Bulletin of Volcanology (2023) 85:61
https://doi.org/10.1007/s00445-023-01662-z

REVIEW ARTICLE

Lateral edifice collapse and volcanic debris avalanches: a post-1980 Mount St. Helens perspective

Lee Siebert[1] · **Mark E. Reid**[2]

Received: 13 July 2022 / Accepted: 17 July 2023 / Published online: 3 October 2023

Abstract

The 1980 eruption of Mount St. Helens was instrumental in advancing understanding of how volcanoes work. Lateral edifice collapses and the generation of volcanic debris avalanches were not widely recognized prior to that eruption, making assessment of their hazards and risks challenging. The proliferation of studies since 1980 on resulting deposits and evaluation of processes leading to their generation has built on the insights from the 1980 eruption. Volcano-related destabilizing phenomena, such as strength reduction by hydrothermal alteration, deformation and structural modifications from shallow magma intrusion, and thermal pressurization of pore fluids supplement those factors also affecting nonvolcanic slopes and can lead to larger failures. Remote and ground-based monitoring techniques can aid in detecting potentially destabilizing dynamic processes and in forecasting the size and location of future large lateral collapses, although forecasting remains a topic of investigation. More than a thousand large lateral collapse events likely ≥ 0.01 km^3 in volume have now been identified from deposits or inferred from source area morphology, leading to a recognition of their importance in the evolution of volcanoes and the hazards they pose. Criteria for recognition of debris-avalanche deposits include morphological factors and textural characteristics from outcrop to microscopic scale, allowing discrimination from other volcaniclastic deposits. Lateral edifice failure impacts a broad spectrum of volcanic structures in diverse tectonic settings and can occur multiple times during the evolution of individual volcanoes. Globally, collapses ≥ 0.1 km^3 in volume have been documented 5–6 times per century since 1500 CE, with about one per century having a volume ≥ 1 km^3. Smaller events < 0.1 km^3 are underrepresented in the earlier record but also have high hazard impact.

Keywords Lateral edifice collapse · Debris avalanche · Failure causes · Sedimentology · Collapse frequency · Mount St. Helens

Introduction

The cataclysmic events of May 18, 1980, at Mount St. Helens led to major advances in the understanding of how volcanoes work. Not the least of these was a recognition of the instability of volcanic edifices and their propensity to collapse, producing large-scale volcanic debris avalanches (VDAs) that extend far from their volcano source. The 1980 eruption of Mount St. Helens was instrumental in calling attention to this process that had received relatively little prior notice. Although large-scale lateral collapse of volcanic edifices and generation of debris avalanches had been recognized prior to 1980 at volcanoes such as Bandai in Japan in 1888 (Sekiya and Kikuchi 1889) and at oceanic volcanoes in the Hawaiian (Moore 1964) and Canary Islands (Bravo 1962), many now well-known examples such as Bezymianny in Kamchatka in 1956 (Gorshkov 1959), Ritter Island in Papua New Guinea in 1888 (Hoyt

Editorial responsibility: A. Harris

This paper constitutes part of a topical collection:

Over forty years since the May 1980 Mount Saint Helens eruption: Lessons, progress and perspectives.

✉ Lee Siebert
siebertlc71@gmail.com

Mark E. Reid
mreid@usgs.gov

[1] Smithsonian Institution, Global Volcanism Program, Washington, DC, USA

[2] U.S. Geological Survey, Volcano Science Center, Moffett Field, CA, USA

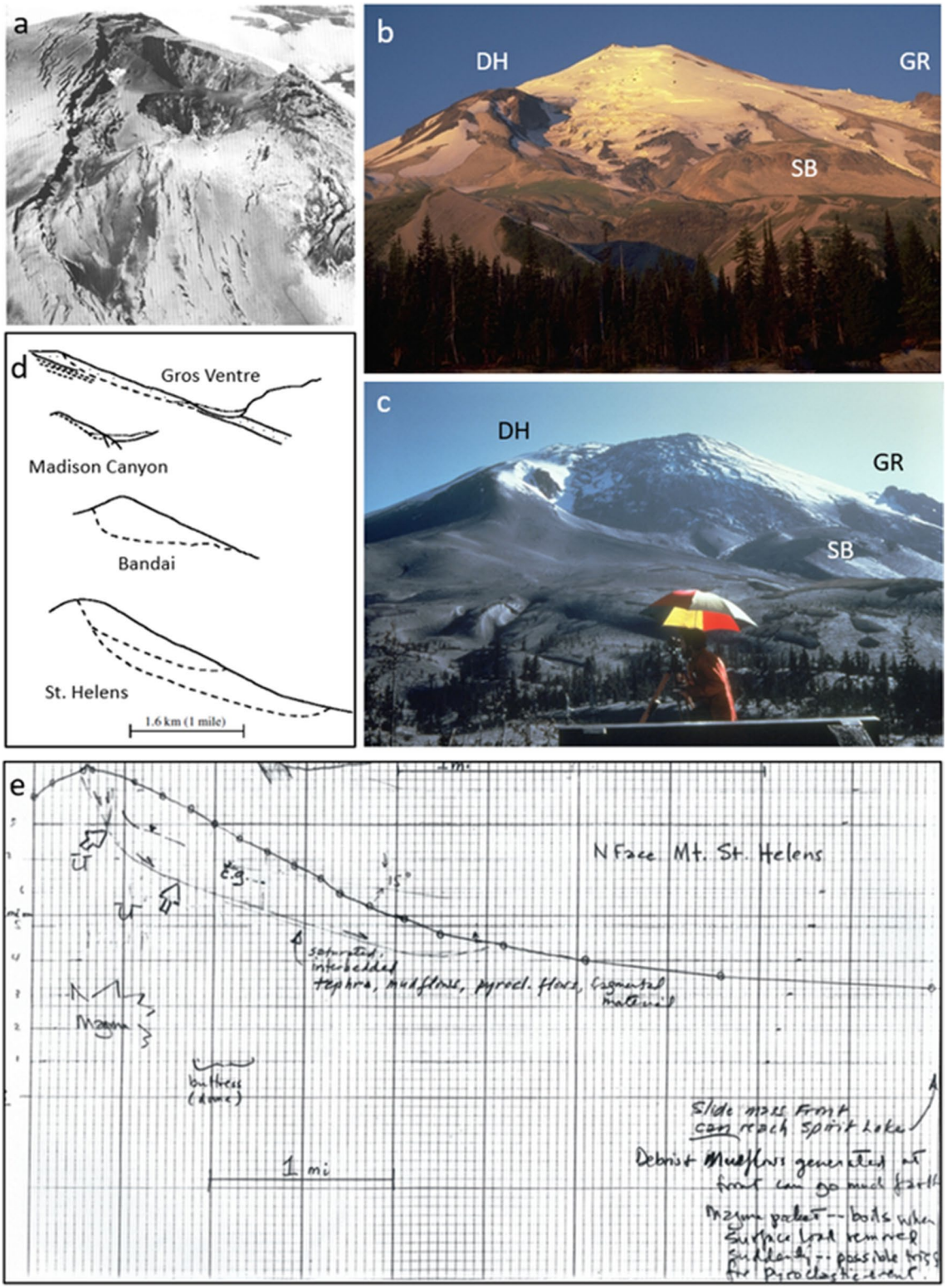

1978), and Mount Shasta in California (Hotz 1977) had been interpreted otherwise. Much of the pre-1980 recognition of VDAs at other volcanoes was in less accessible regional or non-English publications and resulting deposits were most often attributed to a wide variety of other volcanic and nonvolcanic processes, including volcanic mudflows or lahars (Siebert and Roverato 2021).

The 1980 collapse was the first such event to be witnessed and documented at the time of occurrence. An impressively detailed compilation and analysis of the events of 1980 was

◂**Fig. 1** Precursory activity at Mount St. Helens in 1980. **a** Aerial oblique view of summit from east on March 30, 3 days after the onset of eruptive activity showing two small craters and abundant fractures on summit and upper flank with initial development of summit graben (Krimmel and Post 1981). **b** Summit of Mount St. Helens from Timberline viewpoint prior to 1980 volcanic unrest with older lava domes. DH Dogs Head dome, SB Sugar Bowl dome, GR Goat Rocks dome. August 1979 L. Siebert photo. **c** View from nearly same location as **b** (with same features labeled) on May 1, 1980 (Lipman et al. 1981). Base of deformation stretches from Dogs Head to above the top of Sugar Bowl dome and incorporates Goat Rocks and areas to the north. Photo by P. Lipman. **d** Modified Fig. 16 of Voight (2000), with redrafted version of original sketch by Voight posted on wall at the USGS office in Vancouver on April 15, 1980, showing failure surface cross-sections of Gros Ventre (Voight 1978) and Madison Canyon (Hadley 1978) nonvolcanic landslides and potential Mount St. Helens failure surfaces. Bandai volcano was added to final May 1 report. **e** Mount St. Helens portion of original hand-drawn April 15, 1980, sketch showing potential failure surface and including notation that slide mass could reach Spirit Lake and debris and mudflows travel much farther. Image courtesy of B. Voight

rapidly published the following year (Lipman and Mullineaux 1981) while the U.S. Geological Survey (USGS) and other scientists were caught up in dealing with an ongoing major volcanic crisis. We summarize the events leading up to and including the May 18 edifice collapse at Mount St. Helens at a time when the phenomenon of volcanic debris avalanches was not widely recognized, leading to great uncertainty about the future course of the eruption, with attendant difficulties in understanding and communicating risk implications. As part of this special issue on the lasting scientific influence of the 1980 eruption of Mount St. Helens, we then focus on the advances made in understanding and recognizing these events at Mount St. Helens and world-wide in the more than four decades since that catastrophic collapse.

Terminology

We use both *edifice failure* and *edifice collapse* to refer to landslide-generated lateral collapse of volcanic edifices producing debris avalanches. Such landslides are predominantly gravitational but may also be promoted by dynamic volcanic processes such as internal magma "push." The adjective "lateral" is used here to distinguish from vertical caldera collapse resulting from magma chamber evacuation. We apply the generic term *landslide* to both volcanic and nonvolcanic settings. *Pyroclastic flow* and *pyroclastic density current* are generalized terms referring to hot, gravity-driven flows with variable mixtures of air, gas, and pyroclastic particles. We generally use the former term, although both can encompass more specific processes such as *pyroclastic surges, block-and-ash flows, lateral blasts, and ignimbrites* and we also use those more specific terms in context. The terms *lateral blast* or *directed blast* have been applied to several processes including dome explosions (Lerner et al. 2022), but we restrict usage here to laterally directed explosions associated with landslide-generated edifice failures (Belousov et al. 2020).

1980 Mount St. Helens lateral edifice collapse and debris avalanche

Pre-May 18 precursory activity

Prior to the rapid collapse on May 18, 1980, pre-failure deformation at Mount St. Helens began at the onset of the eruptive event in March 1980. Deformation may have begun with the initial seismic events detected on March 20; minor surface fractures cutting the upper northern flank seen on March 25 (Christiansen and Peterson 1981) may have been seismically induced. Summit uplift could have begun slightly before the initial small explosions on March 27, when a 1.5-km-long E-W-trending fracture was first apparent that heralded subsequent formation of a 1.5-km-long, 0.4-km-wide, E-W-trending summit graben. Three days later, deformation at the summit and upper north flank was quite prominent in aerial photos (Fig. 1a). Early explosions were centered within the summit graben that incrementally subsided and expanded to the north, with an uplifted block or bulge forming north of the graben that dramatically pushed the north flank northward prior to May 18. The frequency of small explosions declined slowly in early to mid-April and stopped from April 22 to May 6, resuming intermittently from May 7 to May 14 (Christiansen and Peterson 1981); these explosions were thought at the time to be solely phreatic, but later found to include a magmatic component (Cashman and Hoblitt 2004).

Deformation monitoring on the lower northern flank that included spirit-level tilt stations and the frozen surface of Spirit Lake as a large liquid tiltmeter (Lipman et al. 1981) began on March 30. Tilt measurements at Timberline overlook on the north flank were intensified on April 20 to include geodetic measurements of points higher on the volcano in response to visual evidence of the dramatic bulging on the upper north flank that was not detectable with the early flank tilt measurements (Lipman et al. 1981). Figure 1b and c show the impressive contrast between the pre-eruption profile of the summit and the same view on May 1 after more than a month of deformation. Sequential topographic maps documented that by April 7 the prominent north-flank bulge that formed north of the summit graben was about 1.8 km in diameter (Moore and Albee 1981). It pushed the north flank northward, mostly in a horizontal direction, at a rate of about 1.5–2 m/day, with a peak of 2.5 m/day (Lipman et al. 1981). The bulge was attributed to intrusion of a cryptodome into the upper north flank deflected to the north by the pre-existing summit dome. By May 12 the bulge had

a height of 150 m above the previous slope at that point, with the Goat Rocks dome at the base of the bulge having moved northward by 106 m. By May 18, the cryptodome had an estimated volume of 0.11 km^3 (Moore and Albee 1981).

Ongoing concern about the potential failure of the bulge had prompted the USGS to engage landslide expert Barry Voight to assess the probability of collapse. His report, submitted on May 1, was based on observations during his April 11–19 visit (appended to Voight 2000) and was a prescient analysis of what could happen at Mount St. Helens. Voight noted similarity of events at Mount St. Helens to that at nonvolcanic landslides. He also diagramed potential failure zones at Mount St. Helens (Fig. 1d, e), modeled the tsunami potential from an avalanche reaching Spirit Lake, and noted potential failures as much as a kilometer thick with a volume of 1 km^3 or more. He did not focus on potential explosions triggered by a rapid landslide at Mount St. Helens but noted the volcanic landslide at Bandai volcano in Japan in 1888 and stated that removal of overburden pressure by a landslide could precipitate hydrothermal or possibly magmatic explosive activity. Voight had included the Bezymianny 1956 eruption (Gorshkov 1959) in his draft report outline but did not refer to the widespread 1956 Bezymianny lateral blast in the final report due to ambiguities in Gorshkov's interpretations and his lack of linking landslide and blast (B. Voight, 2021 Pers. Comm.). Voight concluded by noting that data on rates of deformation were difficult to directly inform stability decisions. This proved to be the case at Mount St. Helens. The extensive deformation monitoring of the ominous bulge was intended to determine whether an increase in the rate of movement would be an indication of potential failure. However, measurements on May 16 (delayed due to poor weather since May 5) noted an average deformation rate that had slowed to 1.4 m/day between May 4 and May 16. Measurements on May 17 and early on May 18, the latter made only an hour and a half before the May 18 cataclysmic eruption by David Johnston from the Coldwater ridge field station above the North Fork Toutle River valley, showed further slowing to about 0.5 m/day (Lipman et al. 1981).

Events of May 18

The 2 months of accumulating deformation at Mount St. Helens reached its culmination at 0832 Pacific Daylight Time (PDT) on May 18 when the summit and northern flank suddenly failed, producing one of history's largest landslides. Geologists Keith and Dorothy Stoffel were serendipitously flying above the summit in a small plane (Stoffel 1980) when they saw small avalanches from the summit crater walls, after which the upper north flank begin to ripple in place and then collapse rapidly to the north. Failure of the edifice was retrogressive, involving several slide blocks referred to as slide blocks I, II, and III (Voight 1981; Voight et al. 1981) (Fig. 2). Rapid unloading of the hydrothermal-magmatic system in the upper edifice by failure of slide block I exposed the intruded cryptodome and triggered a directed volcanic explosion (lateral blast) that devastated 600 km^2 over a broad arc WNW to ENE of the volcano, removing trees proximally and causing extensive radial and flow-parallel blowdown with standing singed trees at the deposit margins (Hoblitt et al. 1981; Moore and Sisson 1981; Waitt 1981).

Following emplacement of the debris avalanche and the lateral blast, an open-vent stage of the eruption began from a vent about a kilometer below the former summit, producing a powerful Plinian eruption column that rose to an altitude of 30 km (Sparks et al. 1986). Thick deposits of pumice lapilli blanketed areas near the volcano and distal ashfall reached eastward across the country, causing darkness more than 200 km from the volcano (Sarna-Wojcicki et al. 1981; Carey and Sigurdsson 1982; Eychenne et al. 2015; Criswell 2021; Mastin et al. 2023). Collapse of the eruption column produced pumiceous pyroclastic flows that traveled 7–8 km from the vent, forming a large debris apron extending into Spirit Lake referred to as the Pumice Plain (Rowley et al. 1981; Criswell 1987, 2021; Brand et al. 2016).

May 18 lahars, including those that traveled down the South Fork Toutle River and other valleys to the west and south, formed when pyroclastic surges melted snow and ice. A larger, fines-rich lahar formed several hours later due to liquefaction of the VDA deposit that had traveled down the North Fork Toutle River (Cummins 1981; Janda et al. 1981; Pierson 1985; Fairchild 1987; Brantley and Waitt 1988; Scott 1988a; Waitt 1989). The lahars caused major damage downstream to bridges, roads, houses, and logging camps, reaching the Columbia River and impacting shipping channels. Eyewitnesses located around the volcano provided photographic and other input to interpretation of the eruption (Rosenbaum and Waitt 1981; Waitt 2015; Olsen 2016).

Edifice-failure research at Mount St. Helens

Timely photographs taken by Gary Rosenquist from a location about 17.5 km NE of the summit at Bear Meadow just outside the blast zone showed the volcano before the eruption, the onset of the landslide, and the ensuing eruption. A series of 21 rapid photographs taken over a ~ 45-s interval captured the evolving collapse until the advancing blast cloud obscured views and he and other photographers at Bear Meadow fled the scene. This series allowed detailed assessment of the initial movements of the landslide and the lateral blast (Voight 1981; Voight et al. 1981) (Fig. 2). While the Stoffels were flying overhead, an apparently new fracture about 1.5 km long formed within about 5–10 s after they observed initial small avalanches on the crater walls at

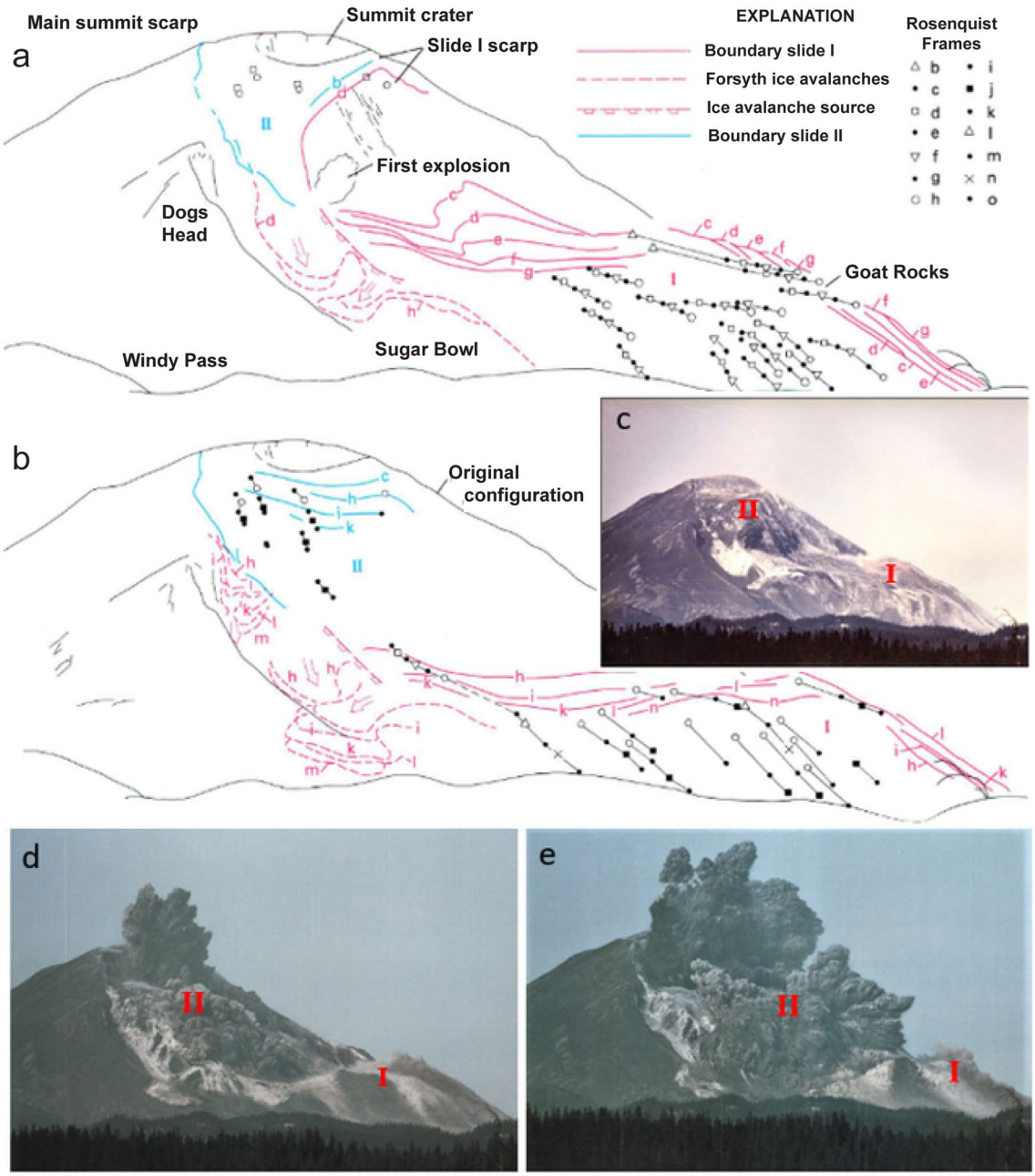

Fig. 2 Initial sequence of edifice collapse showing incremental movement of slide blocks I and II as seen from series of photographs by Gary Rosenquist (Voight et al. 1981). Connected points in Voight et al.'s (1981) diagrams **a** and **b** indicate movement path for objects identified on several images. Photos **c**, **d**, and **e** can be matched to individual slide block movement locations with Rosenquist frame labels c, l, and o, respectively, from Voight diagrams **a** and **b**. Red Roman numerals on photos were added to mark approximate locations of the tops of slide blocks I and II on those photos. **c** Initial post-collapse Rosenquist photo (frame c) at approximately 0832:47 PDT, ca. 36 s after initial earthquake, with no explosive activity showing slide block I at lower right, which had moved 700 m with a scarp 600 m high and had reached a velocity of about 50 m/s. Slide block II at the summit had been displaced about 100 m. White areas in between slide blocks are ice avalanches. **d** Rosenquist frame l taken 10.0 s after frame c. Summit vertical explosions begin from area behind the top of slide block II and the initial explosions of the lateral blast begin through slide block II. **e** Rosenquist frame o 16.7 s after frame c showing growth of summit plume and blast cloud. **c**, **d**, and **e** copyrighted by Gary Rosenquist 1980, used with permission. Figure modified from Voight et al. (1981) and Pierson et al. (2018)

about the time of a 5.1 magnitude earthquake at 0832:11.4 PDT (Endo et al. 1981; Malone et al. 1981). Observable rockslide motion apparently initiated about 0832:21 PDT (Voight 1981). The initial landslide block (slide block I) originated from the area between two northern summit peaks and rapidly unroofed the cryptodome forming the north flank bulge. The initial detachment plane dipped to the north at about a 50–60° angle (Voight et al. 1981). Slide block I had moved 700 m, reaching a velocity of about 50 m/s in about 26 s after its detachment prior to initiation of the blast explosions, which occurred as slide block II was impacting the source of the explosions upslope of slide block I. It moved an additional 700 m downward in only 11 s, attaining a velocity of 70–80 m/s (Voight et al. 1981). The blast cloud soon overtook the still moving slide block I. Calculations of the initial movement of the blast cloud based on the photographs and subsequent destruction of a seismic station at Sugar Bowl dome likely due to arrival of the blast cloud suggested an average horizontal blast cloud velocity of 156 m/s, with a possible instantaneous velocity at Sugar Bowl exceeding 200 m/s (Voight 1981). Kieffer (1981a, b) modeled velocities up to 325 m/s as the blast cloud expanded.

Sidebar: Barry Voight and Harry Glicken

Two individuals, whose names are inexorably linked to Mount St. Helens, were involved both in pre-May 18 monitoring efforts at the volcano in 1980 and in the scientific response to that eruption. They played an oversized role in the volcanology community's understanding of factors contributing to edifice collapse and in recognition and characterization of the resulting deposits. Landslide expert **Barry Voight** was tapped by the USGS prior to the eruption to evaluate the potential for landslide generation at Mount St. Helens. Following the eruption, he plunged into the evaluation of the debris-avalanche deposit and the causes of the failure, utilizing his engineering geology background to produce, along with his colleagues, rigorously constrained evaluations of causes of the collapse at Mount St. Helens and other volcanoes. He was subsequently involved in other major response efforts to volcanic crises or in hazard assessments around the globe, including at Montserrat and other West Indies volcanoes, and at volcanoes in Colombia, Ecuador, Indonesia, the Philippines, Japan, Alaska, Kamchatka, Mexico, France and Italy. Voight had a long-term involvement with the USGS Volcano Disaster Assistance Program, and his focus expanded to incorporate eruption forecasting concepts and methods to improve early warning and evacuation recommendations. His many awards, both in engineering and volcanology, include the IAVCEI Thorarinsson Medal in 2013 and election to the National Academy of Engineering in 2017.

Harry Glicken was a graduate student of R.V. Fisher at the University of California Santa Barbara (UCSB) at the time of the 1980 Mount St. Helens eruption. The events of May 18 prompted him to focus his dissertation on the newly emplaced debris-avalanche deposit. This remains one of the most detailed evaluations of an avalanche deposit to date, and his insights have informed the understanding of many other debris-avalanche deposits since. In addition to his work at Mount St. Helens, Glicken was involved in debris-avalanche projects at Mount Shasta in California, Augustine Volcano in Alaska, Papandayan volcano in Indonesia, and Bandai volcano in Japan. While working in Japan, his promising career was cut short in 1991 when he lost his life, along with French volcanologists Maurice and Katia Krafft and 40 Japanese residents and journalists, when they were caught in a pyroclastic surge from collapse of a growing lava dome on Unzen volcano. Glicken's passion for work on volcanoes is carried on in subsequent papers by volcanologists building on his ground-breaking work at Mount St. Helens and by the annual award of the "Harry Glicken Memorial Graduate Fellowship" of the Department of Earth Sciences at UCSB.

The initial study of the 1980 VDA deposit at Mount St. Helens by Voight et al. (1981) during the summer of 1980 constrained the timing of the VDA, its extent, and textural and physical properties of differentiated deposit units. Part of the rapidly moving VDA swept into Spirit Lake, raising the water surface of the lake by more than 60 m and generating a > 260-m-high wave that swept trees blown down by the blast into the lake, many of which remain floating on the lake surface today. Another segment of the avalanche swept over an intervening ridge (now known as Johnston Ridge) into the South Fork Coldwater Creek drainage, but the bulk of the avalanche was diverted by the ridge down the North Fork Toutle River. The VDA deposit eventually reached 23 km from the source and covered 60 km^2 of the valley floor to an average thickness of 45 m and a maximum thickness of 195 m. Voight et al. (1981) calculated a 2.8-km^3 volume for the deposit, with 2.76 km^3 missing from the edifice, as well as an "in-place" (prior to expansion) volume of about 2.3 km^3 and noted analogs to the Mount St. Helens avalanche deposit in Japan, Kamchatka (Russia), the Cascade Range (USA), Indonesia, and New Zealand.

Following initial studies of the 1980 Mount St. Helens VDA deposit (Voight et al. 1981, 1983; Ui and Aramaki 1983), the most detailed examination of the deposit widely consulted for understanding landslide events elsewhere was by Harry Glicken (1986) in his PhD dissertation at the University of California Santa Barbara, which was published posthumously by the USGS (Glicken 1996). Glicken prepared detailed maps of the surface morphology of the VDA deposit and detailed lithologic maps at a 1:12,000 scale that distinguished overlying lateral-blast and lahar deposits. This mapping allowed determination of movement and destinations of the various parts of the edifice and their relationship to the three retrogressive slide blocks. Factors contributing to edifice instability and resulting collapse at Mount St. Helens and elsewhere are discussed in a later section.

Deposit geometry, morphology, and sedimentology

Glicken (1986, 1996) recalculated the preliminary deposit volumes of 2.8 km^3 of Voight et al. (1981, 1983) to be 2.5 km^3, including 0.43 km^3 of material deposited in Spirit Lake. Neither figure included the 0.2 km^3 of avalanche material remaining in the post-collapse crater. The deposit thinned considerably downstream of a constriction in the valley west of Coldwater Lake (Fig. 4), where it was dominated by slide block III material and widely overlain by subsequent May 18 lahar deposits. Glicken evaluated the morphology and volumes of hummocks, identifying 675 hummocks on available 1:24,000 maps. Small hummocks (less than about 12 m maximum height constrained by available 40-ft. contours) appeared throughout the deposit, but hummock size decreased with distance, with smaller hummocks forming > 90% of hummocks beyond 24 km. Glicken's detailed map of hummock orientations showed that elongation of hummocks was generally parallel to flow direction, but at valley constrictions or at the distal end orientations were random.

Glicken distinguished two end-member facies in the VDA deposit, a *block facies*, consisting of unconsolidated or poorly consolidated pieces of the edifice that were transported relatively intact, and a *matrix facies* consisting of completely mixed material from the edifice or substrate material incorporated during emplacement. Glicken (1990, 1991) redefined the *matrix facies* to be the *mixed facies*, terminology subsequently widely adopted elsewhere. Both

Fig. 3 Dark-colored hummock is exposed block-facies material rafted within light-colored mixed-facies material in the 1980 Mount St. Helens debris-avalanche deposit. Red circle marks person for scale. Photo modified from Glicken (1986)

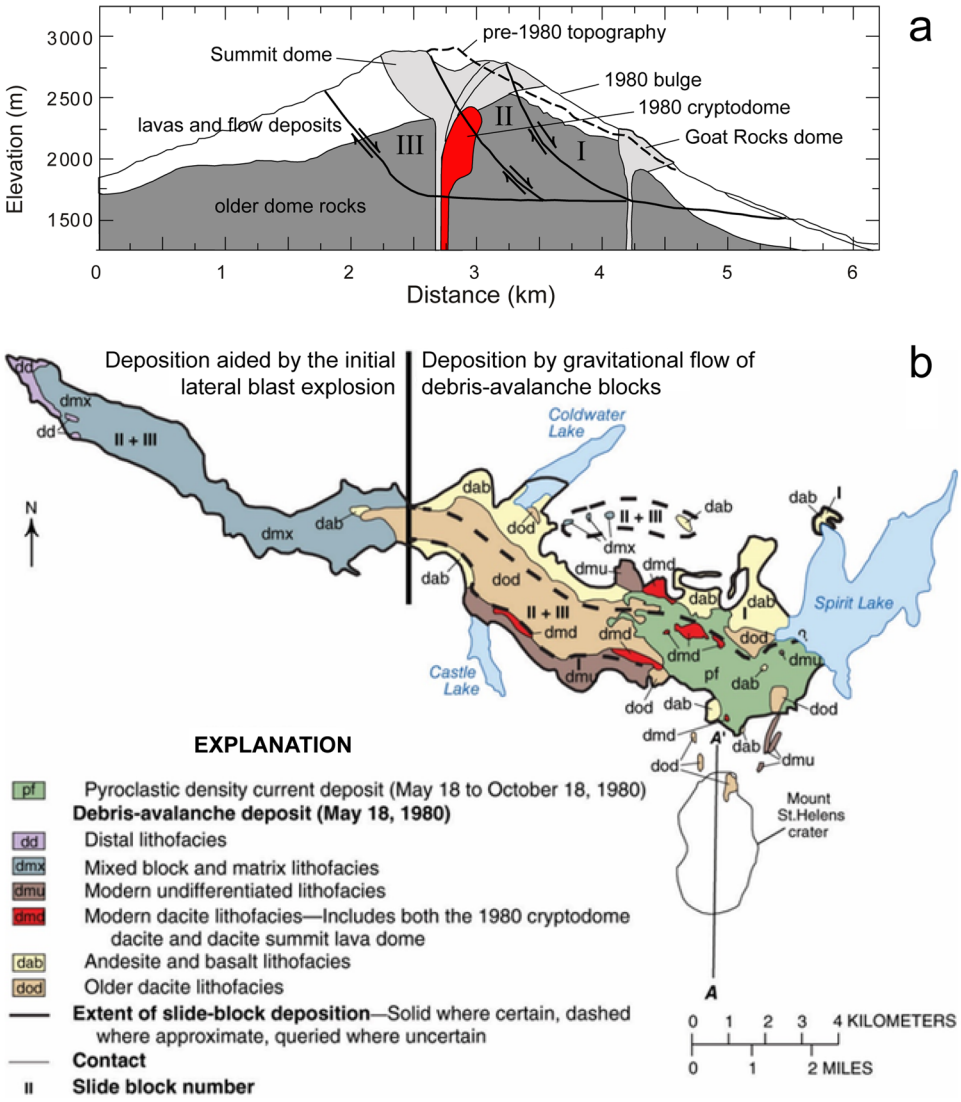

Fig. 4 Summary of 1980 debris-avalanche components before and after edifice collapse. **a** Cross section through pre-collapse Mount St. Helens showing north flank bulge, extent of summit dome (light gray) and older domes (gray), inferred extent of 1980 cryptodome (red) after Donnadieu et al. (2001), and failure surfaces of the three landslide blocks (I, II, and III) after Glicken (1996). Modified from Reid et al. (2010b). **b** Map of the 1980 debris-avalanche deposit showing the distribution of the primary lithofacies. The depositional extent of slide blocks I, II, and III are labeled. Dashed lines to the right of Coldwater Lake indicate area of South Coldwater Creek valley. Figure from Pierson et al. (2018) after Glicken (1996)

block and mixed facies were found at the same exposure, and block-facies material was often surrounded by or carried within mixed-facies material (Fig. 3).

Hummocks were categorized based on facies relationships and attributed to mechanisms such as horst and graben formation or basal or lateral shear. Block-facies material dominated the proximal to medial part of the deposit, with a mixture of block facies and mixed facies dominating distal material to the west. Pervasive fracturing throughout block-facies material produced partially fractured or completely shattered debris-avalanche blocks. Studies on a microscopic scale at Mount St. Helens indicated that pervasive fracturing extended to the size of individual grain fragments (Komorowski et al. 1991).

Glicken conducted the first detailed analysis of the sedimentological properties of a VDA deposit, utilizing pipette and sieve data for finer-grained parts of the deposit supplemented by photographic analysis of larger blocks in a series of 1-m^2 "windows" created by clearing exposures of colluvium and slope wash. Although plots of grain size distributions of different deposit types are often difficult to compare due to different analytical techniques, plots of median grain diameter (Md_ϕ) against Inman sorting coefficient (σ_ϕ) at Mount St. Helens showed that the VDA deposit was commonly coarser than pyroclastic-flow deposits (Walker 1971) and better sorted than lahar deposits from Fisher and Schmincke (1984). Grain size data and clast density measurements at Mount St. Helens suggested that clast fracturing did not occur progressively during transport but primarily originated near the source (Glicken 1986, 1996).

Emplacement processes

Three stratigraphically and lithologically distinct rock types are exposed in the post-collapse crater walls, consisting of *older dacitic* rocks of Pine Creek (ca. 3000–2550 cal BP) or

earlier age exposed at the base of the source scarp, overlain by *andesitic and basaltic* rocks of the Castle Creek, Kalama, and Goat Rocks eruptive periods (ca. 2025 cal BP to 1857 CE), and *modern dacitic* rocks (1479 CE to 1857 CE) from the Goat Rocks and summit lava domes (Mullineaux and Crandell 1981; Clynne et al. 2008; Pallister et al. 2017). Discrimination of these lithologies in VDA deposits outcrops along with deposits of the associated lateral blast allowed determination of sequential slide block movement and their ultimate destinations (Fig. 4).

The 0.96-km^3 slide block I (Glicken 1986, 1996) initially traveled north into Spirit Lake and overrode two low points along Johnston Ridge to the west. Undulating avalanche trimlines to 200 m above the valley floor on the north valley wall above South Coldwater Creek provided evidence for transient wave–like avalanche transport that scoured the hillside of soil and earlier lateral-blast tree blowdown, leaving a thin avalanche veneer well above valley-floor deposits (Fisher et al. 1987). Much of the slide block I material was deflected westward down the North Fork Toutle River valley and broken into smaller blocks, but an area of larger hummocks of the andesite and basalt lithofacies blocked the Coldwater Creek drainage, later forming Coldwater Lake (Fig. 4b).

Slide block II is dominated by stratigraphically lower older dacites from the edifice and contains 8% of juvenile cryptodome dacite. Slightly more than a quarter of the 0.75-km^3 slide block II (Glicken 1996) was incorporated in the lateral blast, and the remainder may have been deposited in Spirit Lake, the South Fork Coldwater Creek drainage, and the North Fork Toutle River valley reaching to the distal end of the deposit. The Rosenquist photos showed the lateral blast erupting through slide block II before overtaking slide block I, and deposits of the lateral blast were found locally beneath the VDA deposit and covered its entire surface before thinner parts of the blast deposit were eroded. Blast deposits were also found intermixed with the VDA deposit, and blast dacite was incorporated within the mixed facies of the VDA deposit. At some locations, mixing of blast and avalanche deposits created a hybrid deposit with textural attributes of both, prompting the use of working field names such as "blavalanche" or "blastalanche," the latter informally used for proximal deposits near the Pumice Plain (Pallister et al. 2017). The interaction of slide blocks II and III with the lateral blast influenced the dynamics and travel distances of the slide blocks. Glicken noted a distinct change in deposit morphology and facies distribution at the valley constriction about 2 km west of Coldwater Lake (Fig. 4b). At this location, the very hummocky terrain of the proximal and medial parts of the VDA deposit dominated by block-facies material changed to a combination of mixed-facies and block-facies material with smaller hummocks surrounded by mixed-facies material. This combination persisted to near the distal end of the deposit.

The 1.29-km^3 slide block III was the largest of the slide blocks (Glicken 1996). Rather than sliding like the discrete blocks I and II, the remaining edifice summit and rim of the landslide scarp forming slide block III appeared to have failed in a piecemeal manner driven by both gravitational sliding and explosive depressurization of the cryptodome (Voight et al. 1981, 1983; Glicken 1986, 1996; Sousa and Voight 1995). The bulk of this slide block traveled as block and mixed facies material that initially covered proximal axial parts of slide block I deposits but formed the dominate downstream component of the western part of the VDA deposit. Later incision of the deposit exposed outcrops unavailable to Glicken, revealing an axial lobe in the North Fork Toutle River with abundant older dacite rocks overlying younger andesite-basalt units in reverse stratigraphic order. Ward (2006) attributed this to slide block III cutting deeper into the edifice, generating more mobile and lower basal friction slide block III material that overrode the higher basal friction material from earlier slide blocks that may have slowed to a stop.

Two-explosion hypothesis and debris avalanche–lateral-blast interactions

Initial studies of lateral-blast dynamics and characteristics of deposits (Kieffer 1981a, b; Hoblitt et al. 1981; Moore and Sisson 1981; Waitt 1981) and many subsequent studies (Fisher et al. 1987; Brantley and Waitt 1988; Kieffer and Sturtevant 1988; Fisher 1990; Druitt 1992; Alidibirov 1995; Esposti Ongaro et al. 2012) were based on the premise of a single explosive event. Moore and Rice (1984) first proposed that a second explosion had taken place from a point either at Johnston Ridge or Spirit Lake using satellite infrared (IR) sensor data and eyewitness photos, and Sparks et al. (1986) also identified multiple plumes.

Hoblitt (2000) attributed the northern explosion of Moore and Rice (1984) to the blast cloud encountering the rugged topography at Johnston Ridge, but also proposed a two-explosion hypothesis, with the second originating on the north flank of the volcano. The second and larger explosion or explosion cluster was associated with a second IR spike and perhaps triggered the collapse of slide block III. It was considered to occur about 60–70 s after slide block II had moved downslope beyond its initial failure plane and re-exposed part of the cryptodome (Hoblitt 2000). In this scenario, the second explosion and IR spike were followed by a second major earthquake (Malone et al. 1981; Kanamori and Given 1982; Kanamori et al. 1984), attributed to the second group of explosions.

Hoblitt (2000) also noted that parts of the lateral-blast deposit contained two coarse basal units with the proportion of dense juvenile and lithic clasts increasing upward, consistent with the initial explosion originating from the more

gas-rich upper part of the cryptodome and a second set of explosions originating from the more degassed lower part. Waitt et al. (2019) described evidence from azimuths of tree blowdown and abrasion that required a source of the second explosion on the north flank of the volcano and noted stratigraphic evidence for two lateral explosive events on May 18.

The hypothesis of a second major lateral-blast explosion from the north flank (Fig. 7 of Hoblitt 2000) is consistent with stratigraphic evidence of the VDA deposit in which blast-dacite-rich slide blocks II and III display an explosively enhanced greater mobility than slide block I, with slide block III forming the dominant distal component of the VDA deposit (Glicken 1986, 1996). The large volume of slide block III, the extent of its deposits, and its association with the second major lateral blast explosion and earthquake series suggest that slide block III could have included an initially large coherent slide block along with smaller incremental piecemeal collapses.

Prehistorical lateral edifice collapse events at Mount St. Helens

The 1980 Mount St. Helens collapse led to the identification of older VDAs at the volcano. The earliest was a late-Pleistocene collapse on the south flank (Mullineaux and Crandell 1981; Newhall 1982; Clynne et al. 2008). The 200–300-m-thick Cougar-stage VDA deposit on the south flank was emplaced at about 24.4 ka during the 28–18-ka Cougar Eruptive Stage at Mount St. Helens (Mullineaux and Crandell 1981; Clynne et al. 2008; Pallister et al. 2017). The volume was roughly estimated to be 1–2 km^3 (Clynne et al. 2008). The VDA traveled about 17 km and dammed the Lewis River at the present site of Swift Creek (Clynne et al. 2008). Subsequent overtopping of the blockage and sudden lake drainage filled the lower Lewis River valley with debris at least 75 m deep and caused flooding downstream to the Columbia River (Major and Scott 1988). A distinctive, very porphyritic, hydrothermally altered hornblende dacite containing about 66% SiO_2 forms at least 80% of the deposit and is called the debris-avalanche dacite. The VDA deposit is found in both the Swift Creek drainage south of the summit and the Cedar Flats area in the Pine Creek drainage SE of the summit, implying an origin from the area of the present-day edifice with subsequent diversion around the broad Marble Mountain massif SE of Mount St. Helens. The avalanche was immediately followed by explosive eruptions that produced a two-pumice dacitic pyroclastic-flow deposit, dated at about 24.4 ka. This deposit overlies the Cougar-stage VDA deposit to depths of 100–200 m without evidence for intervening erosion or soil formation and has a volume of >1.0 km^3 (Clynne et al. 2008).

During the Pine Creek Eruptive Stage of Mount St. Helens about 3000–2500 years BP (Mullineaux and Crandell 1981), two VDA deposits (Fig. 5) were emplaced on the north flank of the volcano (Hausback and Swanson 1990; Hausback 2000). The older of the two deposits is exposed at the bottom of Loowit and Step Creeks and consists of a > 40-m-thick section (base not exposed) of altered fragmental dacitic material with an upper contact suggesting hummocky topography. It is overlain by Pine Creek age pyroclastic-flow deposits and a younger VDA deposit with a 0–3-m-thick basal zone containing abundant uncharred and battered logs up to 40 cm diameter surrounded by an intermixed possible paleosol. These features indicate a time interval between the two VDA deposits sufficient for soil formation and growth of a fir forest. A log in the lowermost part of the upper unit yielded an age of 2590 ± 120 14C years BP. Both VDA deposit units consist of variegated light-gray and pastel-colored yellow, pink, and green unconsolidated lithic dacitic blocks, lapilli, and ash.

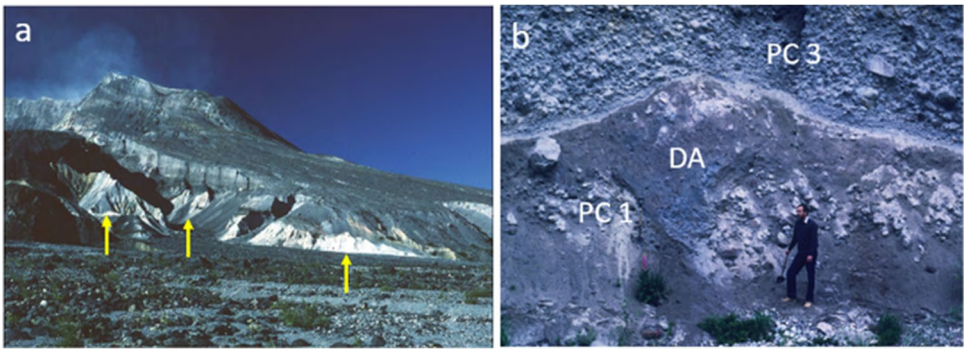

Fig. 5 Pine Creek (PC) age volcanic debris-avalanche deposits of Mount St. Helens. **a** Base of two light-colored volcanic debris-avalanche deposits of Pine Creek age, shown by arrows, incised into north-flank deposits of Mount St. Helens. Upper deposit synchronous in age with the PC lahars (Hausback 2000) and likely dammed Spirit Lake, producing lake breakout floods that transformed into PC1 lahar. Photo by C.J. Harpel from Pierson et al. (2018). **b** Debris-avalanche block (DA) with basal clast-supported dacitic clasts at top of PC1 lahar at Pullen Creek, ca. 30 km northwest of the volcano, overlain by PC3 lahar deposit. Photo by J. Major. The PC1 lahar contains VDA-derived dacitic megaclasts up to 8 m in intermediate dimension (Scott 1988b)

The largest Pine Creek age lahar (PC1) in the Toutle River drainage was likely associated with catastrophic draining of Spirit Lake after it was dammed by a north-flank VDA deposit (Scott 1988a, b). The PC1 lahar contains both rounded lithic clasts entrained from river deposits during a major flood surge and megaclasts of debris-avalanche origin (Fig. 5b). The peak discharge exceeded that of the Amazon River in flood stage (Scott 1989) and ranks among the world's largest floods (O'Conner and Costa 2005). The Pine Creek age VDA deposits have limited exposure near the base of the volcano due to burial by deposits of later eruptions and have been considered relatively small-volume VDAs, but at least one of them must have had considerable volume as it dammed Spirit Lake (Scott 1988b). An avalanche of that volume would also have likely deflected westward down the North Flank Toutle River valley; this could have occurred with both Pine Creek VDA deposits. The broad flat floor of the North Fork Toutle River valley prior to 1980 in contrast to valleys on other sides of the volcano could in part reflect earlier deposition of the Pine Creek age VDA deposits. Hydrothermally altered dacitic megaclasts in unit 8 of Smith Creek-age lahar deposits (ca. 3900–3300 cal BP; Clynne et al. 2008) suggest a possible older VDA deposit in the North Fork Toutle River drainage (Scott 1988b).

Factors leading to edifice instability and subsequent failure

Landslides or slope failures are commonly complex and rarely result from just one factor. Typically, multiple destabilizing conditions predispose a slope toward failure (such as steep slopes or weak rocks) and combine with a dynamic trigger event (such as increases in groundwater pore-fluid pressure or earthquake shaking) to drive failure, although failure can result from slow incremental changes as well. Volcano slopes are afflicted by destabilizing conditions operative on other large mountains, but edifices have additional disrupting factors related to dynamic volcanism and edifice construction, such as shallow magma intrusion and explosive behavior, hydrothermal pressurization of various pore fluids by intrusion and heating, variable loading by magma extrusion, and weakening of rocks by acid-argillic hydrothermal alteration (Fig. 6). Moreover, volcanic edifices can exhibit tremendous geologic complexity and heterogeneity, both at the microscopic and field levels. A wide range of slope failure styles and sizes occur on volcanoes, ranging from relatively small rock falls to enormous, multiple cubic kilometer failure masses that dissect deeply into their edifices (Siebert et al. 1987; McGuire 1996; Ui et al. 2000; van Wyk de Vries and Davies 2015).

Here we primarily focus on causes of these massive and deep flank collapses on subaerial stratovolcanoes; the mechanics and dynamics of motion and emplacement are discussed by others. These failures can be extensive enough to remove edifice summits. Edifice collapses can generate far traveled debris avalanches, with larger edifice collapse volumes typically resulting in greater avalanche runout. Thus, the volume and location of a failure mass can have far reaching ramifications, as these initial conditions influence the downslope transport behavior of an ensuing debris avalanche.

Only a few large edifice collapses have been observed well enough to reasonably ascertain the mechanisms that triggered collapse; these include Unzen-Mayuyama (1792 CE), Bandai (1888 CE), and Ontake (1984 CE) in Japan; Bezymianny (1956 CE) and Shiveluch (1964 CE) in Kamchatka, Russia; and Soufrière Hills (1997 CE) in Montserrat. The massive 1980 Mount St. Helens collapse is one of the best documented major edifice failures, as there were series of

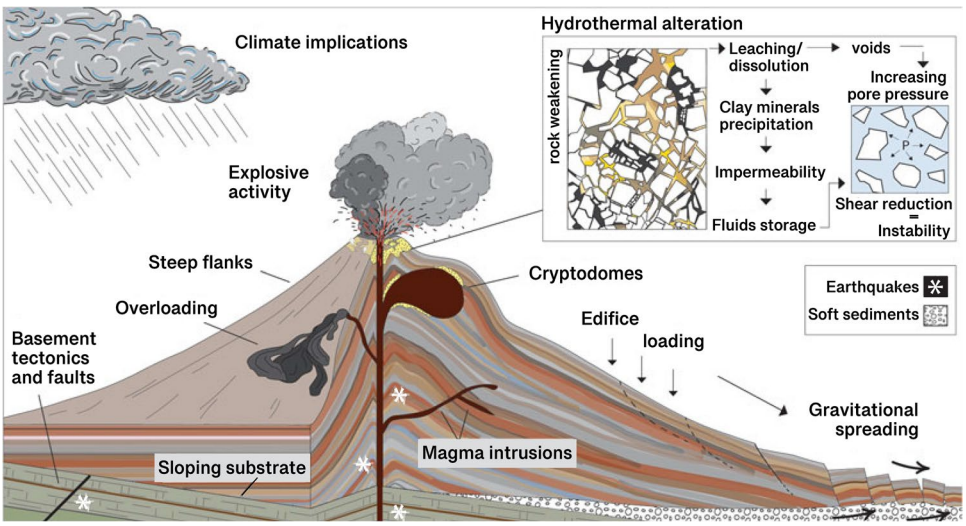

Fig. 6 Schematic diagram showing a few of the numerous volcanic and nonvolcanic factors that can destabilize edifice flanks with top right inset illustrating effects of hydrothermal alteration. Image modified from Roverato et al. (2021a)

photos taken during the event and eye-witnesses, as well as instrumental records, prior to and during the collapse. Observations and analyses of this collapse offer crucial insights into conditions generally applicable to other edifice collapses, such as edifice structure, strength, shallow magma intrusion, and earthquake shaking. Here, we first examine controls on the 1980 Mount St. Helens collapse, then survey other factors that can predispose the flanks of subaerial stratovolcanoes to large-scale failure. We summarize potential triggers for these large collapses and finally discuss techniques for forecasting and (or) monitoring impending large flank collapses.

Lessons from the Mount St. Helens flank collapse

From the many observations made during the 1980 Mount St. Helens collapse, some of the most salient include (1) the intrusion of a shallow cryptodome into the upper edifice, resulting in large scale faulting, graben-formation, and flank bulging; (2) slow deformation over several months, then rapid failure within seconds; (3) massive retrogression of failure in three stages, excavating deep into the edifice and removing its summit; (4) arcuate failure surfaces that cut across, and were not controlled by, geologic contacts within the edifice; and (5) rapid collapse associated with a moderate-sized earthquake. These observations have helped motivate and guide subsequent investigations into the causes of edifice collapse.

Using a variety of methods, including geotechnical deformation analysis, limit-equilibrium slope-stability analysis, analog physical models, and rock testing, investigators have explored both the factors predisposing failure, including slowly changing conditions induced by volcanic activity, and the dynamic triggers leading to the rapid and massive Mount St. Helens collapse. Some of these studies are discussed in detail in Voight (2000). Here, we first discuss the destabilizing factors that promoted instability and then examine potential triggering mechanisms. Factors that modify slope stability involve those that increase stress as well as those that reduce strength.

Topography and internal structural features commonly exert a primary influence on the size and geometry of gravitationally controlled slope failures. Prior to volcanic unrest in 1980, the upper edifice of Mount St. Helens had relatively steep slopes, typically between 20 and 30°, but locally up to 40° (Reid et al. 2000). Strike-slip faulting beneath the edifice may have further predisposed it to slope instability (Lagmay et al. 2000). The dynamic intrusion of a shallow cryptodome over 2 months resulted in dramatic edifice deformation with a large bulge (about 1.5 km by 2 km) on the north flank of the edifice (Fig. 1b, c), as well as a massive east-trending graben and large faults and fractures (about 1.5 km long) near the summit (Lipman et al. 1981; Moore and Albee 1981; Voight et al. 1983). Cryptodome intrusion into the edifice strongly influenced both ground-surface topography and internal structures. Moreover, destabilizing effects associated with intrusion could have included seismic inertial forces, reduction of rock strength, and (or) thermal or stress-related pressurization of pore fluids (Voight et al. 1983).

The destabilizing role from direct magmatic driving forces at Mount St. Helens is not well quantified. In deformation simulations using an interacting assemblage of rigid blocks representing the pre-deformation Mount St. Helens edifice, intruding magma pressure produces the observed surface deformation, including the development of a summit graben and north flank bulge (Paul et al. 1987). Other investigations using analog physical models illustrate the evolution of edifice deformation during shallow intrusion of a cryptodome (Donnadieu and Merle 1998, 2001). Using appropriate scaling of materials, these models show that vertically intruded viscous material creates a series of evolving structural features, including upward shear faulting, bulging of one flank, and an asymmetric graben with normal faulting oriented perpendicular to the bulge. A sill-like shaped cryptodome is not required to induce flank bulging.

Most limit-equilibrium slope-stability analyses of the 1980 Mount St. Helens edifice utilize the observed deformed 1980 topography, including the north flank bulge and summit graben (Voight et al. 1983; Reid et al. 2000, 2010b; Donnadieu et al. 2001). As the observed basal slip surfaces were arcuate, these analyses typically assume arcuate, circular, or spherical slip surfaces. Using two-dimensional analyses, investigations commonly focus on initial failures (such as block I) rather than a deep slip surface such as that associated with block III (Voight et al. 1983; Donnadieu et al. 2001). In these cases, the bulge controls the location of slide block I and the southern bounding normal fault of the graben forms the head of slide block II (Fig. 4a). The relative stability (determined as factor of safety, F) of slide block I and slide block II is similar in most analyses, in keeping with slide observations of block II moving shortly after and in concert with slide block I. Some analyses result in the lowest stability for block I (Voight et al. 1983), whereas others incorporate weak zones along deeper internal structures created by intrusion and determine slightly lower stability for the larger block II (Donnadieu et al. 2001). Three-dimensional slope-stability analyses of millions of potential failures affecting the edifice show that topographic oversteepening alone, caused by the bulge, destabilized the north flank by ~ 3% relative to its undeformed topography and focused instability on a ~ 1.1-km^3 region incorporating the bulge (Reid et al. 2000). These studies reinforce the importance of topography as well as internal structural controls on slope stability.

Another primary control on slope and edifice instability is the distribution of rock strength. The collapse of Mount St. Helens offers insight here as well. Observations indicate that

most of the slip surfaces for all three 1980 slide blocks were predominantly formed in older dacite dome rocks underlying the sloping volcanic layers near the edifice surface (Voight et al. 1983; Reid et al. 2010b) (Fig. 4a). These buried dacite domes and other exposed domes swept away by the 1980 collapse were more plentiful in the northern part of the edifice. The 1980 slip surfaces cut across the thinner, upper edifice layers composed of lava flows and pyroclastic material (Fig. 4a), essentially unaffected by sloping layers in this near-surface region. Early stability analyses assumed relatively high strengths for these older dome rocks (internal friction angle of ~ 40°), and these high strengths necessitated elevated pore-fluid pressures and earthquake shaking to produce slope failure (Voight et al. 1983; Reid et al. 2000; Donnadieu et al. 2001).

Many of the older dome rocks hosting the 1980 slip surfaces, however, are pervasively fractured (Hausback 2000; Kendrick et al. 2013) but contain essentially no hydrothermal alteration (Reid et al. 2010b). Laboratory tests using thermal and cyclic stressing on these older dome rocks demonstrate loss of rock strength and suggest that repeated dome inflation and deflation could progressively weaken them (Kendrick et al. 2013). Other laboratory shear strength testing of shattered dome rocks near the 1980 shear surface reveals that they become weaker through progressive shearing (decreasing in friction angle from ~ 35 to ~ 27°), as might occur during intrusion and flank bulging (Reid et al. 2010b). Slope stability analyses using reduced strengths for these mechanically weaker rocks indicate a propensity for large-scale failure, reducing slope stability by ~ 20% (Donnadieu et al. 2001; Reid et al. 2010b). Moreover, the distribution of Mount St. Helens edifice rock friction fundamentally affects subsequent landslide kinematics and runout (Ward and Day 2006).

Pre-collapse groundwater conditions within the Mount St. Helens edifice are poorly known, although 1980 eruptive activity prior to collapse consisted of predominantly smaller phreatic or phreatomagmatic eruptions (Lipman et al. 1981; Cashman and Hoblitt 2004), suggesting at least some shallow groundwater. Many slope-stability analyses of the collapse assume relatively high pore pressures located on the slip surfaces to provoke instability (e.g., Voight et al. 1983; Reid et al. 2000; Donnadieu et al. 2001). On the other hand, more generalized numerical simulations indicate that water tables may be relatively low within some stratovolcano edifices (Hurwitz et al. 2003; Ball et al. 2018). Analysis of potential failure retrogression induced by undrained unloading of a cold, saturated Mount St. Helens edifice indicates that transiently out-of-equilibrium pore pressures would enable modest retrogression (on the order of block II) (Fig. 7), but less than the amount observed with block III (Reid and Brien 2006). High-temperature magma intrusion into a saturated or partially saturated edifice with accompanying thermally pressurization of pore fluids could have provided another destabilizing effect (discussed below).

The precise triggering mechanism inducing the May 18, 1980, rapid flank collapse remains unclear. The collapse was accompanied by a surface-wave magnitude $M_s = 5.2$ ($m_b = 4.7$) earthquake (Kanamori and Given 1982), but different researchers have argued that the earthquake triggered the massive landslide or that the landslide itself caused the earthquake. The timing of the exceptional photographic observations of the collapse is not precise enough to unequivocally relate them to seismic network timing. Initial analysis suggested that sliding began ~ 7–20 s following the earthquake (Voight 1981). The earthquake has been cited as an abrupt trigger of collapse, in part because the flank did not show accelerating ground displacement in the days preceding collapse as often occurs with failures (e.g., Lipman et al. 1981; Voight et al. 1983; Voight 1989; Intrieri et al. 2019) and in part because inertial forces from earthquake ground acceleration can provoke instability even in relatively strong rocks (e.g., Voight et al. 1983; Reid et al. 2000; Donnadieu et al. 2001).

Nevertheless, the seismic signal accompanying the collapse was not a classic double-couple source typical of tectonic

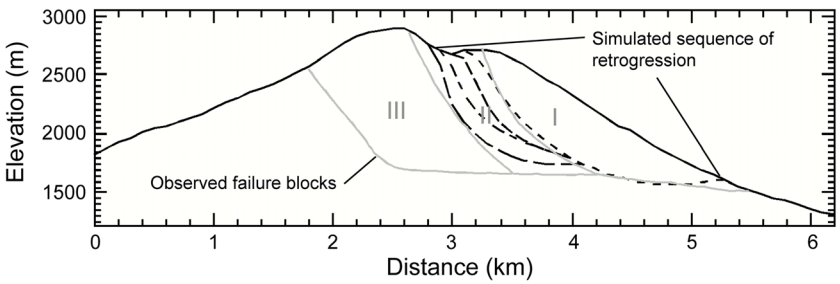

Fig. 7 Simulated three-dimensional (3D) retrogression into a cold, fully saturated Mount St. Helens edifice without a cryptodome intrusion. Light gray indicates observed slide blocks I, II, and III failure surfaces. Leader lines mark sequence of simulated retrogression from right to left, with darker dashed lines representing sequential smaller retrogressive failures due to undrained rapid unloading caused by rapid removal of the previous failure masses. Here, retrogression halts before slide block III is removed. Image modified from Reid and Brien (2006)

earthquakes, but instead was consistent with the onset of sliding by a large landslide (Kanamori and Given 1982; Kanamori et al. 1984). There had been three earthquakes of similar magnitude (7 April 1980, m_b=4.9; 16 April 1980, m_b=4.9, and 12 May 1980, m_b=4.8) in the Mount St. Helens area the month before collapse (Kanamori et al. 1984). In the years since the 1980 collapse, other researchers studying landsides as seismic sources have found that landslides of the Mount St. Helens size are capable of generating Ms ~ 5 earthquakes (Hasegawa and Kanamori 1987; Brodsky et al. 2003; Lipovsky et al. 2008; Ekström and Stark 2013). Other studies indicate that, in general, the smallest earthquakes observed to trigger rock falls are about M_s ~ 5.5 and to trigger rock avalanches about M_s ~ 6 to 6.5 (Keefer 1984; Rodríguez et al. 1999). Other possible triggers for the 1980 collapse, potentially acting in concert with one another, include progressive rock strength reduction from shearing (Reid et al. 2010b) or pressurization of gas or fluid in a shallow hydrothermal system (Voight et al. 1983). Rapid depressurization of the cryptodome and any shallow hydrothermal system caused by the swift movement of slide blocks I and II likely promoted explosive behavior, formation of the directed lateral blast, and retrogression of failure into the edifice (Voight et al. 1983).

Causes of collapse at other edifices

Following the catastrophic Mount St. Helens collapse in 1980, there has been intense interest in understanding the causes of these collapses at other volcanoes. From a simplistic mechanical perspective, slope failure occurs when driving forces on a potential slip surface exceed resisting forces. In an earlier review of collapse causes, Voight and Elsworth (1997) listed 48 categories of possible edifice destabilizing factors grouped by inherent causes, causes that increase shear stress, and causes that reduce shear strength. Other reviews have focused on volcano-centric aspects of collapse; for example, Roverato et al. (2021a) listed instability factors related to (1) basement, tectonics, and faults; (2) slope substrate and gravitational spreading; (3) hydrothermal alteration; (4) dikes and magma intrusions; and (5) past and present climate effects. Acocella (2021) reviewed similar volcano-related factors as well as the destabilizing effects of excess pore-fluid pressures. Here, we use the insights gained from detailed examination of the 1980 Mount St. Helens collapse to focus specifically on controls of large and deep edifice collapses, as these can present immense and far-reaching hazards.

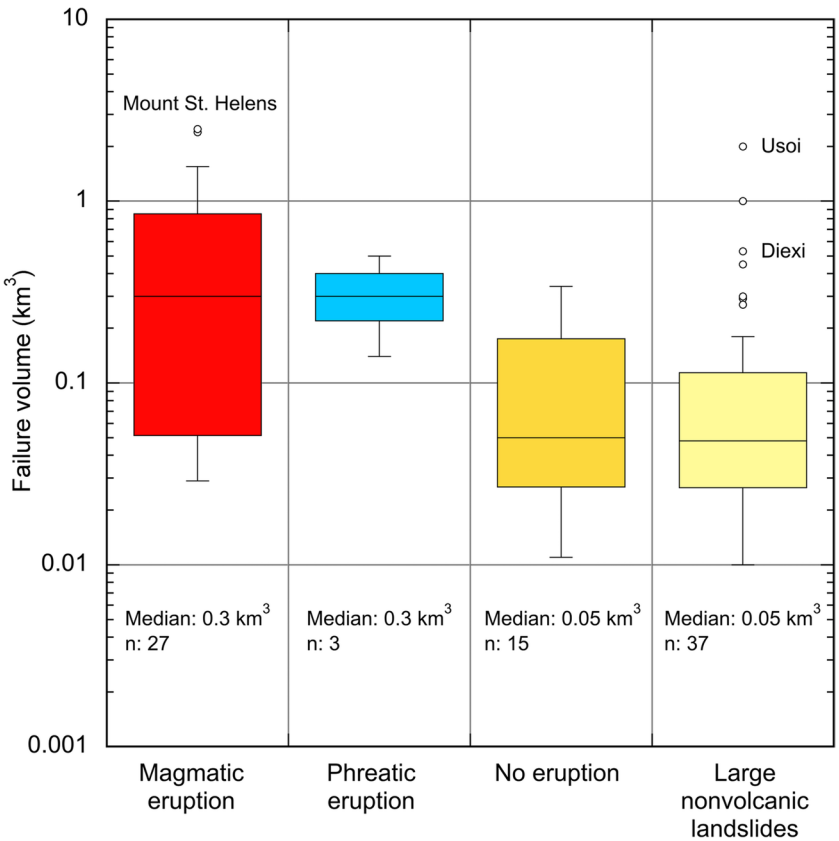

Fig. 8 Box plot of failure volumes ≥ 0.01 km^3 since 1500 CE categorized by event type, including flank failures associated with magmatic eruption, phreatic eruption, and no eruption. Volumes of other large (≥ 0.02 km^3), historical (since 1900) nonvolcanic landslides are shown for comparison; nonvolcanic landslide data from Evans (2006). Smaller, potentially more frequent, failures < 0.01 km^3 not included in plot. Box in each category represents 50% of the data (with median line), whiskers represent the upper and lower quartiles, and circles are outliers

Figure 8 illustrates differences in edifice failure volumes associated with juvenile magmatic eruptions since 1500 CE, with phreatic explosions (with no juvenile magmatic eruption components), and not associated with known eruptive activity. It also shows failure volumes from other historical large nonvolcanic landslides (primarily rockslides and rock avalanches) for comparison. Although there is clear overlap in the sizes found in each category, the median volumes for flank failures associated with magmatic or phreatic eruptions are roughly an order in magnitude greater than either nonmagmatic collapses or other large landslides.

In general, large landslides not on volcanoes have a myriad of factors predisposing them to failure, such as steep slopes and weak rocks. Many of the large catastrophic landslides documented in the twentieth century were triggered by either large tectonic earthquakes ($M > 6$), large rainstorms such as typhoons or hurricanes, or snowmelt, but some have no clear trigger (e.g., Schuster 1996; Hewitt 1998; Schuster et al. 2002; Geertsema et al. 2006; Runqiu 2009). Several of the largest nonvolcanic landslides in Fig. 8 were triggered by large earthquakes, such as the ~ 2-km^3 Usoi Dam rock slide, Tajikistan (1911), associated with a $M_s = 7.6$ earthquake (Schuster and Alford 2004) and the ~ 0.1-km^3 Diexi landslide dam, China (1933), associated with a $M = 7.5$ earthquake (Dai et al. 2021). Large tectonic earthquakes, however, do not necessarily produce failures that dissect deeply into a mountain (see later discussion of VDA source areas). Nevertheless, all these destabilizing and triggering factors could play a role in the failure of volcano slopes.

Large failures on volcanoes without an accompanying known eruption are similar in size to large landslides on nonvolcanic mountains (Fig. 8). Some of these failures were co-seismic, such as the ~ 0.034-km^3 Ontake collapse (1984) associated with a $M = 6.8$ earthquake (Endo et al. 1989). As with many other flank collapses not involving the core of the volcano, this landslide did not excavate deeply into the edifice (Endo et al. 1989; Voight and Sousa 1994), in contrast to the deep failure at Bandai (1888 CE) that was associated with a phreatic eruption (Sekiya and Kikuchi 1889) (Fig. 9). About two-thirds of the historical non-eruptive volcanic edifice collapses were < 0.1 km^3 in size (Fig. 8); many were relatively shallow flank failures. The largest (0.34 km^3), at Unzen-Mayuyama (1792 CE), transpired in association with an estimated $M = 6.4$ earthquake (Sassa et al. 2016) while a nearby vent (Fugen-dake) located ~ 5 km away in the volcanic complex was in eruption (Ota 1969). It is possible that internal stress changes induced by magmatic and (or) hydrothermal fluids from this nearby eruption could have influenced collapse size. Hot fluids issued from the scarp following failure (Ota 1973). The effects from smaller edifice failures (< 0.01 km^3) not shown in Fig. 8 can certainly be hazardous: for example, they can over run nearby towns and

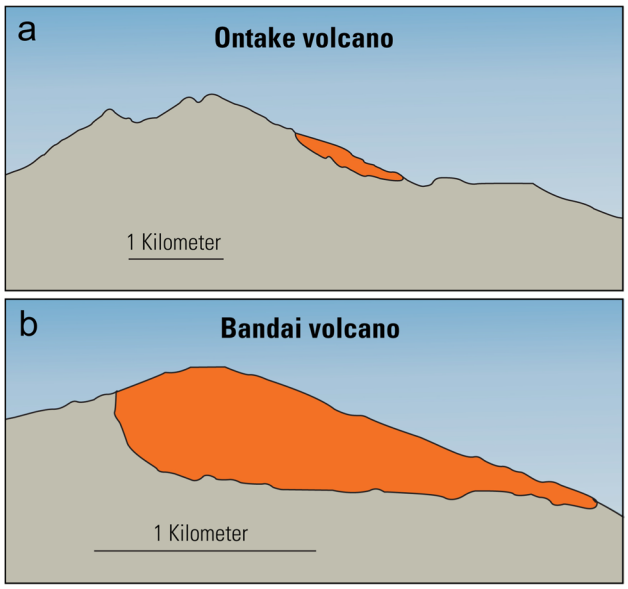

Fig. 9 Cross sections of two volcano flank landslides in Japan. **a** Ontake (1984 CE) triggered without eruption by a M 6.8 earthquake (Okusa et al. 1987). **b** Bandai (1888 CE) associated with a phreatic eruption (Sekiya and Kikuchi 1889). Figures from Siebert et al. (2019)

generate far-traveled tsunamis. Smaller failures, such as the 2012 avalanche at Te Maari in New Zealand (~ 0.0008 km^3), can also be triggered by earthquakes (Procter et al. 2014).

The other two categories in Fig. 8 show events associated with magmatic or exclusively phreatic eruptions. Many of these failures sculpted deeply into an edifice and are deeper and larger than non-eruptive collapses (Fig. 9 and later discussion of VDA source areas). Large non-eruptive collapses may have occurred in the prehistoric record, although evidence for an eruption accompanying such large collapses may be removed or hidden. Relatively few studies of collapse events note the character or existence of associated eruptive activity (Dufresne et al. 2021a). Large, apparently non-eruptive collapses prior to 1500 CE include the > 10-km^3 failure of Gede volcano in Indonesia (Belousov et al. 2015), some in Kamchatka such as the 4–6-km^3 1.2-ka collapse of the extinct Kamen volcano (Ponomareva et al. 2006), and the 18–22-km^3 8.6-ka VDA deposit at Meru volcano in Tanzania (Delcamp et al. 2016a).

We focus below on factors at subaerial stratovolcano edifices that might promote larger, deeper failures atypical of landslides on other mountains. Conditions that can substantially modify the strengths or stresses at depth could promote a series of large retrogressive failures into an edifice core. These conditions, important to slope-stability analyses, include (1) edifice structure, (2) rock strength, (3) pore-fluid effects, and (4) dynamic triggers. Many of these elements are interrelated and can vary over time within an edifice.

Edifice structure

Topography and internal structural features commonly exert a primary influence on the size and geometry of slope failures. Gravitational forces acting on the mass between the ground surface and the landslide slip surface are a major driver of instability. Steep slopes commonly drive instability, but in themselves do not necessarily lead to deeper, larger failures. Internal structures can vary the distribution of loading, create strength discontinuities, and modify pore-fluid flow patterns within an edifice. Here, we examine structural factors that could reduce the stability of crucial regions within an edifice and predispose an edifice to larger, deeper collapses.

Regional tectonic stress fields can influence the growth of edifices, the direction of flank collapses, and potential pathways for destabilizing magma intrusions, as documented in many studies (e.g., Nakamura 1977; Siebert 1984; Delaney et al. 1986; Lagmay and Valdivia 2006; Macías et al. 2010; Paguican et al. 2012; Schaefer et al. 2013; Tibaldi 2015; Delcamp et al. 2016b). In particular, active tectonic faulting under or within an edifice can promote large-scale collapse. Field observations and analog physical models reveal that fault type, geometry, displacement, and motion can affect stability (van Wyk de Vries and Merle 1996; Lagmay et al. 2000; Vidal and Merle 2000; Norini and Lagmay 2005; Norini et al. 2008; Wooller et al. 2009; Paguican et al. 2014). In analog experiments, subsurface faulting can create surface bulging and landslides of different sizes. For example, larger unstable volumes are generated with basal edifice faults located farther from the central axis of the volcano (Wooller et al. 2009).

Other structural conditions can modify the stresses within an edifice and potentially lead to large-scale collapses. Gravitational spreading typically transpires when a volcano is constructed on a base of weak and (or) ductile rocks, such as poorly lithified sediments or unconsolidated pyroclastic deposits (e.g., Borgia 1994; van Wyk de Vries and Borgia 1996; Borgia et al. 2000; Tibaldi et al. 2005; van Wyk de Vries and Davies 2015). The effects of spreading can be complex (van Wyk de Vries and Matela 1998; Byrne et al. 2013), and relatively slow spreading generally leads to gentler slopes and thus can help stabilize an edifice (van Wyk de Vries and Borgia 1996; Andrade and van Wyk de Vries 2010). However, observations at some volcanoes, including Mombacho (Nicaragua), Iriga (Philippines), Socompa (Chile/Argentina), and Parinacota (Chile/Bolivia), indicate that a weak base may have facilitated large-scale collapse (van Wyk de Vries and Francis 1997; van Wyk de Vries et al. 2001; Clavero et al. 2002; Shea et al. 2008; Paguican et al. 2012). Numerical models reveal that spreading can modify internal edifice stresses (Fig. 10) (van Wyk de Vries and Borgia 1996; Norini et al. 2010), and analog models demonstrate that certain spreading conditions, such as outward flow of a weak, low viscosity base or the presence of a weak edifice core, can promote deeper collapses (Merle and Borgia 1996; Cecchi et al. 2004; Delcamp et al. 2008; Andrade and van Wyk de Vries 2010; Kervyn et al. 2014).

A related condition is flank instability promoted by a weak base that slopes under an edifice (e.g., Wooller et al. 2004; Carrasco-Núñez et al. 2006; Norini et al. 2010; Murray et al. 2018) (Fig. 10). Some observed large collapse scars are oriented in the direction of the regional slope, indicating that sloping bases may play a widespread role in predisposing large-scale instability (e.g., Francis and Wells 1988; Vallance et al. 1995; Carrasco-Núñez et al. 2006; Siebert et al. 2006). Shallow intrusion of magma, as occurred during the 1980 Mount St. Helens collapse, can greatly transform edifice topography and internal structure, and is discussed further in the "Dynamic triggers" section below.

Lateral edifice collapse itself can cause major perturbations of stress regimes within volcanoes and modify volcano plumbing systems, petrology and eruptive style (de Silva et al. 1993; Siebert et al. 2004; Ginibre and Wörner 2007; Manconi et al. 2009), and locations of post-collapse vents and fissures (McGuire and Pullen 1989; Tibaldi 2003; Maccaferri et al. 2017).

Rock strength

Material strength is a fundamental factor governing slope instability at any scale. Volcanoes are commonly

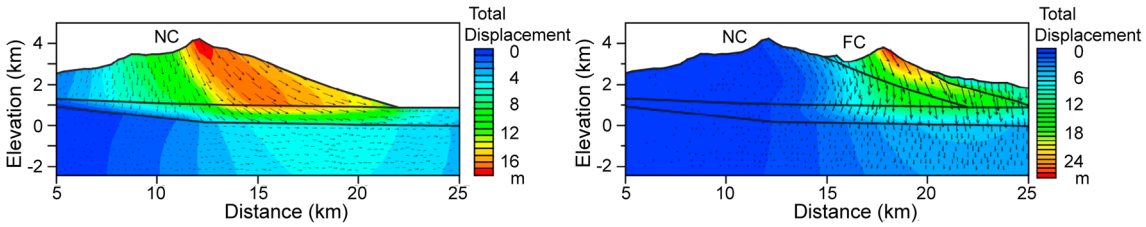

Fig. 10 Cross sections showing simulated two-dimensional (2D) elastoplastic displacements at two edifices with different subsurface structures (faults in black) and weaker basement rocks at the Colima volcanic complex, Mexico. NC, Nevado de Colima volcano; FC, Fuego de Colima volcano. Modified from Norini et al. (2010)

composed of a wide variety of earth materials emplaced during edifice construction, including lava domes as well as essentially slope-parallel lava flows, pyroclastic-flow, and tephra-fall deposits (Fig. 6). Edifices are intruded by dikes, sills, and cryptodomes, and the edifice base may rest on different materials (see previous section). These highly heterogeneous, layered, jointed, and fractured materials can exhibit a wide range in properties (porosity, density, elastic parameters) as well as strengths (compressive, tensile, shear), as documented in many studies (e.g., Watters et al. 2000; Thomas et al. 2004; Apuani et al. 2005a; Apuani et al. 2005b; Moon et al. 2005; Schaefer et al. 2015a; Heap and Violay 2021; Heap et al. 2021c; Kendrick et al. 2021; Lavallée and Kendrick 2021). Many of these studies have focused on scaling up rock properties derived from small samples to values appropriate for an edifice, through methods such as rock mass rating (RMR) or geologic strength index (GSI) rating. Although most studies focus on rocks accessible on the surface of an edifice, the distribution of strength deeper within an edifice is critical to large-scale collapse; thus, some studies have assessed rock strengths from exposed crater walls (e.g., Moon et al. 2005; del Potro and Hürlimann 2009; Reid et al. 2010b) or exhumed systems (Mordensky et al. 2018). Volcanoes have additional dynamic processes that can, over time, reduce rock strength, including mechanical and chemical alteration from an active hydrothermal system or fracturing from thermal or cyclic mechanical stressing.

The circulation of hot fluids and gases within edifice or dome rocks can promote mineral dissolution, precipitation, and (or) replacement. Hydrothermal processes vary in time and space throughout an edifice but can progressively weaken rocks. Acid-sulfate hydrothermal alteration that creates intermediate or advanced argillic mineral assemblages (Meyer and Hemley 1997; Zimbelman et al. 2005; John et al. 2008), in particular, can lead to increased porosity, development of weak clay minerals, and significant reductions in strength (Watters et al. 2000; del Potro and Hürlimann 2009; Pola et al. 2012, 2014; Wyering et al. 2014; Heap et al. 2015; Farquharson et al. 2019; Mordensky et al. 2019; Frolova et al. 2021). If sufficiently pervasive or affecting a potential failure surface, these strength reductions can promote edifice or dome instability (e.g., López and Williams 1993; Reid et al. 2001; Cecchi et al. 2004; Zimbelman et al. 2004; Procter et al. 2014; Ball et al. 2015; Ball et al. 2018; Heap et al. 2019; Heap et al. 2021a; Heap et al. 2021b) (Fig. 11).

The effects of hydrothermal alteration, however, can be complex and not all forms weaken rock — some types of alteration, such as silicification, do not create weak clay minerals and may reduce rock porosity by precipitating minerals. In these situations, alteration may increase strength (Watters and Delahaut 1995; Wyering et al. 2014; Frolova et al. 2015; Mordensky et al. 2018; Heap et al. 2020; Heap and Violay 2021). Geophysical surveys using magnetic and electrical resistivity methods have revealed both extensive and limited altered zones in volcano edifices (e.g., Finn et al. 2001; Finn et al. 2007; Gonzales et al. 2014; Rosas-Carbajal et al. 2016; Usui et al. 2017; Finn et al. 2018; Ghorbani et al. 2018; Kereszturi et al. 2020; Miller et al. 2020; Heap et al. 2021b; Peterson et al. 2021). Some edifices, such as Mombacho (Shea et al. 2008), have both deeper collapse scars in more extensive hydrothermally altered rocks and shallower scars associated with less abundant altered rocks.

Hydrothermally altered rocks are not required for large-scale failure. Notably, some altered clasts were contained in the 1980 Mount St. Helens VDA deposit (Glicken 1996); however, the rocks hosting the primary slip surfaces were essentially unaltered (Reid et al. 2010b). Although many debris-avalanche deposits contain hydrothermally altered rocks (e.g., Siebert 1984; Carrasco-Nuñez et al. 1993; Vallance and Scott 1997; Norini et al. 2020; Roverato et al. 2021a), weakening from hydrothermal alteration needs to be present in crucial locations to play a role in destabilizing large regions. Many volcano edifices have small, localized regions of hydrothermal alteration, commonly near fumaroles, but these typically would be insufficient to destabilize an edifice flank.

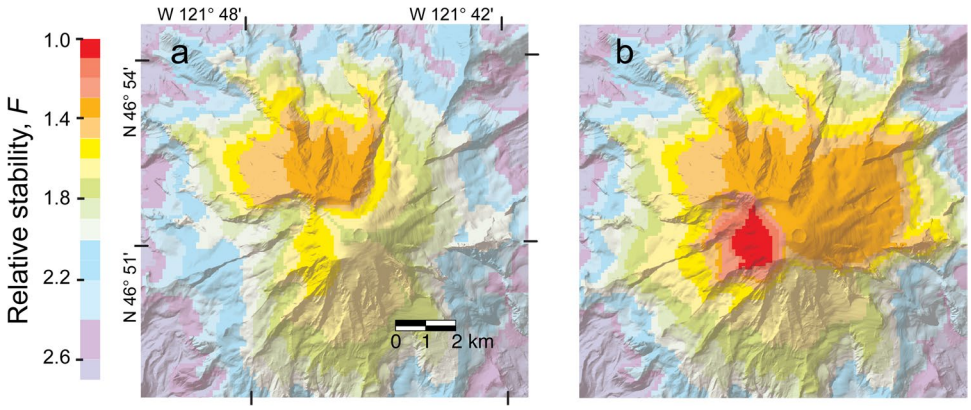

Fig. 11 Computed three-dimensional (3D) slope stability draped on shaded relief of Mount Rainier, Washington, USA. **a** Image of relative slope stability using homogeneous rock strength. **b** Image of relative slope stability using inferred subsurface distribution of weaker hydrothermally altered rocks. Instability (red) is focused on the west flank, a region underlain by highly altered rocks. Modified from Reid et al. (2001)

Magma intrusion can weaken rocks by thermal and (or) mechanical stressing, potentially affecting broad areas within an edifice. Laboratory experiments document that thermal stresses in volcanic rocks can sometimes lead to microfracturing and strength reduction (e.g., Kendrick et al. 2013; Schaefer et al. 2015a; Browning et al. 2016; Heap and Violay 2021). Underlying basement rocks may be weakened by heating as well, thereby promoting long-term deformation of an edifice (Heap et al. 2013). Cyclic stressing of volcanic rocks, as might occur during repeated intrusions, or rapid unloading as might have transpired during prior flank collapses, can also reduce strength (Kendrick et al. 2013; Schaefer et al. 2015a). Magmatic intrusion into an edifice could generate locally weakened fault gouge zones along the intrusion contacts (e.g., Donnadieu and Merle 2001; Cashman et al. 2008; Moore et al. 2008; Kendrick et al. 2012; Pallister et al. 2013: Mordensky et al. 2018), and incipient flank failures may progressively reduce strength through active shearing (Reid et al. 2010b). Thus, dynamic processes can weaken rocks and promote instability over broad regions in crucial zones within an edifice.

Pore-fluid effects

Fluids in pores or fractures are an extremely important destabilizing factor for many landslides, and undoubtedly play a large part in some edifice flank failures that have not been associated with eruption. For example, the Casita, Nicaragua, flank VDA in 1998 was triggered during intense rainfall from Hurricane Mitch (e.g., Kerle et al. 2003; Scott et al. 2005; Devoli et al. 2009). The presence of fluids in a slope can modify the weight distribution and thereby change gravitationally induced stresses. Pore fluids can reduce the strength of clays due to their mineralogy and structure. In many situations, however, the dominant destabilizing effect is from locally elevated pore-fluid pressures that reduce frictional resistance; this modifies the effective stresses acting on a failure surface and can induce failure (Terzaghi 1950; Lambe and Whitman 1969). Moreover, fluid saturated rocks can promote the transition from debris avalanche to debris flow or lahar, as inferred from various field settings (e.g., Voight et al. 1983; Vallance and Scott 1997; Capra and Macías 2000; Capra et al. 2002; Tost et al. 2014; Delcamp et al. 2016b). Thus, the magnitude and distribution of pore-fluid pressures within an edifice can be crucial to instability.

Landslides triggered by infiltrating water or from gravity-driven groundwater flow tend to be relatively shallow, in part because the ratio of shear to normal stresses affecting frictional resistance on a slip surface tends to be largest near the ground surface (e.g., Iverson and Reid 1992; Reid and Iverson 1992; Reid 2004). The presence and distribution of fluids within a volcano is undoubtedly complex, given the heterogeneous materials within an edifice (e.g., Sanford et al. 1995; Aizawa et al. 2009; Delcamp et al. 2016b; Ball et al. 2018), and a variety of driving forces affecting fluid flow including gravity as well as thermal and mechanical stressing conditions induced by nearby magma (e.g., Elsworth and Voight 1995, 1996; Reid 2004). Little data exist about fluid pressures within active stratovolcanoes, but geophysical surveys have revealed varied distributions of saturated rocks (Finn et al. 2001, 2007, 2018; Revil et al. 2004; Aizawa et al. 2009; Peterson et al. 2021). Numerical simulations of coupled groundwater and heat flow indicate that water tables recharged by rain and snowmelt might exist lower within an edifice (Hurwitz et al. 2003; Ball et al. 2018), leading to large unsaturated regions in the upper edifice.

At some volcanoes, groundwater can occur higher in an edifice, as suggested by small phreatic eruptions, for example, at Mount St. Helens in 1980, and indicated by observations of upper flank groundwater expulsion, for example, at Nevado del Huila, Peru, in 2007 (Worni et al. 2012; Johnson et al. 2018). Hydraulic properties such as porosity and permeability vary extensively in volcanic rocks, as noted in many studies (e.g., Wright et al. 2009; Farquharson et al. 2016; Lamur et al. 2017; Heap et al. 2018; Farquharson et al. 2019; Revil et al. 2020; Heap and Violay 2021). Lower permeability rock layers within a slope can produce perched water tables resulting in locally elevated, and potentially destabilizing, pore pressures (e.g., Rulon and Freeze 1985; Sruoga et al. 2004; Delcamp et al. 2016b; Ball et al. 2018) (Fig. 12). Moreover, hydrothermally altered rocks with greater porosity and clay minerals can hold more water, potentially enhancing the transition from debris avalanche to debris flow. Coupled numerical models also demonstrate that heating from deep or shallow magma tends to increase pore-fluid pressures deep within an edifice (e.g., Hurwitz et al. 2003; Reid 2004; Ball et al. 2018; Collard et al. 2020; Heap et al. 2021a). Thus, elevated pore pressures at depth could destabilize deeper regions.

Dynamic triggers

The relatively slow, incremental pre-conditioning processes described above might eventually lead to large-scale flank collapse. Such processes can significantly modify internal stresses or strength distributions and thereby promote larger, deeper failures. Moreover, destabilizing processes common on other mountains (e.g., infiltration of groundwater from storm events) could contribute to long-term instability. However, the 1980 Mount St. Helens collapse and other historical collapses, such as Unzen-Mayuyama (1792 CE), Bandai (1888 CE), Bezymianny (1956 CE), and Shiveluch (1964 CE), have been accompanied by more dynamic triggers, such as seismic shaking or volcanic unrest. Inertial forces from tectonic or volcanic seismicity could play a role in instigating failure (e.g., Voight et al. 1983; Voight and

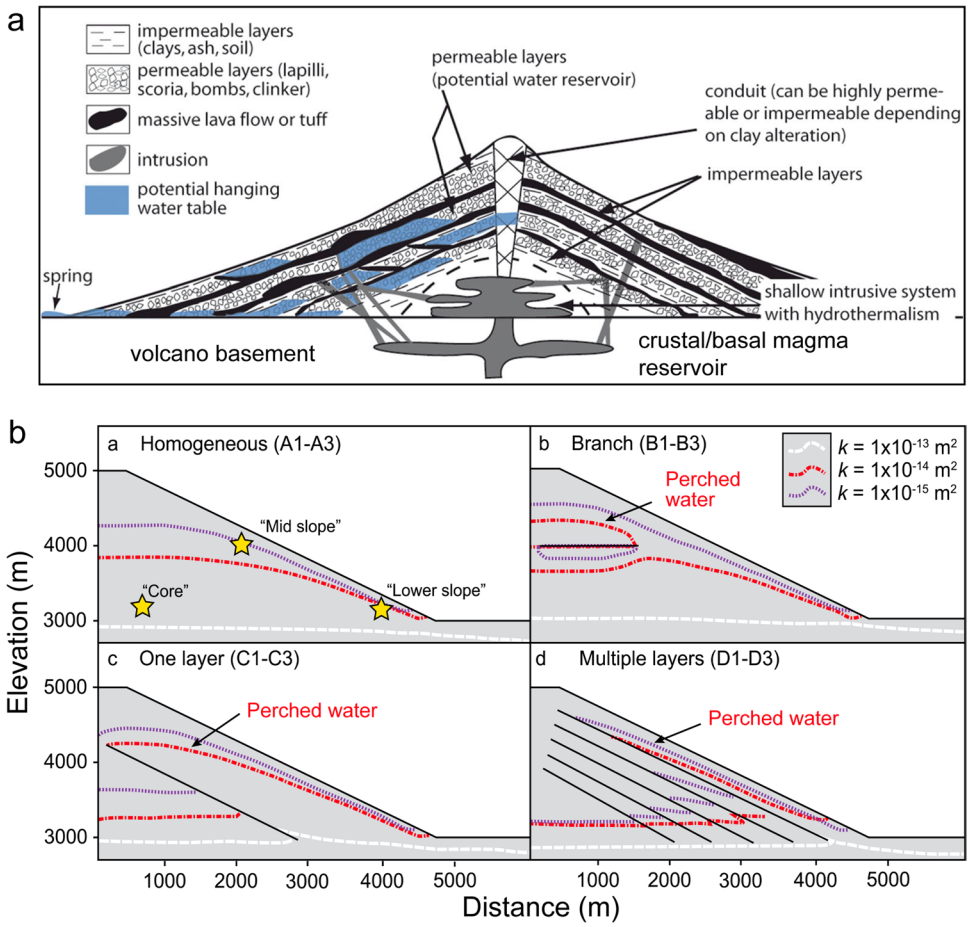

Fig. 12 Cross sections showing possible groundwater configurations within stratovolcanoes. **a** Schematic representation showing perched or hanging water tables on lower permeability layers. Modified from Delcamp et al. (2016b). **b** Simulated gravity-driven groundwater tables in four different scenarios with either homogeneous rocks, a low permeability branch (horizontal layer), a low permeability sloping layer, or multiple low permeability sloping layers. Different water tables (colored lines) represent simulations with different surrounding rock permeability (k). Lower overall permeability leads to higher elevation water tables. Modified from Ball et al. (2018)

Elsworth 1997; Procter et al. 2014), although as noted above, earthquake-induced landslides themselves rarely result in the very deep scars associated with large-scale flank collapses. Subsequent retrogression of an initial failure, as ensued at Mount St. Helens and inferred at other historical collapses (Fig. 13), promotes the development of these deep-seated scars (Voight 2000).

Edifice failures are often associated with volcanic unrest (e.g., Waythomas 2012; Acocella 2021; Roverato et al. 2021a). Very large and deep historical flank failures have most frequently been associated with some type of eruption, either magmatic, phreatomagmatic, or phreatic, and therefore have transpired with either shallow (within the edifice) or deeper magmatic activity (Table 1 and Fig. 8). Shallow intrusions into an edifice have been noted with many collapses, including Bezymianny, Lamington, Mount St. Helens, and Soufrière Hills (Gorshkov 1959; Voight et al. 1983; Siebert et al. 1987; Belousov et al. 2007, 2020). Flank failure in these situations commonly leads to exposure of the intrusion and eruption of juvenile magma, as occurred at Mount St. Helens, Lamington, and Bezymianny. Such shallow magma intrusions can create many destabilizing conditions, including topographic bulging and edifice oversteepening, the development of large grabens and internal faults, and shearing and weakening of rocks in the deformed zones, all of which occurred at Mount St. Helens (discussed above). Physical analog modeling studies as well as computational slope-stability and deformation analyses highlight the importance of these dynamic destabilizing influences (e.g., Voight et al. 1983; Voight and Elsworth 1997; Donnadieu and Merle 1998, 2001; Reid et al. 2000; Donnadieu et al. 2001; del Potro et al. 2013). In addition to intrusions, dome extrusion onto a weak hydrothermally altered edifice can instigate large landslides that incorporate both the dome and the underlying edifice, as occurred at Tutupaca, Peru (Samaniego et al. 2015; Valderrama et al. 2016; Mariño et al. 2021).

Magma pressure from a shallow intrusion exerted on edifice rocks might contribute to instability, although modeling studies vary on the relative importance of this effect. Some indicate that the mechanical (non-pore pressure) effects from magmatic pressures in an intrusion are localized and unlikely to be the dominant factor controlling large-scale instability (Elsworth and Voight 1995; Iverson 1995). Other studies illustrate marked destabilizing effects from magmatic pressures ("push") within an edifice (e.g., Paul et al. 1987;

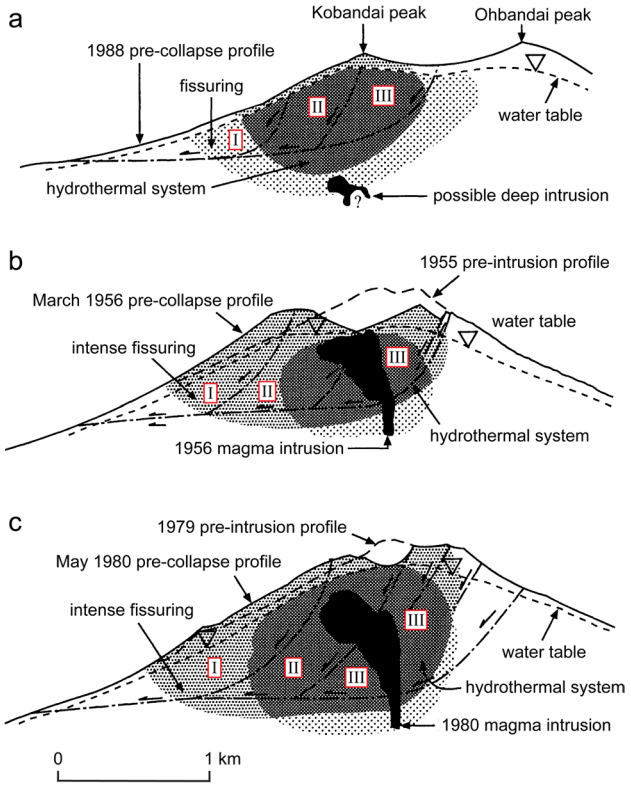

Fig. 13 Schematic cross sections of three large flank collapses on stratovolcanoes associated with phreatic (**a**) or magmatic (**b** and **c**) eruptions. **a** Bandai. **b** Bezymianny. **c** Mount St. Helens. Each collapse is inferred to have three blocks that retrogressively failed in sequence (numerals I, II, and III) resulting in a large, deep scar. Modified from Voight (2000)

McGuire et al. 1990; Voight and Elsworth 1997; Lundgren et al. 2004; Apuani and Corazzato 2009).

Heating of pore fluids or degassing from subsurface magma can lead to Bandai-style phreatic explosions or eruptions without a magmatic component (e.g., Barberi et al. 1992; Germanovich and Lowell 1995; Stix and de Moor 2018; Takahashi and Yahata 2018). Shallow magma intrusion into an edifice can induce mechanical and thermal stressing (Elsworth and Voight 1995; Kendrick et al. 2013), but heating of pore fluids or gases near the intrusion can play a more extensive role in destabilizing an edifice (e.g., Elsworth and Voight 1995; Day 1996; Reid 2004) (Fig. 14). Fluid pressurization results from heating a fluid or gas within restricted pores (Delaney 1982; Mace and Smith 1987); in an edifice, this process is transient, as elevated pressures eventually dissipate. As with other forms of groundwater flow within an edifice, hydraulic properties, including porosity, compressibility, and permeability, greatly control the degree of thermal fluid pressurization (e.g., Reid 2004; Ball et al. 2018; Heap et al. 2021a). Higher permeability rocks can rapidly dissipate pressures whereas lower permeability rocks retain elevated pressures. Pressurization is largest near a heat source, and propagates outward over time; thus, there may be a time lag between magma movement and destabilizing effects in an edifice (Reid 2004), but fluid pressures travel much faster than thermal effects (Delaney 1982). Pressurized gases within an extruded lava dome may also induce failure (e.g., Voight and Elsworth 2000; Elsworth and Voight 2001; Simmons et al. 2005). Deeper fluid pressurization could foster failure retrogression following the unloading from an initial shallower failure.

Forecasting and monitoring potential collapse

Large edifice collapses are much less frequent than volcanic eruptions. The lack of well-studied historical collapse events as well as the complexity of volcanoes can make accurately forecasting the size, location, and timing of collapse events challenging. Prior to volcanic unrest, assessments commonly rely on understanding past collapse events at a particular edifice or at one with similar conditions. Geotechnical-based approaches have proven useful in understanding the causes of specific failure events, such as at 1980 Mount St. Helens (e.g., Voight et al. 1983; Paul et al. 1987; Reid et al. 2000, 2010b; Donnadieu et al. 2001). This back-analysis approach has been applied to other previous edifice collapses, such as White Island (Moon et al. 2005).

Forward-looking, scenario-based assessments of potential edifice collapses using limit-equilibrium slope-stability analysis have been performed at volcanoes, including Augustine Volcano, Alaska (Reid et al. 2010a); Mount Baker, Washington (Finn et al. 2018); Volcán de Colima, Mexico (Borselli et al. 2011); Iliamna Volcano, Alaska (Peterson et al. 2021); Mount Rainier, Washington (Reid et al. 2001); Stromboli, Italy (Apuani et al. 2005a; Apuani et al. 2005b; Schaefer et al. 2019; shown in Fig. 15); and Teide, Tenerife, Canary Islands (del Potro et al. 2013). Continuum or discrete deformation modeling of internal stresses and strains has been applied to assess potential collapses at other volcanoes, including Citlaltépetl, Mexico (Zimbelman et al. 2004); Etna, Italy (Apuani et al. 2013); Pacaya, Guatemala (Schaefer et al. 2013); Soufrière Guadeloupe (Heap et al. 2021b); and Stromboli (Apuani and Corazzato 2009). These slope-stability studies aim to forecast the size and location of future failures. Nevertheless, their insight is limited by uncertainties in defining structures and material properties deep within an edifice. Moreover, dynamic processes that modify internal stresses or weaken rocks can be difficult to quantify.

For volcanoes undergoing unrest, dynamic processes may hint at possible failure, and monitoring changes over time may enable better forecasting of future unstable behavior. Many techniques for volcano monitoring, such as ground deformation, volcano seismicity, and chemical changes in gas or fluid emissions, rely on changes detected by

Table 1 Documented lateral edifice-failure events since 1500 CE

Volcano	Location	Type	Year	km^3	Fatal	Agent	Type	VEI	References
Anak Krakatau	Indonesia	**Stratocone**	**2018**	0.3	>437	T	**M**	3	Priyanto et al. (2021)
Meager	*Canada*	*Stratocone*	***2010***	*(0.0485)*	-	-	*x*	-	Guthrie et al. (2012)
NW Rota-1	*Mariana Is*	***Stratocone***	***2009***	*0.053*	-	-	***M***	*0*	Chadwick et al. (2012)
Monowai	*Tonga*	***Stratocone***	***2004–2007***	*0.042*	-	-	***M***	*0*	Chadwick et al. (2008)
Bawakaraeng	Indonesia	*Stratocone*	**2004**	0.2	32	A	x	-	Tsuchiya et al. (2009)
Stromboli	*Italy*	*Stratocone*	***2002***	*(0.029)*	-	-	***M***	*2*	Tinti et al. (2006)
Monowai	*Tonga*	***Stratocone***	***2002***	*(0.085)*	-	-	***M***	*0*	Chadwick et al. (2008)
Soufriere Hills	*Montserrat*	***Dome***	***1997***	*0.05*	-	-	***Mb***	*3*	Voight et al. (2002)
Fernandina	Galapagos	*Caldera*	**1988**	0.9	-	-	**M**	2	Chadwick et al. (1991)
Bezymianny	*Kamchatka*	*Dome*	***1985***	*0.05*	-	-	***Mb***	*3*	Melekestsev (2006)
Ontake	*Japan*	*Stratocone*	***1984***	*0.034*	-	-	*x*	-	Endo et al. (1989)
St. Helens	Washington	**Stratocone**	**1980**	**2.5**	57	P, A, L	**Mb**	**5**	Voight et al. (1981)
Ili Werung	*Indonesia*	***Stratocone***	***1979***	*0.05*	*539*	*A, T*	*x*	-	Yudhicara et al. (2015)
Meager	*Canada*	*Stratocone*	***1975***	*±0.0285*	*4*	*A*	*x*	-	Mokievsky-Zubok (1977)
Shiveluch	Kamchatka	**Dome**	**1964**	**1.5**	-	-	**M**	**4**	Gorshkov and Dubik (1970)
Rainier	*Washington*	*Stratocone*	***1963***	*0.011*	-	-	*x*	-	Crandell and Fahnestock (1965)
Bezymianny	Kamchatka	**Stratocone**	**1956**	0.8	-	-	**Mb**	**5**	Gorshkov (1959)
Lamington	*Papua NG*	***Stratocone***	***1951***	*0.03*	*3000?*	*P*	***M***	***4***	Belousov et al. (2020)
Kliuchevskoi	*Kamchatka*	*Stratocone*	***1945***	*0.05*	-	-	***M***	*3?*	Ponomareva et al. (2006)
Harimkotan	Kurile Is	**Dome**	**1933**	0.5	2	T	**M**	**5**	Belousova and Belousov (1995)
Paluweh	Indonesia	**Dome**	**1928**	n/a	226	T, A	**M**	3	Primulyana et al. (2017)
Mageik	*Alaska*	*Stratocone*	***1912***	*±0.075*	-	-	*x*	-	Griggs (1920)
Hakuba-Oike	Japan	*Compound*	**1911**	0.15	-	-	x	-	Yoshida (2016)
Baker	*Washington*	*Stratocone*	***1891***	*±0.018*	-	-	*x*	-	Scott et al. (2001)
Ritter Island	Melanesia	**Stratocone**	**1888**	**(>2.4)**	3000?	T	**M**	2?	Johnson (1987)
Bandai	Japan	**Stratocone**	**1888**	(0.5)	461	A, P	**P**	**4**	Sekiya and Kikuchi (1889)
Augustine	Alaska	**Dome**	**1883**	0.3	-	-	**M**	**4**	Siebert et al. (1995)
Krakatau	Indonesia	**Stratocone**	**1883**	(<<3.8)	(?)	T, P	**M**	**5**	Camus et al. (1992)
Sinarka	Kurile Is	**Stratocone**	**1878**	0.5?	(?)	A	**M**	**4**	Belousova and Belousov (2011)
Tate-yama	Japan	Stratocone	**1858**	0.2	Many	L	x	-	Nozaki (2015)
Garibaldi Lake	*Canada*	*Stratocone*	***1855–1856***	*0.025*	-	-	*x*	-	Moore and Mathews (1978)
Baker	*Washington*	*Stratocone*	***1845–1847***	*±0.025*	-	-	*x*	-	Scott et al. (2001)
Ararat	Turkey	*Stratocone*	**1840**	0.3	1900	P	**P**	3?	Karakhanian et al. (2002)
Suwanose-jima	Japan	**Stratocone**	**1813**	**>1.0**	-	-	**M**	**4**	Shimano et al. (2013)
Tutupaca	Peru	**Stratocone**	**1802?**	0.7?	-	-	**M**	**4?**	Samaniego et al. (2015)
Unzen	Japan	**Dome**	**1792**	0.34	15,030	T, A	x	-	Ota (1969)
Asama	Japan	**Stratocone**	**1783**	0.14	1491?	A, P, L	**M**	**4**	Tamura and Hayakawa (1995)
Papandayan	Indonesia	**Stratocone**	**1772**	0.14	2957	A	**P**	3	Glicken et al. (1987)
Oshima-Oshima	Japan	**Stratocone**	**1741**	**2.5**	1475	T	**M**	**4**	Satake and Kato (2001)
Augustine	Alaska	**Dome**	**1700?**	0.15	-	-	**M**	?	Siebert et al. (1995)
Nabukelevu	*Fiji*	***Dome***	***1650?***	*>0.1?*	-	-	***M***	*?*	Cronin et al. (2004)
Callaqui	Chile	**Stratocone**	**1630?**	<0.7	-	-	**M**	?	Polanco and Naranjo (2008)
Chaos Crags	California	**Dome**	**1650?**	0.15	-	-	x	-	Crandell et al. (1974)
Komagatake	Japan	**Stratocone**	**1640**	**1.55**	700	T	**Mb**	**5**	Yoshimoto and Ui (1998)
Augustine	Alaska	**Dome**	**1540?**	0.5	-	-	**Mb**	**4?**	Siebert et al. (1995)
Soufrière	*Guadeloupe*	***Stratocone***	***1530***	*±0.05*	-	-	***M***	*3*	Boudon et al. (2008)
Rainier	Washington	*Stratocone*	**1500?**	0.23	-	-	x	-	Scott et al. (2001)

Events with VDA deposit volumes ≥ 0.1 km^3 in normal font; italicized lines are smaller volumes 0.01–0.1 km^3. Bolded volcano Type entries mark deep-seated failures typically involving the summit and core of the volcano; non-bolded events are shallow, mostly flank failures lower on the edifice. Volume data in parentheses are in situ source area volumes; without parentheses are from deposit volumes. Volume estimates of the 1888 Ritter Island collapse vary widely from a 2.4-km^3 shallower volcanic edifice failure surface to a 7.34-km^3 deeper failure surface involving significant submarine substrate (Karstens et al. 2020). **Agent** (cause of fatalities): *A*, avalanche; *L*, lahar; *P*, pyroclastic flow; *T*, tsunami, listed in order of cause of known or inferred number of fatalities. Known tsunami fatalities at Krakatau in 1883 are not listed because, although large-volume submarine VDA deposits have been identified (Camus et al. 1992; Deplus et al. 1995), the number of potential avalanche-related tsunami fatalities is not known. **Type** of collapse: *M*, magmatic eruptions; *Mb*, magmatic eruption with lateral blast; *P*, phreatic eruption; *x*, no eruptive activity. At Unzen volcano in 1792, there was no eruption at the Mayu-yama dome complex where collapse occurred, although neighboring Fugen-dake volcano was erupting. *VEI*, Volcanic Explosivity Index (Newhall and Self 1982). VEIs of 4 or higher are bolded. Frequent historical ice-rock avalanches from Iliamna Volcano are typically from ice-rock interface (Huggel et al. 2007) and are not included. Single reference listed for each deposit focuses on early work pertaining to edifice collapse event. Data updated from Siebert and Roverato (2021) and Dufresne et al. (2021a)

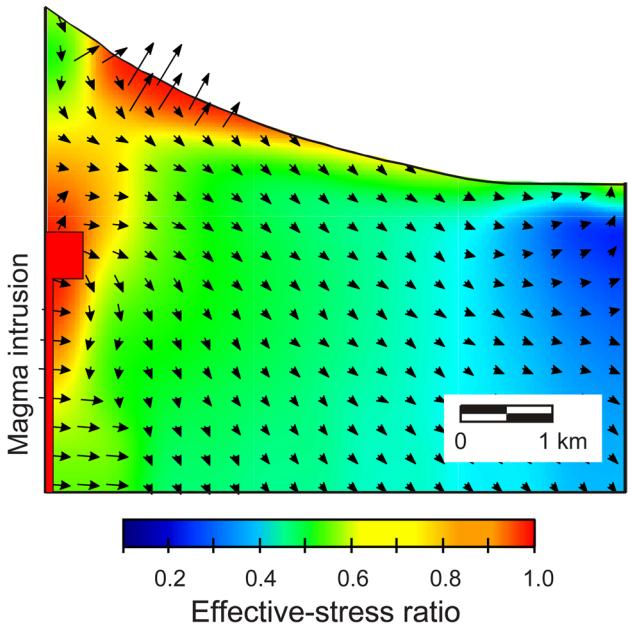

Fig. 14 Simulated effects of coupled pore-fluid pressurization and stress changes induced by the thermal effects of a shallow magma intrusion beneath an edifice. Vectors indicate direction of fluid flow. Higher values of effective-stress ratio indicate more unstable areas. Figure from Reid (2004)

ground-based or remote sensors (e.g., Chouet 1996; Dzurisin 2007; Scarpa and Tilling 2012; Schaefer et al. 2019; Kern et al. 2022). Monitoring can help distinguish shifting conditions that could predispose a flank to collapse. For example, seismic monitoring or repeated seismic tomography can detect shallow magma intrusions that might incite collapse (Patanè et al. 2006; Giampiccolo et al. 2020). Also, repeat aerial geophysical surveys could detect changes in rock properties (such as porosity or strength) due to acidic hydrothermal alteration that might weaken an edifice flank over time (e.g., Rouwet et al. 2014; Miller et al. 2020; Heap et al. 2021a; Kereszturi et al. 2021).

Monitoring ground deformation is one of the fundamental tools in slope-stability forecasting — it can identify specific regions or kinematic elements actively bulging or displacing downslope as well as quantify rates of change that might portend catastrophic failure. Deformation monitoring at edifices commonly focuses on detecting magma movement, understanding magma plumbing systems, and forecasting potential eruptions (e.g., Poland et al. 2006; Dzurisin 2007; Segall 2013; Biggs and Pritchard 2017). Although conventional landslide investigations can use subsurface instruments installed in boreholes to characterize the size and location of a sliding mass, this is rare at volcanoes due to cost and logistical difficulties. Instead, monitoring ground-surface deformation at edifices is the norm. A myriad of active tectonic, hydrothermal, and magmatic processes can affect edifice surface deformation (Poland et al. 2006) and hinder precise interpretation of observations. Persistent deep-seated deformation due to spreading or sagging, inflation or deflation from magma movement, surficial mass wasting processes, thermal contraction, compaction, or transient loading from magma extrusion can overprint or combine with flank deformation (e.g., Lanari et al. 1998; Stevens et al. 2001; Lundgren et al. 2004; Lu et al. 2005; Sturkell et al. 2006; Ebmeier et al. 2014; Poland et al. 2017; Schaefer et al. 2017; Ebmeier et al. 2018; Schaefer et al. 2019). Nevertheless, transient surface deformation of a flank or dome has preceded catastrophic collapse, as demonstrated at Mount St. Helens, Bezymianny, Lamington, and Soufrière Hills (e.g., Gorshkov 1959; Lipman et al. 1981; Voight 2000; Voight et al. 2002; Belousov et al. 2020).

There are a wide variety of techniques for monitoring and detecting geodetic changes over time in the surface of an edifice. They range from repeat campaign-style, ground-based techniques using leveling or Global Positioning System (GPS)/Global Navigation Satellite System (GNSS) surveys (e.g., Nishi et al. 1999; Murray and Wooller 2002; Dzurisin 2007; Clarke et al. 2013) to photogrammetry including structure-from-motion techniques (Baldi et al. 2008; Diefenbach et al. 2012), lidar (e.g., Neri et al. 2008; Favalli et al. 2009; Okyay et al. 2019), or satellite-based interferometric synthetic aperture radar (InSAR) (Wicks et al. 2002; Solaro et al. 2010; Ebmeier et al. 2013; Pinel et al. 2014; Bonforte and Guglielmino 2015; Froger et al. 2015; Schaefer et al. 2015b, 2019; Di Traglia et al. 2018). Some of these techniques are not continuous, for example, ground-surface changes detected by satellite-based InSAR depend on the frequency (often days to weeks) of satellite passes over an edifice. Future satellite capabilities with higher frequency passes could greatly improve this monitoring technique. Better temporal resolution of changes can be recorded using fast-repeat methods such as ground-based InSAR (e.g., Wadge et al. 2005; Macfarlane et al. 2006; Wadge et al. 2008; Intrieri et al. 2013; Nolesini et al. 2013; Di Traglia et al. 2014a; Di Traglia et al. 2014b; Bonforte et al. 2016; Di Traglia et al. 2018; Kuraoka et al. 2018; Schaefer et al. 2019) (Fig. 15) or more continuous GPS/GNSS techniques (e.g., Segall et al. 2001; Bartel et al. 2003; Dzurisin 2003; Biggs et al. 2010; Hotta et al. 2016; De Guidi et al. 2018).

Trilateration using electronic distance measurements and differences between aerial photographs were used at Mount St. Helens in 1980 (Lipman et al. 1981; Moore and Albee 1981). Given their large extent, potential hazards, and difficult ground access, edifices are now commonly monitored with GPS/GNSS and (or) satellite-based InSAR techniques. To understand the amounts and rates of downslope edifice flank motion, however, standard analysis techniques such as vertical elevation differences between sequential DEMs

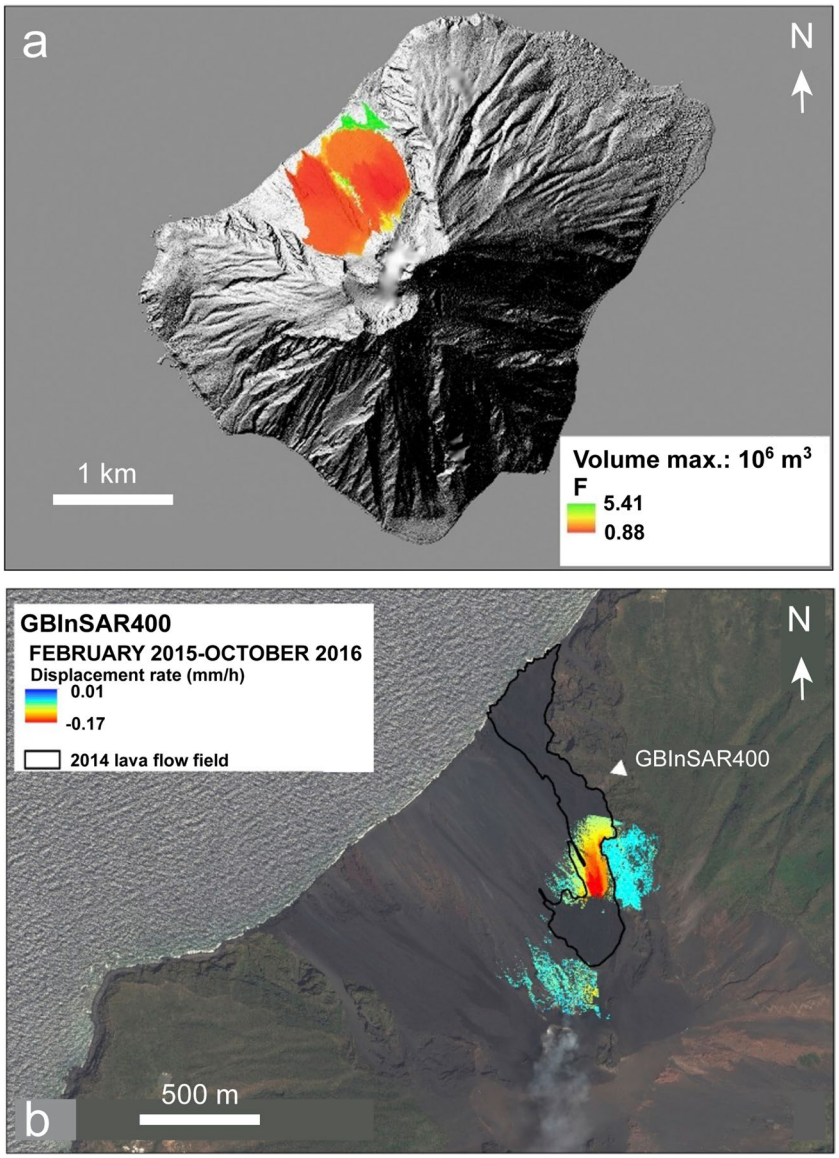

Fig. 15 Examples of slope-stability analysis and ground-based InSAR monitoring for potential collapse at Stromboli, Italy. **a** Limit-equilibrium stability results for potential landslides with volumes between 10^5 and 10^6 m^3. Warmer colors (lower *F* values) are less stable. **b** Displacement rates from ground-based InSAR monitoring (February 2015–October 2016) of part of the summit crater. Warmer colors indicate higher rates. Modified from Schaefer et al. (2019)

or changes in line-of-sight (LOS) distances from radar over time may not be sufficient, as they do not track the actual downslope ground motion. Three-dimensional positional changes over time obtained from ground-based GPS/GNSS measurements, InSAR techniques such as permanent scatters or amplitude pixel offset measurements (e.g., Hooper 2008; Crosetto et al. 2016; Schaefer et al. 2017), or a combination of techniques for both spatial and temporal coverage (e.g., Palano et al. 2008; Chen et al. 2017; Wang et al. 2019) can more accurately determine slope displacements from large-scale flank landsliding.

In addition to identifying where a potential slope failure might transpire, deformation monitoring can sometimes provide insights into when slow creeping motion will transition into catastrophic failure. With some landslides, velocity or acceleration thresholds or reciprocal of velocity relations have provided sufficient time to issue warnings or estimate time of failure (e.g., Saito 1965; Salt 1988; Voight 1989; Crosta and Agliardi 2003; Federico et al. 2012; Dick et al. 2015; Loew et al. 2016; Segalini et al. 2018; Intrieri et al. 2019). Such failure forecasting techniques have been applied to volcanic rocks and edifice failures with varying levels of success (e.g., Voight 1989; Murray et al. 1994; Kilburn 2003; Bell et al. 2011a; Bell et al. 2011b; Heap et al. 2011; Hao et al. 2016; Kilburn 2018). In addition, increasing frequency of smaller landslide or earthquake activity may serve as a precursor to a large slide (e.g., Kilburn and Voight 1998; Voight et al. 2002; Di Traglia et al. 2018). However, the reciprocal of velocity approach did not work well at Mount St. Helens (Lipman et al. 1981; Voight et al. 1983). Rapid failure of landslides is a complex process

(Fell et al. 2007), and many slides move and stop without catastrophic movement (e.g., Petley et al. 2002; Rose and Hungr 2007; Intrieri and Gigli 2016); volcanic edifices also can exhibit these mutable behaviors (e.g., Carracedo 1999; Schaefer et al. 2015b; Giampiccolo et al. 2020).

If a stratovolcano edifice experienced a large bulge during a cryptodome intrusion with phreatic explosions (similar to 1980 Mount St. Helens), it would likely be intensely monitored and analyzed. Both perceived hazards and nearby risk would influence monitoring strategies, including temporal and spatial coverage of the ongoing volcanic unrest and deformation. Potential landslide location and collapse magnitude could be well estimated with appropriate monitoring, such as InSAR, and might contribute to a reasonable overall estimate of failure likelihood. However, this can be more challenging in the more common cases without dramatic Mount St. Helens–style deformation or active magmatic involvement. Despite advancements in understanding these high-impact but low-frequency failures, accurately forecasting the timing of failure remains elusive and a topic of investigation.

Characteristics and identification of volcanic debris-avalanche deposits

Although deposits from large-scale lateral collapse of volcanic edifices had been recognized prior to 1980, such as at Bandai in 1888 (Sekiya and Kikuchi 1889) and in the Hawaiian (Moore 1964) and Canary Islands (Bravo 1962), evidence was not widely known and the resulting deposits were attributed to a broad range of primary and secondary volcanic or nonvolcanic processes, including volcanic mudflows or lahars (Siebert and Roverato 2021). The 1980 eruption of Mount St. Helens motivated an increasing number of field studies of these deposits and illuminated their characteristics. VDAs differ from their nonvolcanic counterparts (e.g., Hsü 1975; McSaveney 1978; Plafker and Ericksen 1978; Strom et al. 2019) in that they tend to involve larger volumes with higher fine-grained proportions and have proportionally longer runout distances (Lucas et al. 2014; Dufresne et al. 2021a) (Fig. 16). VDA deposits have some characteristics similar to other volcaniclastic deposits such as those of lahars and pyroclastic flows but have distinguishing attributes ranging from deposit-scale morphological features to textural features at outcrop and microscopic scale. Numerous reviews of the characteristics of VDA deposits include those of Ui et al. (2000) and van Wyk de Vries and Davies (2015) in two *The Encyclopedia of Volcanoes* editions, and papers in Roverato et al. (2021b). A book on volcaniclastic deposits (Pierson et al. in review) includes discussion of VDA deposits and a photo glossary to aid in their distinction.

Unlike debris flows or lahars, VDAs are typically not water-saturated, although the variable amounts of available water within the edifice influences avalanche behavior (Fig. 17). Volcanic edifices can develop localized and evolving saturated regions above low permeability layers that can then contribute to landslide initiation, avalanche transport processes, and post-avalanche dewatering (Delcamp et al. 2016b; Ball et al. 2018). If sufficient water is present within an avalanche body, partial or complete transformation to debris flow/lahar may occur, almost immediately after failure or after the avalanche has traveled some distance (e.g., Voight and Sousa 1994; Scott et al. 1995; Vallance and Scott 1997; Evans et al. 2001; Bernard et al. 2019; Dufresne et al. 2021a; Paguican et al. 2021). Avalanches that liquefy during flow and transform to lahars can flow farther and inundate larger areas.

Although water is the most efficient mechanism for partial fluidization of debris avalanches (Legros 2002), complete

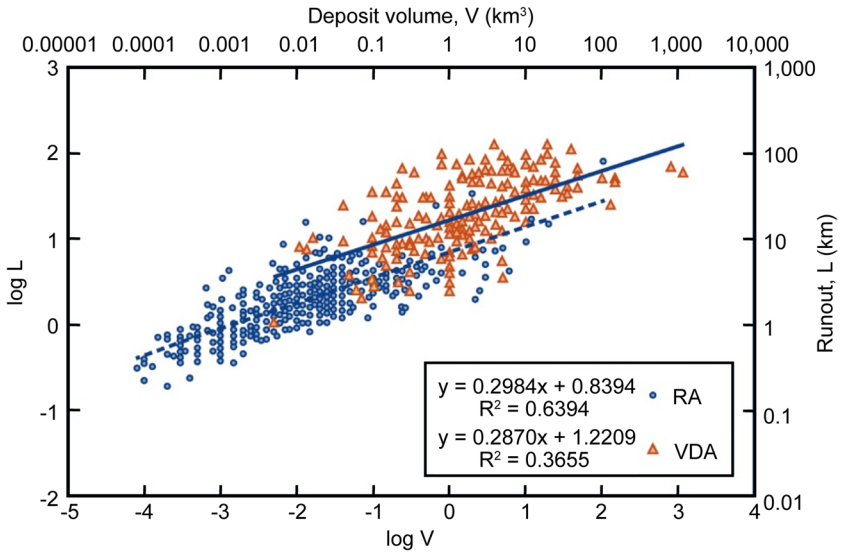

Fig. 16 Comparison of volume (V) versus runout (L) for volcanic and nonvolcanic debris avalanches. Orange triangles, volcanic debris avalanches (VDAs); blue circles, nonvolcanic debris (rock) avalanches (RA). Solid trend lines are for VDAs, dashed lines for nonvolcanic events. Figure modified from Dufresne et al. (2021a)

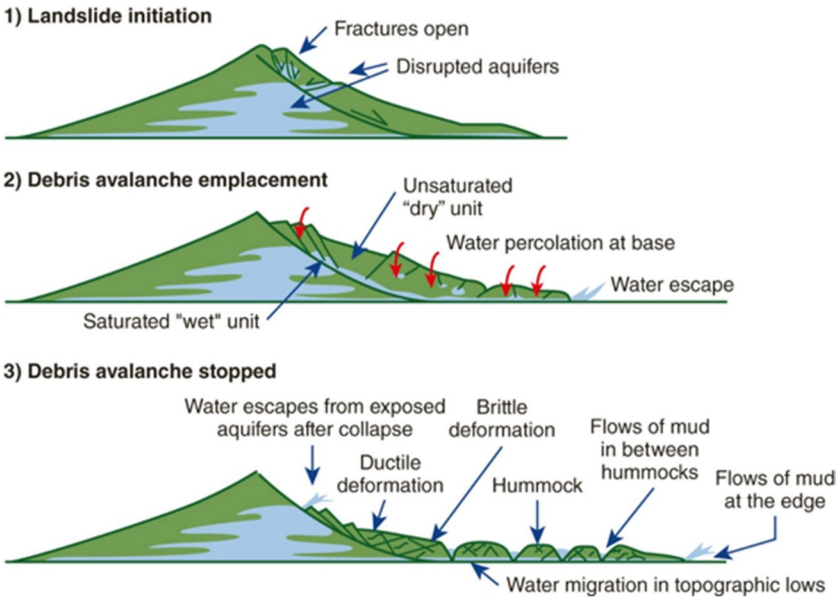

Fig. 17 Model of water migration and influence during landslide initiation and mass transport. Modified from Delcamp et al. (2016b)

water saturation is not an essential component of debris-avalanche mobility (Weidinger et al. 2014). Contingent on the degree to which VDAs truncate zones of groundwater within an edifice, deposits can display both saturated regions with ductile deformation and non-saturated regions with brittle deformation, often in close contact with each other (Delcamp et al. 2016b). Most lateral edifice collapses behave as debris avalanches (Vallance and Iverson 2015), which can be locally saturated but retain sedimentological and textural characteristics of unsaturated flow throughout their extent, including lower clay content, open voids without mud fills, and non-dispersed clast clusters (Siebert et al. 2004; Yoshida and Sugai 2010; Roverarto et al. 2015).

Most VDAs are emplaced at relatively low temperatures, even during magmatic eruptions. At Mount St. Helens in 1980 (Banks and Hoblitt 1981, 1996) and Bezymianny in 1956 (Belousov and Belousova 1998), temperatures were under 100° C. Clement et al. (1993) found paleomagnetic evidence for variable primary temperatures up to 350–580° C in medial parts of a VDA deposit from Volcán de Colima. Pseudotachylites or frictionites, resulting from frictional heating, have been reported at the base of VDA deposits in Peru (Legros et al. 2000; Bernard et al. 2019; Hughes et al. 2020), France (Bernard and van Wyk de Vries 2017), and in the massive mid-Cenozoic megaslides in Utah (Hacker et al. 2014; Biek et al. 2019).

Morphologic evidence

Most VDAs exhibit a characteristic surface morphology with variable proportions of hummocky terrain and areas of closed depressions. Hummocky terrain (discussed below) can dominate deposits but can also be separated by wide areas of topographically subdued terrain formed during emplacement or after the failure event. Deposit geometry can help distinguish VDAs from other volcaniclastic deposits as VDAs are often unusually thick in comparison with saturated volcaniclastic flows such as lahars, hyperconcentrated flows, or volcanic muddy floods. Thickness tends to be greater in valley-confined deposits but can also be significant in broad areas of unconfined deposits.

Source areas and proximal features

The morphology of VDA source areas differs from other volcanic depressions and from those of nonvolcanic landslides (Fig. 18). Lateral edifice failures are often referred to as *sector collapses* although Bernard et al. (2021) noted ambiguities in use of the term. They range in scale from those that involve the summit and core of the volcano and are characteristically deep (to ~ 10^3 m from original ground surface), breached depressions that are open on the downslope side, with relatively flat floors and steep head walls and subparallel side walls, to more shallow and smaller collapses on the flanks of volcanoes (Fig. 9a). Most avalanche source areas are U-shaped in plan view, with somewhat broader breaches than that of a horseshoe shape and are distinct from the narrow breaches typical of erosional depressions (Siebert 1984)—although actual morphology can vary considerably (Bernard et al. 2021). Source area terminology varies widely, including terms such craters or calderas (sometimes with genetic or morphologic modifiers), amphitheaters (to avoid comparisons with calderas), and scars or scarps (Bernard et al. 2021; Siebert and Roverato 2021). Bernard et al. (2021), following terminology of the nonvolcanic landslide community, prefer the use of the term *volcanic landslide*

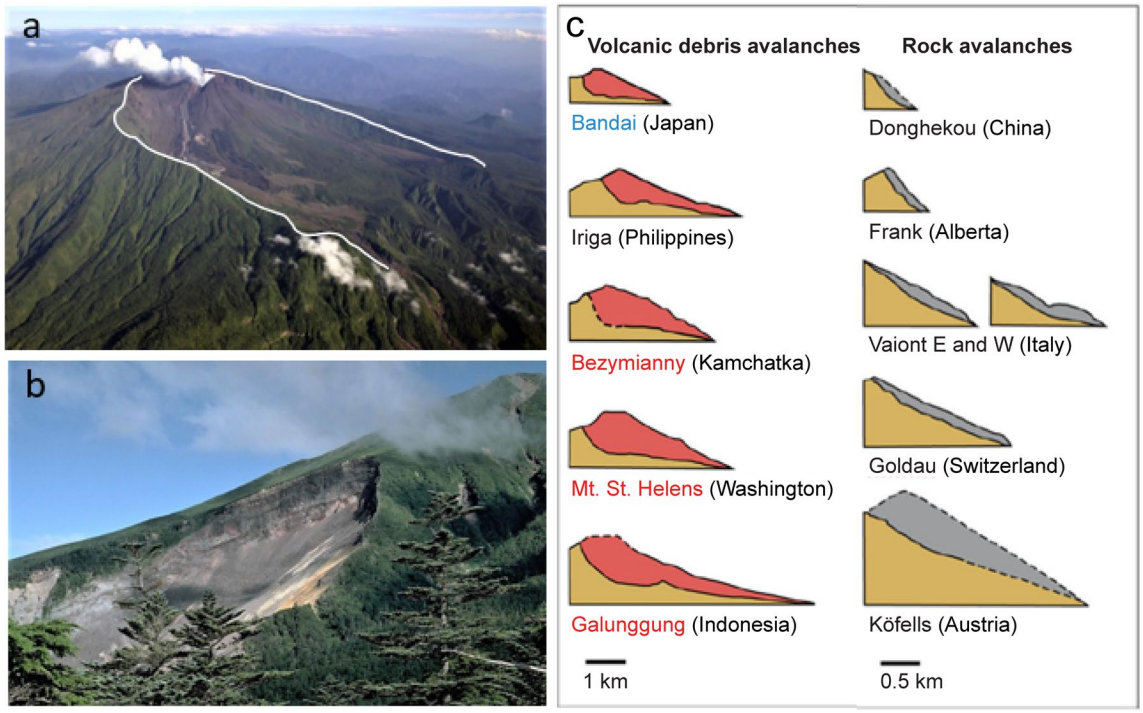

Fig. 18 Edifice collapse scars. **a** Large-scale, ca. 4×6 km collapse scar (white outline) from two Pleistocene collapse events at Reventador volcano in Ecuador involving summit and core of volcano (Johnson et al. 2006). Steam plume rises from the post-collapse cone, whose eruptive products fill much of the originally deep-seated scar. Photo by P. Ramon modified from https://volcano.si.edu/gallery/ShowImage.cfm?photo=GVP-11671. **b** Small-scale, shallow ca. 0.6×1.5 km 1984 flank collapse scar at Ontake volcano in Japan (Endo et al. 1989). Photo by L. Siebert. **c** Differences in source geometry between volcanic edifice and rock slope failures illustrating deeper failures and potentially higher landslide volumes for VDA sources. Volcano profiles and those of Frank and Goldau rock avalanches after Siebert (1984). Additional rock avalanche profiles from Donghekou (Qi et al. 2011), Vaiont (Dykes and Bromhead 2018), and Köfels (Prager et al. 2009). Note difference in scale between the two slope failure types (volcanic are larger). Volcano name font colors show failures associated with magmatic eruptions (red), phreatic eruptions (blue), and non-eruptive events (black). **c** Modified from Dufresne et al. (2021a)

scar for these features. These failure scars are commonly partially or completely filled by the products of post-avalanche eruptions, and at many volcanoes the VDA deposits themselves are the only evidence for lateral edifice failure.

During failure, large segments of the volcanic edifice may slide relatively short distances without disaggregating into a debris avalanche. Reiche (1937) described these features at nonvolcanic landslides, referring to them as *toreva blocks* after the Toreva landslide in Arizona. They represent remnants of the initial edifice failure block and commonly display rotational, backward dipping structures as they slide, tilt, and rotate along listric faults (e.g., Andrade and van Wyk de Vries 2010; Paguican et al. 2014, 2021; Dufresne and Geertsema 2020). At Socompa volcano (Francis et al. 1985; Wadge et al. 1995; Grosse et al. 2022), backward-tilting toreva blocks up to 2.5 km in length and 11.5 km^3 in volume lie within and near the base of the collapse scar, perpendicular to the scar sidewalls and failure direction. Similarly oriented backward-tilting toreva blocks up to about 5 km in length with a volume of ~ 5 km^3 occur at Volcán Barú in Panama (Siebert et al. 2006; Sherrod et al. 2007; Herrick et al. 2013). Analog modeling shows the toreva blocks form early in the collapse process and can transition to downslope hummock formation (Andrade and van Wyk de Vries 2010; Paguican et al. 2014, 2021). Toreva blocks can occur at large, deep-seated collapses but are not preserved where topography drops steeply away from the base of the volcano (van Wyk de Vries and Davies 2015).

A prominent proximal feature seen in analog modeling of collapse processes is the formation of a graben perpendicular to the failure direction (Andrade and van Wyk de Vries 2010; Paguican et al. 2014). The graben originates high on the edifice during the onset of failure, as observed at Mount St. Helens in 1980, and migrates downslope, forming a depression at the base of the failure scar between upslope toreva blocks and the downslope hummocky terrain of the VDA deposit (Fig. 19). This graben area is the transitional point between the listric, high-angle normal faults of the collapse zone and the low-angle normal faults of the depositional zone (Paguican et al. 2014). Field evidence for this graben is often obscured by deposition of post-collapse eruptive or volcaniclastic products.

Hummocky terrain

The typical irregular surface topography forming hummocky terrain (Fig. 20) is characteristic of both subaerial and submarine VDA deposits. Large avalanche deposits can contain hundreds to thousands of hummocks that range from a meter to several hundred meters in height and more than a kilometer in length. Hummock formation occurs under varying conditions but is dominated by extensional horst-and-graben formation during lateral spreading of a moving VDA (e.g., Voight et al. 1981, 1983; Paguican et al. 2012; van Wyk de Vries and Davies 2015). Extensional formation of hummocks can be accentuated by spreading on a weak base (van Wyk de Vries et al. 2001; Roverato et al. 2021a). Hummocks may also form by individual blocks rafted in finer-grained material or during compressional thrusting and faulting at deposit margins or where the VDA is constricted by topography (Glicken 1986, 1996). Analog modeling shows hummock formation as a natural progression during edifice failure from initial toreva block formation within the edifice to hummock generation beyond the edifice as extensional spreading and normal faulting separates slide blocks (Andrade and van Wyk de Vries 2010; Paguican et al. 2014, 2021).

Hummock orientations are often elongated in a radial pattern from the source, but orientations can be variable due to lateral spreading, or transverse to flow direction (Fig. 21). Elongated hummocks produced by flow-parallel shear may form long longitudinal ridges, which themselves may be broken up into hummock chains (Fig. 21). Hummock chains may reflect additional extensional ridge breakup into individual aligned hummocks when the fronts of ridges have greater velocity/momentum than upslope ridge components to the rear (Dufresne and Davies 2009). Hummock concentrations are also influenced by pre-avalanche topography. Many hummocks at the Acajutla VDA deposit in El Salvador (Siebert et al. 2004) preferentially lie adjacent to buried ridges of Tertiary bedrock, and at Raung volcano in Java they are near bedrock hills (Siebert 2002). Valley wall constrictions at Mount St. Helens (Glicken 1986, 1996) and Volcán Barú (Herrick et al. 2013) also stranded coherent block-facies material against topographic barriers.

Extensional spreading of hummocks creates closed depressions between hummocks that can be closely spaced and contain ponds and small lakes. VDA deposits also can display broad, flat intrahummock areas that can encompass the dominant proportion of deposit surface areas. These intrahummock areas initially form from grabens between hummock horsts but reflect zones of intense extensional strain in a mixture of brecciated block-facies, mixed-facies material (see lithofacies discussion below), and substrate material (van Wyk de Vries and Davies 2015). These areas can be composed of large concentrations of mixed facies

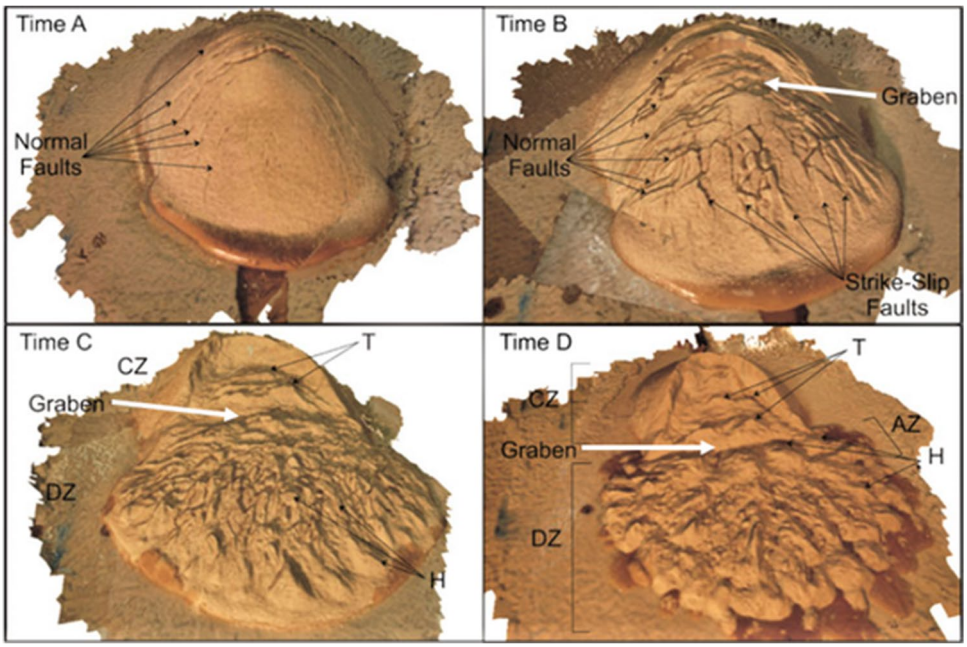

Fig. 19 Analog model, < 1 m in long dimension, of the evolution of a landslide on a cone into a debris-avalanche. Time A: initial landslide stage with formation and subsequent sliding along normal faults. Time B: formation of additional normal and strike-slip faults with onset of upper graben formation (white arrow). Time C: toreva blocks (T) that began forming earlier are prominent in the collapse zone (CZ) and abundant hummocks (H) have formed in the depositional zone (DZ) below the expanding graben. Time D: hummocks break up as the avalanche spreads, although new hummocks may form in the accumulation zone (AZ) when large hummocks form as those in front decelerate and stop. Figure modified from Paguican et al. (2014)

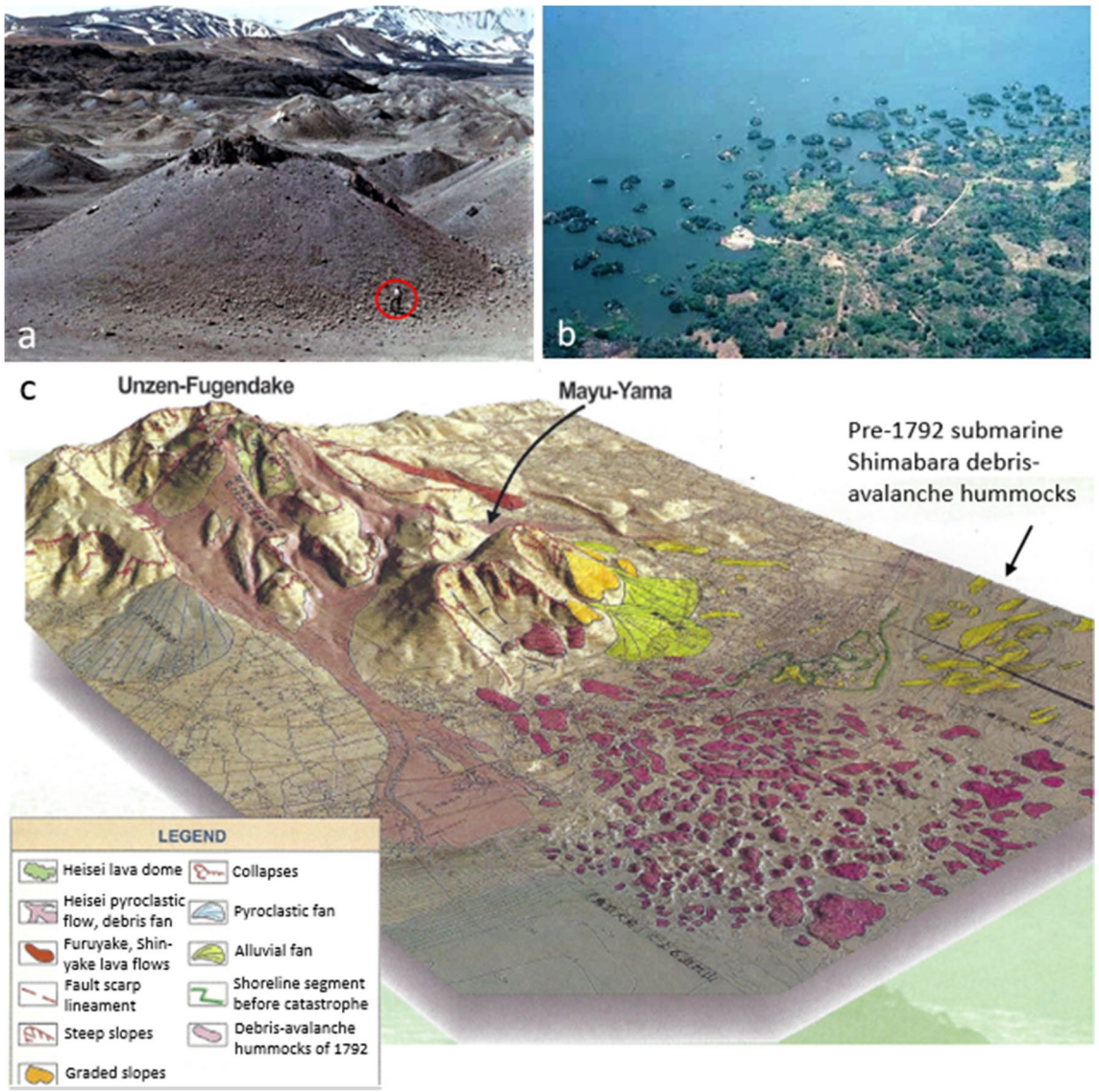

Fig. 20 Hummock topography from volcanic debris-avalanche (VDA) deposits. **a** Hummocks at 1956 CE Bezymianny, Kamchatka. Hummocks at this location have a spatial density of ~ 700/km^2 (Belousov and Belousova 1998, with photo modified to show red-circled person for scale). **b** Hummocks deposited in Lake Nicaragua from collapse of Mombacho volcano in Nicaragua form the Las Isletas peninsula and adjacent islands. Photo by J. Incer (https://volcano.si.edu/gallery/ShowImage.cfm?photo=GVP-04203). **c** Aerial oblique map view of 1792 CE Mayu-yama VDA deposit from the Unzen volcanic complex, Japan. Collapse from Mayu-yama lava dome (center) produced VDA that swept into the Ariake Sea and produced a catastrophic tsunami. Note change in hummock orientation from largely radial subaerial hummocks to transverse hummocks just outboard of pre-collapse shoreline (partial location shown by dark green line). Unzen-Fugendake was source of 1792 CE lava flow (in red at top center) and pyroclastic-flow and debris-flow fan produced during the 1990–1995 eruption (in pink at left). Older Shimabara VDA deposit forms olive-colored submarine deposits at right and subaerial deposits above dark green line depicting pre-1792 shoreline segment. Figure modified from Koga (2002), after Inoue (1999)

or, when sufficient water is present, lahar-facies deposits. Hummock formation dominates in block-facies deposits but can also be found in mixed-facies deposits as noted at Mount St. Helens (Glicken 1986, 1996) and in parts of transformed lahar deposits as at Mount Rainier (Vallance and Scott 1997).

Statistical studies of morphometric and distribution features of hummocks for both topographically confined and unconfined VDAs (Glicken 1986, 1996; Yoshida et al. 2012; Herrick et al. 2013; Yoshida 2013, 2014) document the decrease in size and proportion of hummocks with distance from the source. Hummock concentrations can also be found in compressional regimes adjacent to valley walls or at the terminus of deposits (e.g., Glicken 1986; Siebert et al. 2004; Herrick et al. 2013; Paguican et al. 2014; Roberti et al. 2017). Yoshida et al. (2012) noted that the rate of decrease in

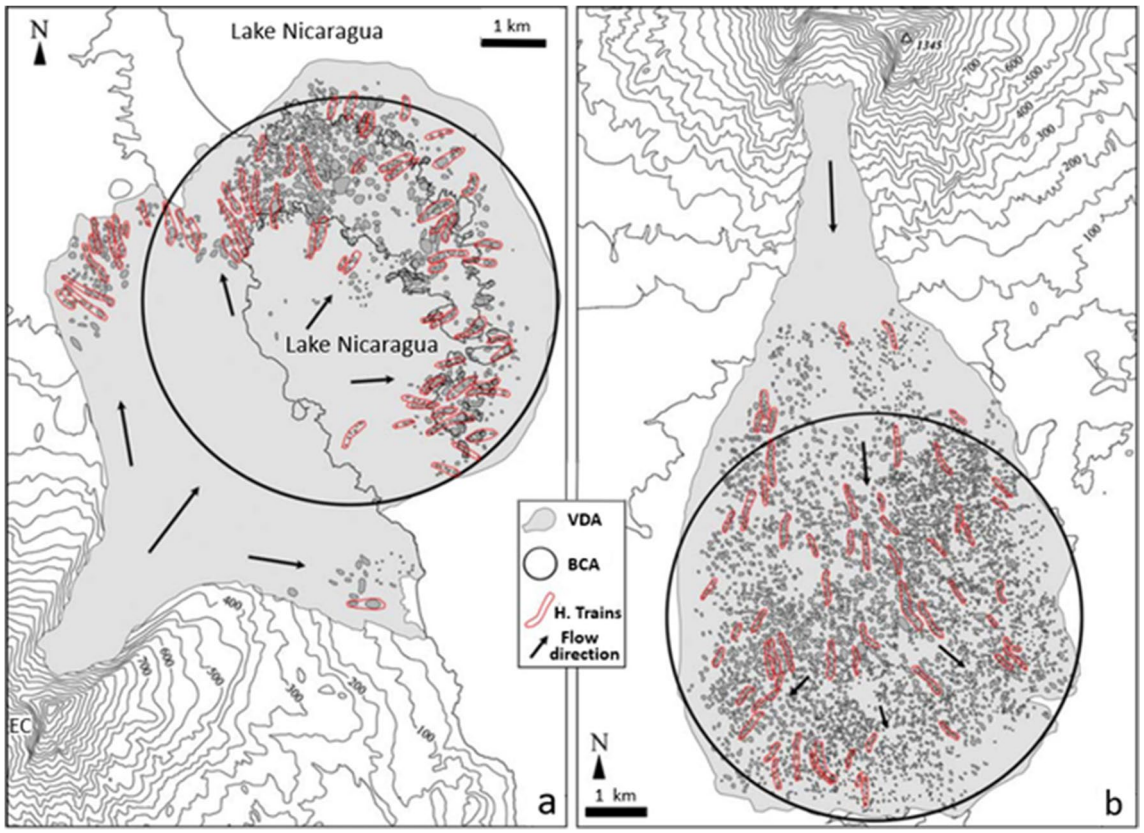

Fig. 21 Map of hummock distribution and hummock trains (red outlines) of two volcanic debris-avalanche (VDA) deposits at Mombacho volcano, Nicaragua. **a** Las Isletas VDA deposit. **b** El Crater VDA deposit. Hummocks shown in dark gray, VDA deposit area in lighter gray. BCA shows best circular approximation of deposits. Label EC at lower left in Las Isletas image shows upper part of El Crater collapse scar also shown in **b**. Hummock trains at the El Crater VDA deposit are dominantly radial from source, whereas hummock trains on the Las Isletas peninsula and adjacent islands extending into Lake Nicaragua are more variable and show effect of lateral spreading. Figure modified from Shea et al. (2008)

hummock size was inversely related to the overall mobility of the avalanche and that hummock size parameters correlate with avalanche volume and mobility. Yoshida (2013) documented that the average size of proximal hummocks positively correlates with the volume of the failure mass. Paguican et al. (2014) concluded that hummock size, shape, and density are influenced by interplay of the density of normal, thrust, and strike slip faults, material properties, and emplacement topography.

Other medial-to-distal features

More distal morphologic features on VDA deposits include lateral levees, longitudinal and transverse ridges, longitudinal flow banding, and substrate sediment deformation at the deposit terminus (Fig. 22). Levee formation reflects shear boundaries due to changes in velocity gradients at valley sides or at the margins of unconfined VDAs and can be formed within deposits due to multiple lobes emplaced over time. Levees can reach ~ 50 m above the adjacent deposit surface and are significantly higher than those of lahars and pyroclastic flows. They can represent the fully dilated height of the VDA during emplacement or that of valley margin VDA material pushed aside by the moving flow (Shea and van Wyk de Vries 2008). Levees of VDAs at valley margins are typically taller than at unconfined locations. Blockage of tributary drainages by VDA deposits can form large lakes, such as those at Bandai (Sekiya and Kikuchi 1889), Mount St. Helens (Scott 1988b), and Volcán de Colima (Capra and Macías 2002; Cortés et al. 2010). Such lakes can overtop catastrophically, forming massive floods and breakout lahars long after their formation.

A variety of longitudinal and transverse features can form in VDA deposits. Flow-parallel elongated ridges up to tens of meters in height can be found in deposits from both non-volcanic landslides and VDAs (Dufresne and Davies 2009) (Fig. 22). Flow-parallel ridges are on the order of hundreds of meters in length, while *flowbands* (sometimes called *striations*) are lower in height, separated by narrow "furrows," and can extend for kilometers along much of the length of

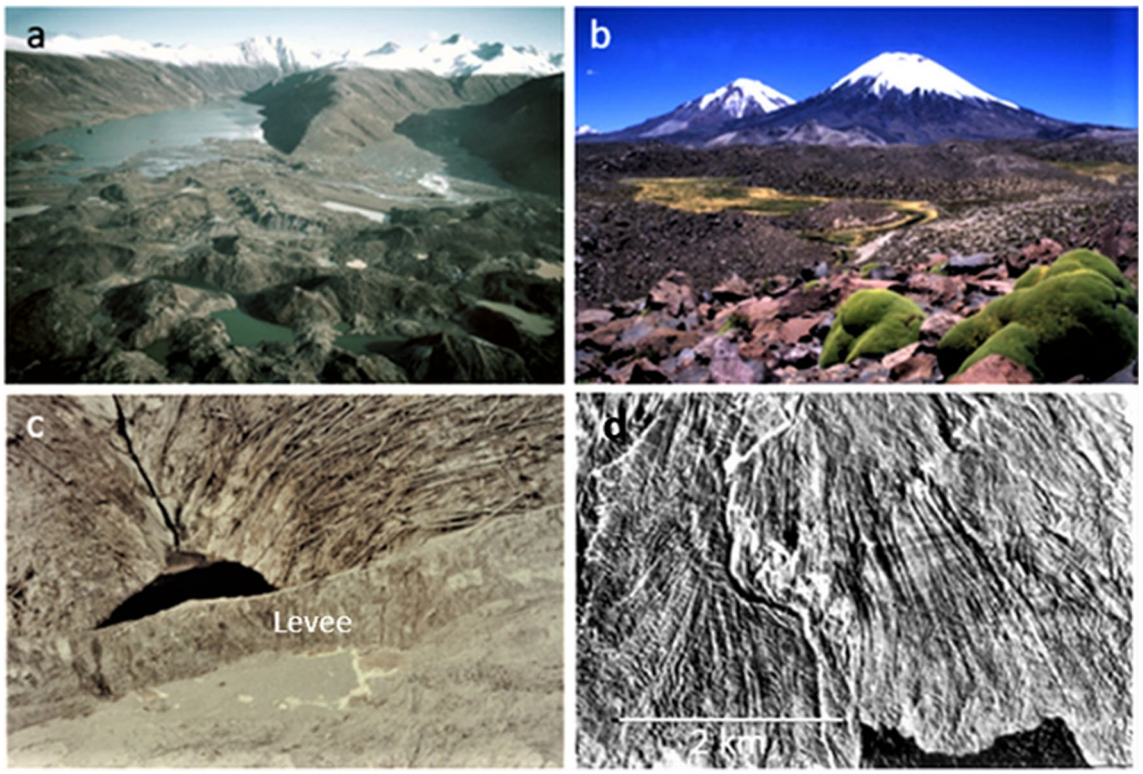

Fig. 22 Volcanic debris-avalanche (VDA) deposit surface features. **a** Closed depressions between large hummocks at Mount St. Helens, Washington (USA), in foreground were often filled by small ponds post 1980. Coldwater Lake in left background was formed through damming of drainage by 1980 VDA deposit. USGS photo. **b** Larger vegetated closed depression at VDA deposit from Parinacota volcano (right) in Chile (Clavero et al. 2002). Photo by L. Siebert. **c** ca. 30-m-high 1980 Mount St. Helens VDA deposit marginal levee formed small lake from drainage blockage. Lateral-blast tree blowdown visible at upper right. Photo from Glicken (1986). **d** Flow-parallel ridges at the distal end of the 1964 Shiveluch VDA deposit, Kamchatka; these features also occur at nonvolcanic landslide deposits, pyroclastic-flow deposits, and those of snow and ice avalanches (Dufresne et al. 2009). Belousov et al.'s (1999) photo modified from Dufresne and Davies (2009)

the deposit (Dufresne and Davies 2009). Prominent examples of flow banding at volcanic deposits are present at Llullaillaco in Chile/Argentina (Richards and Villeneuve 2001), Tutupaca in Peru (Valderrama et al. 2018), and the 1964 CE Shiveluch VDA deposit (Belousov et al. 1999) (Fig. 22d). Ridges within VDA deposits are thought to form in strong, competent, material that can travel over a mechanically weak base, whereas flowbands, the longer and thinner expressions of ridges, are more likely created from flow-parallel size segregation of weak, loose, low-density, small-clast-size source material (Inokuchi 1985; Dufresne and Davies 2009). Analog modeling shows that ridged features occur when coarse irregular particles segregate and concentrate at the flow front surface and are then recirculated into the advancing flow front (Pouliquen et al. 1997; Johnson et al. 2012; Valderrama et al. 2016, 2018). Analog modeling has shown that more homogeneous sources areas generate flow-parallel ridged morphologies, rather than hummocky terrain (Shea and van Wyk de Vries 2008). Typically, more limited fragmentation and ensuing segregation leads to block sliding without ridge formation (Valderrama et al. 2018).

Stress regimes can vary widely during emplacement in VDAs due to differential movement of VDA segments, with cross-cutting fault relationships indicating multiple generations of deformation during emplacement (Roberti et al. 2017) (Fig. 23). Sudden deceleration of VDAs can produce compressional transverse ridge or hummock orientation features near the terminus of deposits or individual lobes as they slow to a halt (Roberti et al. 2017). These features can also form from a VDA moving over deformable substrate (Dufresne and Davies 2009) or due to changes in substrate slope angle or from substrate obstructions (Yoshida et al. 2012; Herrick et al. 2013). Longitudinal hummocks can also change to transverse orientations from deceleration when an avalanche enters the sea, as at Augustine Volcano in 1883 CE, Unzen in 1792 CE, Santa Ana volcano in El Salvador (Siebert et al. 1987, 1995, 2004), and at Harimkotan (Kharimkotan) volcano in 1933 in the Kuril Islands (Belousov and Belousova 1996). In terrain with fine-grained, ductile

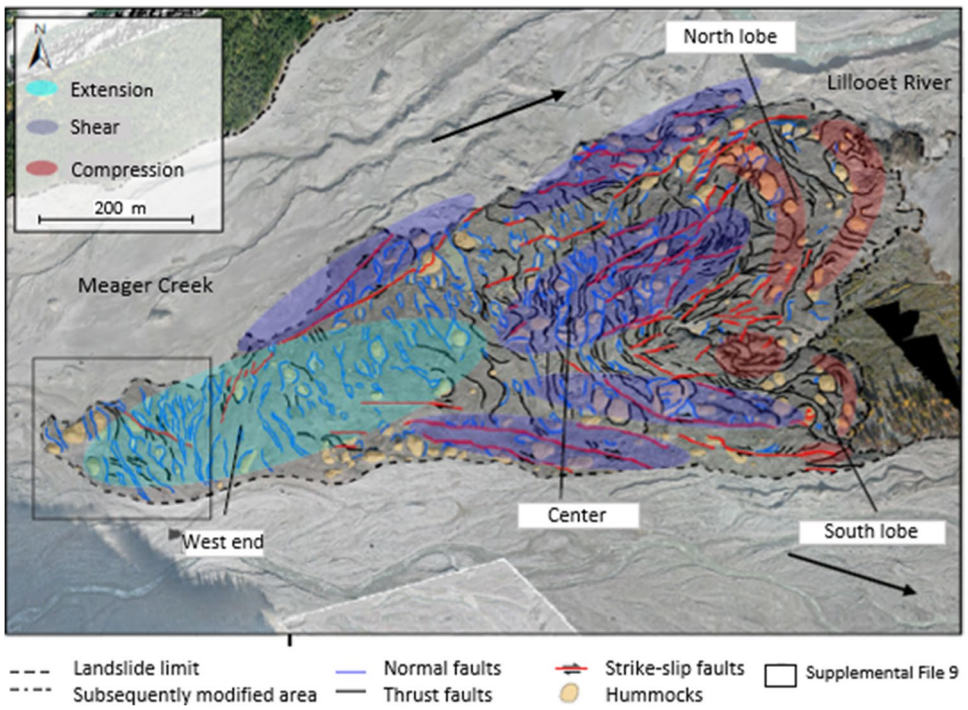

Fig. 23 Variable deformation regimes in distal portion of 0.0485 km^3 2010 CE volcanic debris-avalanche (VDA) deposit from Meager volcano in British Columbia with source area to left of this image. The 1.2-km-long segment near terminus of VDA at intersection of Meager Creek and Lillooet River valleys shows zones of proximal extension (blue) with normal faulting and graben formation, a central zone of shear (purple) with dominant flow-parallel strike-slip faults displacing thrust faults, and distal compression (red) dominated by thrust faults and transverse hummock chains. Arrows show overall flow directions. Figure modified from Roberti et al. (2017)

substrate, transverse distal and terminal hummock ridges at the terminus can be dominated by bulldozed substrate material producing thrust faults and soft-sediment deformation as at Shiveluch (Belousov et al. 1999), Ollagüe in Chile (Clavero et al. 2004), and Iriga volcanoes (Paguican et al. 2012). Very abrupt deceleration of debris avalanches can create ballistic impacts from large clasts tossed hundreds of meters beyond the steep distal fronts of some avalanche deposits (Plafker and Ericksen 1978; Siebe et al. 1992).

Lithofacies

The literature on VDA deposits is populated by a wide range of lithofacies terminology that reflect the complex variety of rock types, structures, and textures in these deposits as well as ambiguities in criteria and definitions of terms (see discussion in Bernard et al. 2021 and Dufresne et al. 2021b). A first-order distinction between *block facies* and *mixed facies* (formerly *matrix facies*) has been widely used to characterize these deposits (e.g., Glicken 1986, 1991, 1996; Ui and Glicken 1986; Ui et al. 2000; van Wyk de Vries and Davies 2015; Bernard et al. 2021; Dufresne et al. 2021b). *Block-facies* material is dominated by coherent and disrupted blocks and fragmented segments of the edifice that are transported relatively intact, preserving recognizable remnants of the original volcanic structures and stratigraphy, although with variable degrees of shear and internal deformation. The intense color variations produced by the juxtaposition of debris-avalanche blocks of variable composition and degrees of hydrothermal alteration with more subdued hues of disaggregated segments of the VDA can be one of the defining characteristics of VDA deposits. These variations are typically much more pronounced than in other mass flow deposits (Fig. 24a, b). Clasts are dominantly angular to very angular (Fig. 24c). In unconfined VDAs, the block facies is generally concentrated along the thick central axis of the deposit, but can persist to distal regions, although with diminishing block size. Bernard et al. (2021) distinguished edifice-derived block facies from that derived from incorporated substrate material. VDA deposits may include significant amounts of entrained substrate rock (Wadge et al. 1995; Shea et al. 2008) and scoured surficial soil or sediment (Palmer et al. 1991; Bernard et al. 2008).

Mixed-facies material becomes progressively more abundant with distance from the source, and contrasts with block facies in being more homogeneous in color and texture (Fig. 24d), with smaller, more rounded, more broadly polymictic, and dispersed clasts. This facies, with its typically subdued brownish or grayish colors, contrasts with multi-hued block-facies material and these materials can be intruded into block-facies material (Fig. 24e). Along with transformed laharic material (discussed above), it can form the most widespread and voluminous part of VDAs (Vallance and Scott 1997; Tost et al. 2014). Contacts between facies are typically gradational but can also be sharp. van Wyk de Vries and Delcamp (2015) and van Wyk de Vries and Davies (2015) distinguished a monomictic matrix facies (produced by milling of clasts of one rock type) from a polymictic mixed facies. Palmer et al. (1991) also described a *marginal facies* with characteristics of transformation to a

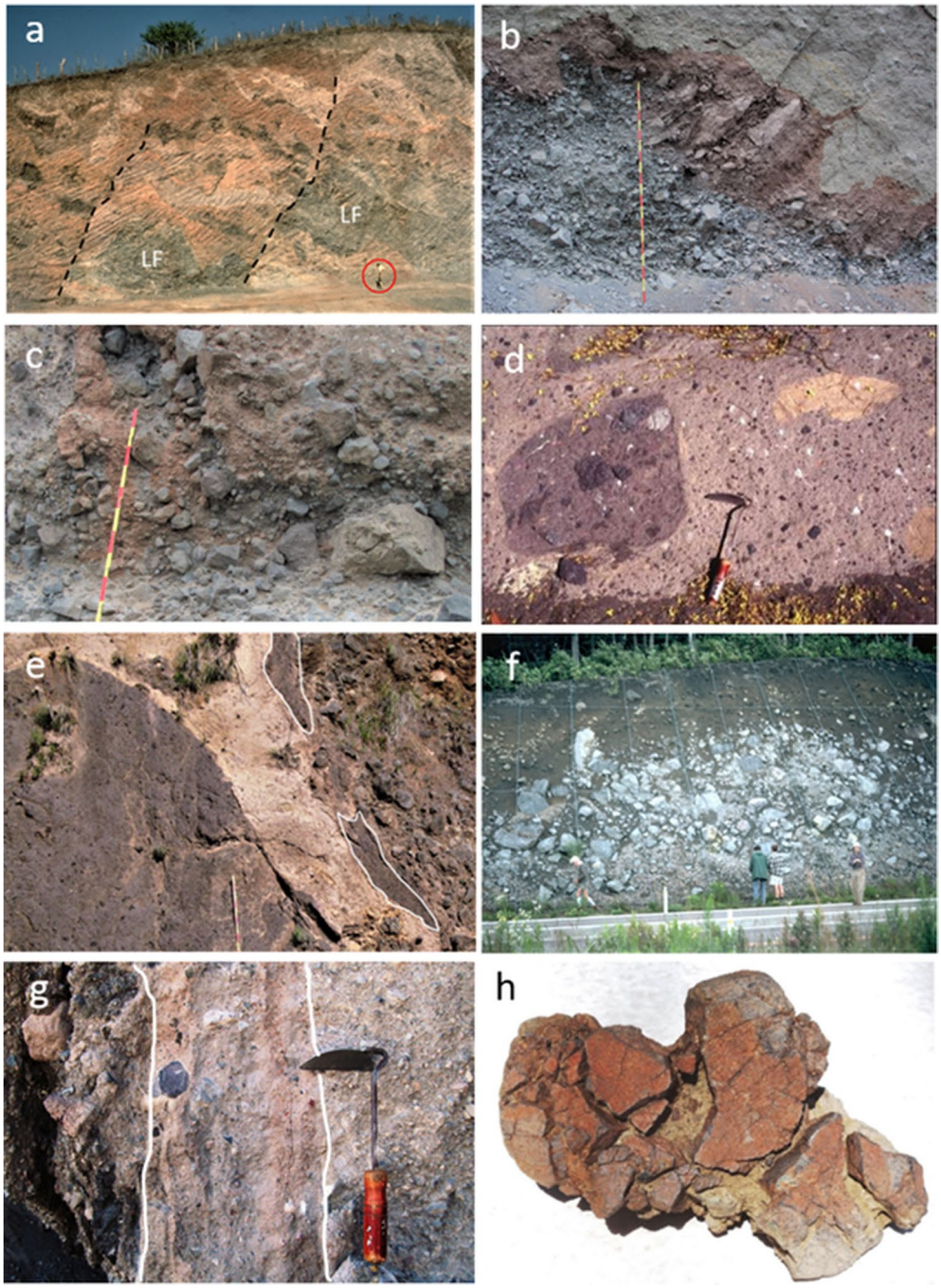

debris flow (e.g., Neall 1979; Scott et al. 2001; Zernack et al. 2011; Dufresne et al. 2021b; Zernack 2021), which can also be considered the *lahar facies* of an edifice collapse event (Siebert 2002; Pierson et al. in review). A *basal facies* on the scale of centimeters to a few meters in thickness reflects basal shear and substrate incorporation (Schneider and Fisher 1998; Ui et al. 2000; van Wyk de Vries and Davies 2015), and a *bulldozer facies* describes areas of terminal, often soft sediment, folded, and sheared substrate (Belousov et al. 1999; Paguican et al. 2012; Dufresne et al. 2021b). The textural features visible at outcrop scale can be critical in distinguishing VDA deposits from other types of mass flows, including debris flow/lahars, pyroclastic flows, and glacial deposits. Diagnostic textural characteristics, however, are commonly not visible on surficial exposures, making cross-sectional views in riverbanks, cliffs, road cuts, and quarries essential, which themselves may be partially obscured by slope wash or weathering.

◂**Fig. 24** Outcrop-scale volcanic debris-avalanche (VDA) deposit textures. **a** Roadcut through freshly excavated hummock in VDA deposit from the Fuego-Acatenango volcanic complex, Guatemala (Vallance et al. 1995). Outcrop shows pervasive normal faulting and shear, with boudinage and both brittle and ductile (top of outcrop) deformation. Dashed lines mark selected normal faults, LF offset large lava flow segments, circled person at lower right for scale. **b** Chimborazo VDA deposit, Ecuador (Bernard et al. 2008), with fractured gray debris-avalanche block in irregular contact with reddish clasts. Top of exposure is obscured by smooth, light-gray slope wash, emphasizing importance of fresh outcrops to reveal textures. **c** Dominantly angular clasts of VDA deposit from Tenerife volcano, Canary Islands (Martí 2019) with variably colored domains. **d** Acajutla VDA deposit from Santa Ana volcano, El Salvador (Siebert et al. 2004), showing relatively homogeneous, uniformly colored mixed-facies material containing small dark debris-avalanche block at left and light-brown substrate material at upper right. Polylithologic matrix contains both dark-colored lithic clasts and white pumice clasts. **e** VDA deposit from Dittmar volcano, California (Muffler and Clynne 2015), with light-colored mixed-facies material cutting through ignimbrite block at left and breccia block at right. Ignimbrite and remnants (outlined in white) at right indicate ignimbrite block and breccia block were in direct contact prior to mixed-facies injection. **f** Clast cluster surrounded by brown clast-poor matrix material in Okinajima VDA deposit from Bandai volcano, Japan (Mimura and Endo 1997). Persons along road for scale. **g** Vertical multi-hued shear bands in center at fault contact of dark-colored debris-avalanche block at left with light-colored block at right at Shasta Valley VDA deposit in California (Crandell 1989). **h** Jigsaw-fracture clast from the voluminous Oligocene Sevier megaslide in the Markagunt Plateau, Utah (Biek et al. 2019). Clast is 20-cm wide. Note incipient fractures within clast fragments and separation of clast fragments by lighter-color, now indurated, mixed-facies material. Photos by L. Siebert. Individual colored segments on scale bars in photos **b**, **c**, and **e** are 10 cm long, trowel in **d** and **g** is 26 cm long

Sedimentology

Deposits of VDAs are typically massive without internal bedding or fabric, although bedding or fabric can be retained in block-facies material containing transported bedded deposits from the edifice or in sedimentary deposits incorporated during emplacement. In addition, transported logs or trees may be aligned parallel to flow direction (Takarada et al. 1999). Fluid escape structures are not common in VDAs, although clastic dikes of mixed facies materials with vertical to irregular orientations and lengths from meters to tens of meters are commonly intruded into debris-avalanche block fractures. Bubble vesicles common in lahar deposits are largely absent in VDA deposits outside of transformed lahar-facies deposits (Pierson et al. 2018). A unique characteristic of VDA deposits is the frequent occurrence of clustered clasts that are not widely dispersed within surrounding mixed-facies material (Fig. 24f). Clast distributions typically become more random with distance from source, but clast clusters may be present in distal areas of even very long-runout deposits (Siebert et al. 2004; Roverarto et al. 2015).

Localized shear is common within faulted debris-avalanche blocks (Fig. 24a, g), with brittle deformation structures including block elongation, conjugate reverse faults, and a variety of minor faults (Takarada et al. 1999). Basal shear is pervasive at the lower parts of VDAs and nonvolcanic landslides in contact with substrate and can produce parallel striations in bedrock similar to those generated by glaciers, distinguished by their occurrence in previously unglaciated locations (Glicken 1996; Mehl and Schmincke 1999). Striations and grooves of variable orientation also appear in isolated individual blocks and incorporated substrate blocks within VDA deposits due to shear and collisional impacts (Mehl and Schmincke 1999; Bernard et al. 2022). On softer substrate, "groove casts" at the cemented bottom surface of a VDA deposit at Popocatépetl, Mexico, were interpreted to have been formed by sliding blocks scratching over soft clayey paleosols or sediments (Siebe et al. 2017). Shear can also occur at the base of fragmenting debris-avalanche blocks throughout the VDA during emplacement (Roverarto et al. 2015) and at contacts of VDAs with co-eval pyroclastic-flow deposits (Bernard et al. 2022).

Clasts within VDAs vary widely in size from clay-sized particles to large blocks but are typically angular to very angular in contrast to those of other volcaniclastic mass flow deposits. Mixed-facies clasts reflect more differential movement and can be more rounded, although are commonly in association with angular fragments. Dynamic disintegration of isolated clasts by collision and frictional grain-grain abrasion during transport increases the proportion of finer-grained matrix with distance (Perinotto et al. 2015; Roverarto et al. 2015). As with nonvolcanic landslides (Shreve 1968), VDA deposit outcrops often display clasts with jigsaw cracks or jigsaw fractures (Ui 1983), where fractured clasts may remain in close proximity and can be visually refitted together like a jigsaw puzzle (Fig. 24h). Jigsaw fractures can be found throughout VDA deposits and distinguishes them from lahars, although their frequency is variable within individual deposits and among different deposits. Jigsaw-fit textures also occur in a more localized context in hyaloclastites and peperites generated primarily by in situ non-explosive quench fragmentation at the margins of subaqueous lava flows, domes, or sills (e.g.,Scutter et al. 1998; Schmidt and Schmincke 2002; Skilling et al. 2002).

Jigsaw cracks have been attributed to compression and rarefaction waves early in the landslide process at Mount St. Helens (Glicken 1986, 1996; Komorowski et al. 1991). Later work also notes collisional comminution close to the depositional sites of jigsaw-cracked clasts, without disruption from long transport distances, as suggested by analysis of fractal dimensions and circularity of jigsaw-cracked clasts at Piton des Neiges volcano (Reunion Island) (Perinotto et al. 2015). Jigsaw fracturing and localized crushing of particles continues down to microscopic scale, as first demonstrated by the scanning electron microscopy of Komorowski et al. (1991) at Mount

St. Helens and subsequently seen at other volcanoes (e.g., Belousov et al. 1999; Pulgarín et al. 2004; Caballero and Capra 2011; Keigler et al. 2011; Roverato and Capra 2013; Perinotto et al. 2015; Roverarto et al. 2015; Bernard and van Wyk de Vries 2017; Bernard et al. 2019; Hughes et al. 2020; Procter et al. 2021). These investigations show a wide range of microscopic textures indicative of crushing from repeated high-pressure collisional contacts between sand-sized grains during flow that differs from textures in other volcaniclastic flows (Fig. 25).

Following the pioneering grain-size distribution studies of Glicken (1986, 1996) at Mount St. Helens, subsequent VDA deposit grain-size distribution studies, primarily from other stratovolcanoes and lava domes, have been summarized by Dufresne et al. (2021b). Full-deposit grain-size distributions from VDA deposits overlap considerably with other volcaniclastic deposits, particularly those of lahars and pyroclastic flows. VDA deposits are often as coarse or coarser than the pyroclastic-flow field of Walker (1971) and more poorly sorted than Walker's pyroclastic-fall field (Siebert et al.

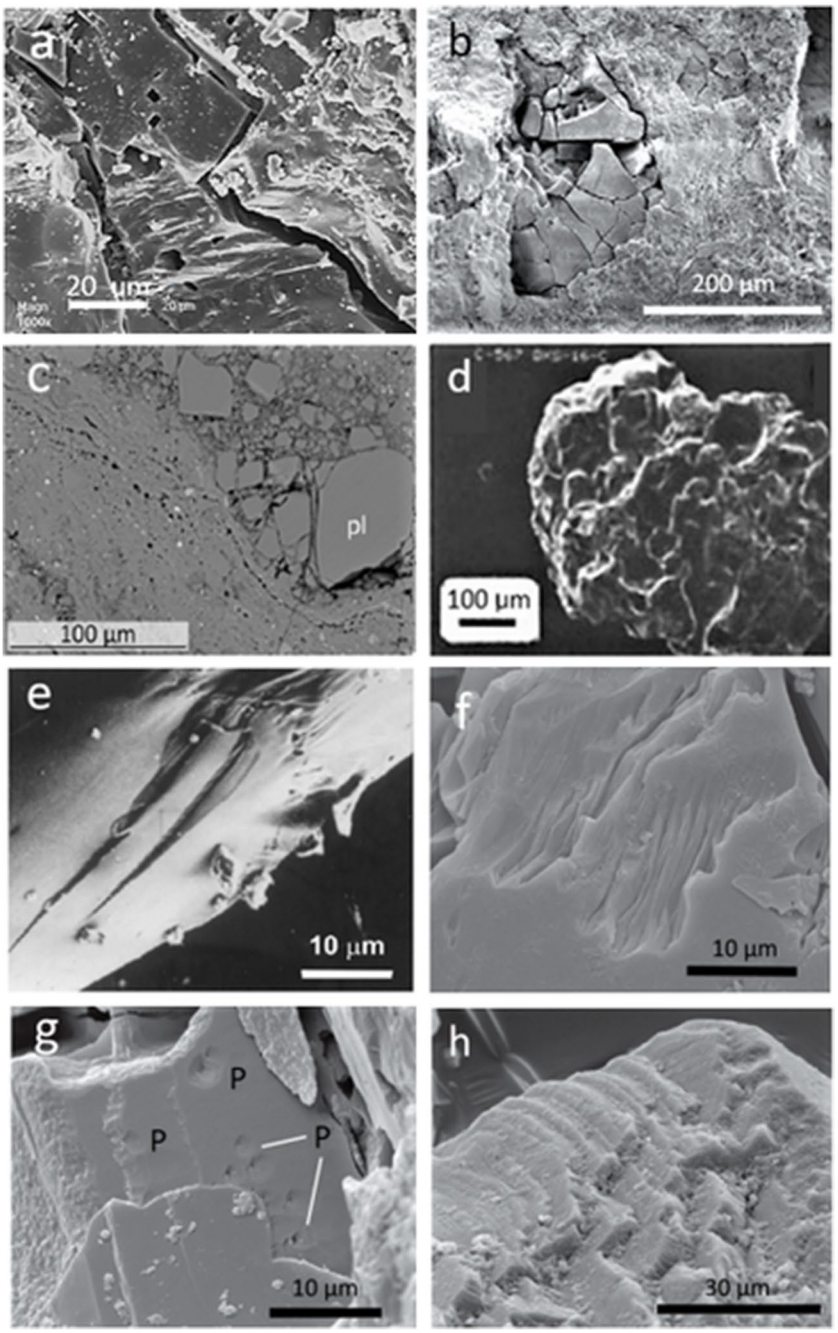

Fig. 25 Scanning electron microscope (SEM) images of microtextures of volcanic debris-avalanche (VDA) deposit grains. **a** Fracture generation with separation of cracks and small-scale displacements. **b** Jigsaw fractures in lithic clast. **c** Shattered plagioclase crystal (pl) adjacent to glass at left along basal shear zone. **d** Hackly texture on projecting parts of glass-covered pyroxene crystal from highly irregular breakage by repeated high-pressure grain contacts in contrast to smooth topographic lows on the surface. **e** Pair of diagonal lip structures wider and deeper at top of image. **f** Grooves and scratches of variable size and depth. **g** Percussion marks (P) from grain-to-grain impact. **h** Truncated crystal with staircase geometry. Modified images: **a** Shiveluch volcano, Kamchatka (Belousov et al. 1999); **c** Pichu Pichu volcano, Peru (Hughes et al. 2020); **d** Mount St. Helens, Washington, 1980 CE VDA deposit (Komorowski et al.1991); **e** Nevado de Toluca volcano, Mexico (Caballero and Capra 2011). Images **b**, **f**, **g**, and **h** from Taranaki volcano, New Zealand (Roverarto et al. 2015)

2004; Dufresne et al. 2021b). Data collected after Walker (1971) show considerable overlap between pyroclastic-flow and pyroclastic-fall fields, and pyroclastic-surge data overlap broadly with both fields (Fisher and Schmincke 1984), who noted that these size and sorting diagrams should be used with caution. Standard grain-size distribution parameters including graphical statistics on size, sorting, kurtosis, skewness, and size-component distribution can characterize VDA deposits. However, varying analytical and sampling techniques can complicate direct data comparison, and grain-size distribution data alone may not be indicative of processes. Deposit morphology and outcrop- and microscopic-scale textures can be essential tools for VDA deposit identification.

Post-1980 understanding of lateral edifice collapse and volcanic debris avalanches

Magnitude and global distribution

The 1980 collapse and eruption of Mount St. Helens spawned an intense burst of research on individual VDA deposits. Regional and global surveys of VDA deposit occurrences have been produced at a rate of more than one yearly since then, roughly equally divided between continental and oceanic compilations. Regional surveys included those in **Tanzania** (Delcamp et al. 2016a), **New Zealand** (Palmer et al. 1991; Neall 2002), **Papua New Guinea** (Johnson 1987; Silver et al. 2009), **Indonesia** (MacLeod 1989), **Philippine**s (Geronimo-Catane 1995), **Japan** (Ui et al. 1986; Inokuchi 1988, 2006; Yoshida 2016), **Hokkaido** in Japan (Yamagishi 1996), **Kuril Islands and Kamchatka** (Melekestsev and Braitseva 1988; Ponomareva et al. 2006; Belousova and Belousov 2011), the **Aleutian Islands** (Coombs et al. 2007; Montanaro and Beget 2011), the **Cascade Range** (Siebert and Vallance 2017), **Hawaiian Islands** (Moore et al. 1989, 1994; Normark et al. 1993; McMurtry et al. 2004), the **Society and Austral Islands** (Clouard and Bonneville 2004), **Mexico** (Capra et al. 2002), **Guatemala** (Vallance et al. 1995), **Costa Rica** (Alvarado et al. 2004), **Central America** (Siebert et al. 2004, 2006), **Ecuador** (Andrade 2009; Bernard and Andrade 2019), the **Central Andes** (Francis and Wells 1988), the **West Indies** (Deplus et al. 2001; Boudon et al. 2007), the **Madeira Islands** (Quartau et al. 2018), the **Canary Islands** (Krastel et al. 2001; Masson et al. 2002; Acosta et al. 2004; Hunt et al. 2014), and the **Cape Verde Islands** (Masson et al. 2008). **Global** surveys of VDAs included Ui (1983), Siebert (1984), Siebert et al. (1987), Holcomb and Searle (1991), Mitchell (2003), Bernard (2008), Dufresne et al. (2008), Blahůt et al. (2019), Dufresne et al. (2021a), Siebert and Roverato (2021), and Rowberry et al. (2023).

VDA deposits originate from a broad spectrum of volcanic structures, most commonly from steep-sided stratovolcanoes that compose about three-fourths of all known collapse events (Dufresne et al. 2021a). Over-steepened lava domes like Augustine Volcano (Siebert et al. 1989, 1995; Waitt and Begét 2009), Soufriere Hills (Sparks et al. 2002; Voight et al. 2002; Young et al. 2002), or Shiveluch (Belousov et al. 1999) are also highly susceptible to lateral edifice collapse. Large VDA deposits can result from collapse of caldera walls during (Rinjani volcano, Indonesia; Lavigne et al. 2013) or after caldera formation, as occurred at Fernandina, Galápagos Islands, in 1988 (Chadwick et al. 1991). Much smaller syn-eruptive VDA deposits have been noted at features as small as monogenetic cinder cones (Romero et al. 2020). Larger failures are not limited to steep slope angles, however, as demonstrated by the large-scale lateral volcanic collapses occurring on low-angle shield volcanoes in the Hawaiian Islands (Moore et al. 1989) and many other volcanic island chains as well as comparably sized massive collapses (> 1000 km^3) from continental volcanic fields (Hacker et al. 2014; Biek et al. 2019). Submerged seamounts can fail both in island arc (Wright et al. 2006; Chadwick et al. 2008) and mid-plate (Smoot and King 1993; Moore et al. 1994; Staudigel and Clague 2010; Omira et al. 2016) settings. A 19-km^3 VDA deposit has been documented along the Mid-Atlantic Rift (Tucholke 1992). Partially submerged VDA deposits are common on edifices ranging from massive shield volcanoes to smaller stratovolcanoes or lava domes. VDA deposits have likewise been documented at volcanic constructs on other planets (Bulmer and Wilson 1999; McGovern et al. 2004). Individual VDA deposits have been identified on all continents. The vast majority of documented VDA deposits are Quaternary in age, but they have been documented as far back as the Precambrian in Australia (Trofimovs et al. 2004) and Brazil (Roverato 2016). Dufresne et al. (2021a) analyzed known geometric and associated data on VDA deposits, including mobility, travel distance, volumes, areas, and poorly known associated eruptive activity.

Frequency of occurrence

The surge of interest in lateral edifice failure events has led to the identification of more than 1000 cases globally with known or inferred volumes ≥ 0.01 km^3, most of these thought to be ≥ 0.1 km^3, from more than 600 volcanoes, based on VDA deposits or inferred from source-area geometries (Dufresne et al. 2021a; Siebert and Roverato 2021; this study). On a regional scale, more than half of large-volume stratovolcanoes have undergone edifice failure at least once in regions such as Japan (Ui et al. 1986; Inokuchi 2006), Kamchatka (Ponomareva et al. 2006), the Cascade

Range (Siebert and Vallance 2017), and Mexico (Capra et al. 2002). Other regions such as Turkey and the Philippines have far fewer documented failures from their volcanoes. As VDA deposits have been investigated in more detail at individual volcanoes, it has been documented that many have undergone more edifice failures than initially realized. Ten or more collapse events have occurred at Piton des Neiges (Oehler et al. 2008), Taranaki (Zernack et al. 2009), Bandai (Chiba and Kimura 2001), Augustine Volcano (Waitt and Begét 2009), Colima volcanic complex (Cortés et al. 2019), Soufrière Hills (Boudon et al. 2007), and Tenerife (Hunt et al. 2014). At a small-volume volcano such as Augustine Volcano, a high magma production rate promotes rapid reconstruction following failure and collapses have recurred as often as ~ 200 years during the past ~ 2500 years (Waitt and Begét 2009). At Las Derrumbadas dome complex in Mexico, as many as 10 VDA deposits > 0.01 km^3, seven of which are > 0.1 km^3, occurred during an eruptive episode at about 2 ka that lasted perhaps decades to centuries (Guilbaud et al. 2022).

During historical time after 1500 CE, known lateral edifice-failure events ≥ 0.01 km^3 in volume averaged about nine per century globally, with larger avalanches ≥ 0.1 km^3 averaging 5–6 per century and those > 1 km^3 about one per century (Table 1). These are likely undercounts, as data show an apparent progressive decrease in events with age, going from nearly 20 events per century since 1900 CE and about 16 per century since 1800 CE to only a dozen known events in the three centuries prior to 1800 CE. This decline suggests that collapse occurrence data since 1800 CE may be a more representative frequency for larger events ≥ 0.1 km^3. The systematic decline in known smaller events from more current values reflects the lower likelihood of earlier observations and documentation (Fig. 26).

Three-fifths of total events involved deep-seated failures, most often involving the summit and core of the volcano, with the remainder being smaller volume, typically flank failures. These smaller failures included more than half of the total events since 1900 CE, likely reflecting the tendency for underreporting of less dramatic collapse events in earlier centuries (Fig. 26). This underreporting trend matches pronounced eruption undercounting, particularly of smaller eruptions, during the same intervals (Siebert et al. 2011) and for eruptions of all sizes throughout the geologic record (Deligne et al. 2010; Brown et al. 2014; Kiyosugi et al. 2015).

Two-thirds of events since 1500 CE (Table 1) were associated with eruptive activity, all but three of which were magmatic, the remainder associated with only phreatic eruptions. Lateral blasts such as at Mount St. Helens in 1980 and Bezymianny in 1956 were identified at only four of the other magmatic events. This is consistent with lateral-blast generation associated with edifice failure

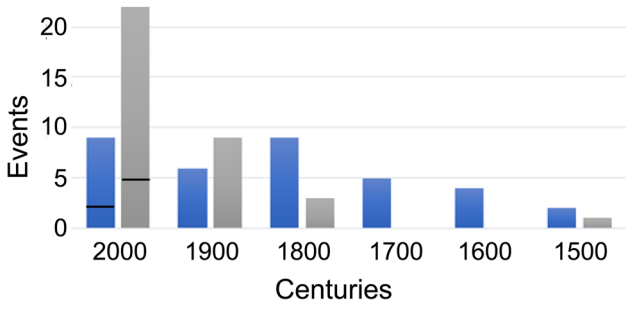

Fig. 26 Age distribution of lateral edifice collapse events since 1500 CE. Blue bars are volcanic debris-avalanche (VDA) events with deposit volume ≥ 0.1 km^3; gray bars are events ≥ 0.01 and ≤ 0.1 km^3. The total twenty-first century data extrapolated from data through early 2023 with black lines showing known twenty-first century events. Data from Table 1

requiring the precise coincidence of collapse at the time of explosions, typically when a magma body is high in the edifice and collapsing slide blocks deflect decompression-generated explosions (Belousov et al. 1999, 2007, 2020; Siebert 2002). Elsewhere, as at Shiveluch volcano in 1964 (Belousov 1995), collapse can be completed prior to the onset of magmatic eruptions, resulting in open-vent eruptions and more typical vertical explosions (Fig. 27). A vertically directed, magmatic blast explosion occurred at Lamington volcano, Papua New Guinea, when the basal failure plane truncated only the upper tip of the intruding magma body (Belousov et al. 2020). When magma is even deeper, explosions may be only phreatic, as at Bandai volcano in 1888 (Nakamura 1978).

Lateral edifice failure can also frequently occur in absence of eruptive activity, with attendant hazards implications. Half of the smaller-volume, shallower events ≤ 0.1 km^3, few of which involved the summit of the volcano, had no reported eruptive activity (Table 1). Much larger deep-seated non-eruptive collapse events have also been reported in the geologic past, although the "historical" interval of Table 1 is too short to include these. The existence or character of associated eruptive activity is addressed at far too few earlier collapse events (Dufresne et al. 2021a) to adequately assess the degree of active magmatic involvement in past lateral edifice-failure events.

Hazards from lateral edifice-failure events include those from the VDAs themselves, as well as those associated with magmatic or phreatic eruptions accompanying the collapse event, including pyroclastic flows, lahars, and tsunamis created by the rapid impact of VDAs into the sea or large lakes (Latter 1981; Begét 2000; McGuire 2006; Day 2015). Fatalities are known to have occurred at many of the events listed in Table 1 (including more than half of those with volumes ≥ 0.1 km^3). The impact

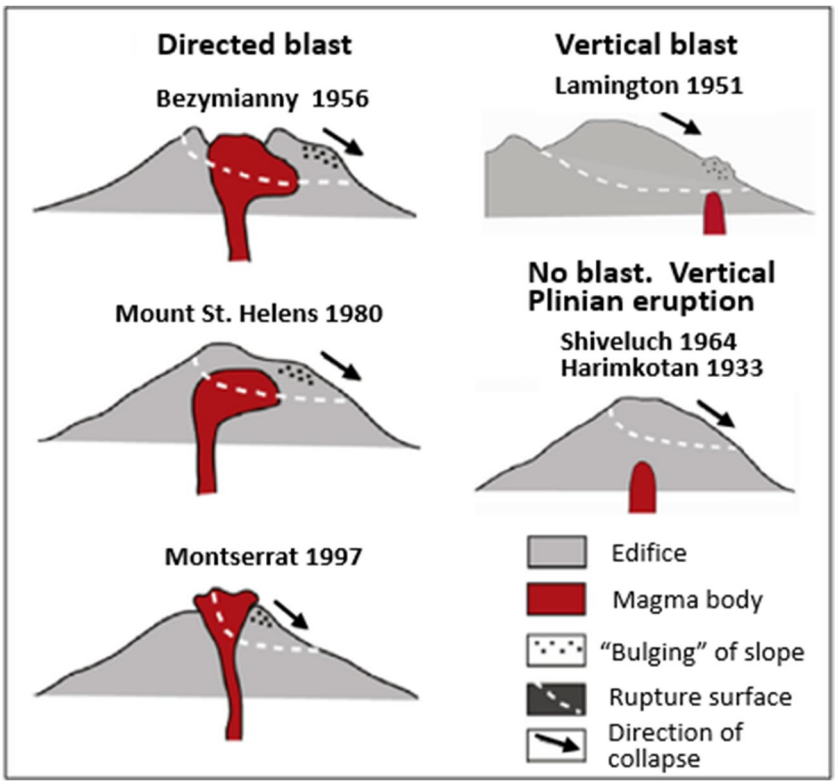

Fig. 27 Sketches illustrating positions of magma bodies inside volcanic edifices before gravitational collapses. Directed (lateral) blasts occurred when failure planes truncated a combination of dome and cryptodome (Bezymianny, Kamchatka), cryptodome (Mount St. Helens, Washington), and dome (Soufrière Hills, Montserrat). At Lamington (Papua New Guinea), the rupture surface intersected only the uppermost part of the cryptodome and vertical "blast explosions" with radial pyroclastic-flow distribution resulted. At Shiveluch (Kamchatka) and Harimkotan (Kuril Islands), collapse occurred before ascending magma reached the failure plane and no lateral blast occurred, although failure was followed by major vertical Plinian eruptions. Figure modified from Belousov et al. (2020)

would have been much higher had many not occurred in areas uninhabited or sparsely populated at the time. Edifice collapse events led to more than 30,000 known fatalities since 1500 CE (Table 1), about equally distributed between eruptive and non-eruptive events. Even smaller events than those considered here can have considerable impact as seen by the > 2500 non-eruptive fatalities from an avalanche-induced 0.0016-km^3 debris flow at Casita volcano in 1998 (Scott et al. 2005). Tsunamis have by far been the leading cause of collapse-related deaths, dominated by those in Japan and Indonesia. Thus, secondary hazards to humans during historical time have proven even more devastating than the considerable primary hazards from the VDAs themselves.

Summary

Lateral edifice collapse and the generation of volcanic debris avalanches were not widely recognized prior to the 1980 Mount St. Helens collapse and eruption. The more than four decades since have seen a proliferation of studies on the resulting deposits and evaluation of processes leading to debris-avalanche generation, which build on the insights from the 1980 eruption. The Mount St. Helens VDA deposit is one of the best studied modern examples of a large-scale lateral collapse. Important aspects of the flank failure at Mount St. Helens include (1) a shallow cryptodome intrusion destabilized the north flank through deformation, bulging, and faulting; (2) slow deformation over months led to rapid catastrophic failure; (3) massive retrogression of three large slide blocks sculpted deeply into the edifice; (4) the accompanying $Ms \sim 5$ earthquake may have been induced by the enormous landslide; and (5) failure did not occur in hydrothermally altered rocks.

Slope instability is promoted by a myriad of factors — some act to predispose a slope to failure whereas others act as dynamic triggers. Volcanic edifices experience the destabilizing conditions present on other large mountains, such as earthquake shaking and elevated pore-fluid pressures, but additionally have volcano-related destabilizing phenomena, such as hydrothermal alteration, deformation from shallow magma intrusion, and pressurization of pore fluids by heating.

Recent lateral edifice collapses after 1500 CE accompanied by magmatic eruption or phreatic explosions are typically about an order of magnitude larger compared to those without these dynamic processes or large nonvolcanic landslides, although very large non-eruptive collapses have been reported in the geologic record. Factors that could enhance or promote large, deep failures, initially or through retrogression, involve modifying stresses or strengths at depth.

These stresses include changes in internal structures relating to gravitational spreading, possibly on a weak base; degradation of highly variable rock strength by certain styles of hydrothermal alteration; locally elevated pore-fluid pressures; and dynamic triggers such as earthquake shaking, magma intrusion, and thermal pressurization of pore fluids.

Scenario-based geotechnical assessments can aid in forecasting the size and location of future large lateral collapses. Monitoring volcanic unrest, such as increased seismicity and changes in volcanic gas emissions, can herald the onset of potentially destabilizing dynamic processes. A primary tool for detecting potential collapses is ground deformation, monitored using a variety of techniques. Satellite-based InSAR is useful for detecting changes in remote settings or over large areas whereas ground-based InSAR and continuous GPS/GNSS can provide near-real time assessments. Changes in ground velocity and (or) acceleration over time can sometimes forecast rapid failure. However, failures occur within a broad spectrum of magmatic and non-magmatic conditions with attendant difficulties in assessing and communicating short-term and long-term risk. Forecasting these high-impact but low-frequency events remains a topic of investigation.

Catastrophic edifice failure impacts a broad range of volcanic structures in diverse tectonic settings. More than a thousand events, primarily ≥ 0.1 km^3 in volume, have now been identified from deposits or inferred from source area morphology, leading to a recognition of their importance in the evolution of volcanoes and the hazards they pose. These deposits had often previously been interpreted otherwise and morphological factors and textural characteristics from outcrop to microscopic scale are now known that distinguish VDA deposits from other volcaniclastic deposits.

Documented edifice failure events ≥ 0.01 km^3 in volume averaged about 9 per century globally since 1500 CE, with larger avalanches ≥ 0.1 km^3 averaging 5–6 per century and those > 1 km^3 about one per century. An apparent progressive decline in collapse events in earlier centuries reflects diminished likelihood of observation and documentation, particularly of less dramatic smaller volume events. This underrepresentation is consistent with pronounced eruption undercounting for eruptions of smaller sizes since 1500 CE and for those of all sizes throughout the geologic record. In addition to hazards from the VDAs themselves, collapse-related hazards include those from associated magmatic or phreatic eruptions. Directed volcanic explosions such as at Mount St. Helens in 1980 and Bezymianny in 1956 require precise coincidence of collapse and decompression-related explosions, conditions not found at most magmatic collapse events. Associated secondary hazards also originate from lahars and collapse-generated tsunamis, with the latter being the primary cause of known collapse-related fatalities.

Acknowledgements The extensive reference list cited here acknowledges but a fraction of those who have contributed to the recognition and understanding of lateral edifice failure phenomena. We thank Barry Voight for discussion and providing figures regarding events leading up to the May 18, 1980, collapse at Mount St. Helens. LS acknowledges concurrent work on characteristics of volcanic debris-avalanche deposits with Tom Pierson as part of a Pierson et al. (in review) book on volcaniclastic deposits. Lauren Schaefer provided valuable insights to discussion of failure causes. We thank Chris Harpel, Claus Siebe, and an anonymous reviewer for improvements to the manuscript.

References

Acocella V (2021) Volcano flank instability and collapse. In: Volcanotectonic processes, Springer, Cham, 205–244. https://doi.org/10.1007/978-3-030-65968-4_6

Acosta J, Uchupi E, Muñoz A, Herranz P, Palomo C, Ballesteros M, ZEE Working Group (2004) Geologic evolution of the Canarian Islands of Lanzarote, Fuerteventura, Gran Canaria and La Gomera and comparison of landslides at these islands with those at Tenerife, La Palma and El Hierro. Mar Geophys Res 0:1–38

Aizawa K, Ogawa Y, Ishido T (2009) Groundwater flow and hydrothermal systems within volcanic edifices: delineation by electric self-potential and magnetotellurics. J Geophys Res Solid Earth 114(B1). https://doi.org/10.1029/2008JB005910

Alidibirov MA (1995) A model for the mechanism of the May 18, 1980 Mount St. Helens blast. J Volcanol Geotherm Res 66:217–225. https://doi.org/10.1016/0377-0273(94)00065-O

Alvarado GE, Vega E, Chaves J, Vásquez M (2004) Los grandes deslizamientos (volcánicos y no-volcánicos) de tipo debris avalanche en Costa Rica. Rev Geol Am Central 30:83–99

Andrade SD (2009) The influence of active tectonics on the structural development and flank collapse of Ecuadorian arc volcanoes. Dissertation, Université Blaise Pascal-Clermont-Ferrand, France

Andrade SD, van Wyk de Vries B (2010) Structural analysis of the early stages of catastrophic stratovolcano flank-collapse using analogue models. Bull Volcanol 72:771–789. https://doi.org/10.1007/s00445-010-0363-x

Apuani T, Corazzato C (2009) Numerical model of the Stromboli volcano (Italy) including the effect of magma pressure in the dyke system. Rock Mech Rock Eng 42(1):53–72. https://doi.org/10.1007/s00603-008-0163-1

Apuani T, Corazzato C, Cancelli A, Tibaldi A (2005a) Physical and mechanical properties of rock masses at Stromboli: a dataset for volcano instability evaluation. Bull Eng Geol Environ 64(4):419–431. https://doi.org/10.1007/s10064-005-0007-0

Apuani T, Corazzato C, Cancelli A, Tibaldi A (2005b) Stability of a collapsing volcano (Stromboli, Italy): limit equilibrium analysis and numerical modelling. J Volcanol Geotherm Res

144(1–4):191–210. https://doi.org/10.1016/j.jvolgeores.2004.11.028
Apuani T, Corazzato C, Merri A, Tibaldi A (2013) Understanding Etna flank instability through numerical models. J Volcanol Geotherm Res 251:112–126. https://doi.org/10.1016/j.jvolgeores.2012.06.015
Baldi P, Coltelli M, Fabris M, Marsella M, Tommasi P (2008) High precision photogrammetry for monitoring the evolution of the NW flank of Stromboli volcano during and after the 2002–2003 eruption. Bull Volcanol 70:703–715. https://doi.org/10.1007/s00445-007-0162-1
Ball JL, Stauffer PH, Calder ES, Valentine GA (2015) The hydrothermal alteration of cooling lava domes. Bull Volcanol 77(12):1–16. https://doi.org/10.1007/s00445-015-0986-z
Ball JL, Taron J, Reid ME, Hurwitz S, Finn C, Bedrosian P (2018) Combining multiphase groundwater flow and slope stability models to assess stratovolcano flank collapse in the Cascade Range. J Geophys Res Solid Earth 123(4):2787–2805. https://doi.org/10.1002/2017JB015156
Banks NG, Hoblitt RP (1981) Summary of temperature studies of eruptions of 1980 deposits. In: Lipman PW, Mullineaux DR (eds) The 1980 eruptions of Mount St Helens Washington. U S Geol Surv Prof Pap 1250:295–313
Banks NG, Hoblitt RP (1996) Direct temperature measurements of deposits, Mount St. Helens, Washington. U S Geol Surv Prof Pap 1387:1–76. https://doi.org/10.3133/pp1387
Barberi F, Bertagnini A, Landi P, Principe C (1992) A review on phreatic eruptions and their precursors. J Volcanol Geotherm Res 52(4):231–246. https://doi.org/10.1016/0377-0273(92)90046-G
Bartel BA, Hamburger MW, Meertens CM, Lowry AR, Corpuz E (2003) Dynamics of active magmatic and hydrothermal systems at Taal Volcano, Philippines, from continuous GPS measurements. J Geophys Res Solid Earth 108(B10). https://doi.org/10.1029/2002JB002194
Begét JE (2000) Volcanic tsunamis. In: Sigurdsson H (ed) Encyclopedia of volcanoes. Academic Press, Amsterdam, pp 1005–1013
Bell AF, Greenhough J, Heap MJ, Main IG (2011a) Challenges for forecasting based on accelerating rates of earthquakes at volcanoes and laboratory analogues. Geophys J Int 185(2):718–723. https://doi.org/10.1111/j.1365-246X.2011.04982.x
Bell AF, Naylor M, Heap MJ, Main IG (2011b) Forecasting volcanic eruptions and other material failure phenomena: an evaluation of the failure forecast method. Geophys Res Lett 38(15). https://doi.org/10.1029/2011GL048155
Belousov AB (1995) The Shiveluch volcanic eruption of 12 November 1964—explosive eruption provoked by failure of the edifice. J Volcanol Geotherm Res 66:357–365. https://doi.org/10.1016/0377-0273(94)00072-O
Belousov A, Belousova M (1996) Large scale landslides on active volcanoes in the 20th century - examples from the Kurile-Kamchatka region (Russia). In: Senses K (ed) Landslides. Balkema, Rotterdam, pp 953–957
Belousov A, Belousova M (1998) Bezymyannyi eruption on March 30, 1956 (Kamchatka): sequence of events and debris-avalanche deposits. Volcanol Seismol 20:29–47
Belousov A, Belousova M, Voight B (1999) Multiple edifice failures, debris avalanches and associated eruptions in the Holocene history of Shiveluch volcano, Kamchatka, Russia. Bull Volcanol 61:324–342. https://doi.org/10.1007/s004450050300
Belousov A, Voight B, Belousova M (2007) Directed blasts and blast-generated pyroclastic density currents: a comparison of the Bezymianny 1956, Mount St Helens 1980, and Soufrière Hills, Montserrat 1997 eruptions and deposits. Bull Volcanol 69:701–740. https://doi.org/10.1007/s00445-006-0109-y
Belousov A, Belousova M, Krimer D, Costa F, Prambada O, Zaennudin A (2015) Volcaniclastic stratigraphy of Gede Volcano, West Java, Indonesia: how it erupted and when. J Volcanol Geotherm Res 301:238–252. https://doi.org/10.1016/j.jvolgeores.2015.05.018
Belousov A, Belousova M, Hoblitt R, Patia H (2020) The 1951 eruption of Mount Lamington, Papua New Guinea: devastating directed blast triggered by small-scale edifice failure. J Volcanol Geotherm Res 401(2020):106947. https://doi.org/10.1016/j.jvolgeores.2020.106947
Belousova M, Belousov A (1995) Prehistoric and 1933 debris avalanches and associated eruptions of Harimkotan Volcano (Kurile Islands). Per Mineral 64:99–101
Belousova M, Belousov A (2011) Tsunamigenic volcanic landslides of Kurile-Kamchatka arc. Geophys Res Abstr 13:2011 European geosciences union general assembly, Vienna, Austria 3–8 April, 2011
Bernard B (2008) Étude des dépôts d'avalanche de debris volcaniques: analyse sédimentologique d'exemples naturels et identification des mécanismes de mise en place. Dissertation, Université Blaise Pascal-Clermont-Ferrand
Bernard B, Andrade SD (2019) Large volcanic debris avalanches in Ecuador. In: Abstracts volume 8th International Symposium Andean Geodynamics, Quito, Ecuador, 24–26 September 2019
Bernard B, Takarada S, Andrade SD, Dufresne A (2021) Terminology and strategy to describe large volcanic landslides and debris avalanches. In: Roverato M, Dufresne A, Procter J (eds) Volcanic debris avalanches. Advances in Volcanology. Springer, Cham 6:51–73. https://doi.org/10.1007/978-3-030-57411-6_3
Bernard B, van Wyk de Vries B, Barba D, Leyrit H, Robin C, Alcaraz S, Samaniego P (2008) The Chimborazo sector collapse and debris avalanche: deposit characteristics as evidence of emplacement mechanisms. J Volcanol Geotherm Res 176(1):36–43. https://doi.org/10.1016/j.jvolgeores.2008.03.012
Bernard K, van Wyk de Vries B (2017) Volcanic avalanche fault zone with pseudotachylite and gouge in French Massif Central. J Volcanol Geotherm Res 347:112–135. https://doi.org/10.1016/j.jvolgeores.2017.09.006
Bernard K, van Wyk de Vries B, Thouret J-C (2019) Fault textures in volcanic debris-avalanche deposits and transformations into lahars: the Pichu Pichu thrust lobes in south Peru compared to worldwide avalanche deposits. J Volcanol Geotherm Res 371:116–136. https://doi.org/10.1016/j.jvolgeores.2019.01.008
Bernard K, van Wyk de Vries B, Samaniego P, Valderrama P, Mariño J (2022) Collisional interactions and the transition between lava dome sector collapse and pyroclastic density currents at Tutupaca volcano (Southern Peru). J Volcanol Geotherm Res 107668. https://doi.org/10.1016/j.jvolgeores.2022.107668
Biek RF, Rowley PD, Hacker DB (2019) The gigantic Markagunt and Sevier gravity slides resulting from mid-Cenozoic catastrophic mega-scale failure of the Marysvale volcanic field, Utah, USA. Geol Soc Am Field Guide 56:1–121
Biggs J, Lu Z, Fournier T, Freymueller JT (2010) Magma flux at Okmok Volcano, Alaska, from a joint inversion of continuous GPS, campaign GPS, and interferometric synthetic aperture radar. J Geophys Res Solid Earth 115(B12). https://doi.org/10.1029/2010JB007577
Biggs J, Pritchard ME (2017) Global volcano monitoring: what does it mean when volcanoes deform? Elements 13(1):17–22. https://doi.org/10.2113/gselements.13.1.17
Blahůt J, Balek J, Klimeš J, Rowberry M, Kusák M, Kalina J (2019) A comprehensive global database of giant landslides on volcanic islands. Landslides 16:2045–2052. https://doi.org/10.1007/s10346-019-01275-8
Bonforte A, Guglielmino F (2015) Very shallow dyke intrusion and potential slope failure imaged by ground deformation: the 28 December 2014 eruption on Mount Etna. Geophys Res Lett 42(8):2727–2733. https://doi.org/10.1002/2015GL063462

Bonforte A, González PJ, Fernández J (2016) Joint terrestrial and aerial measurements to study ground deformation: application to the Sciara Del Fuoco at the Stromboli Volcano (Sicily). Remote Sens 8(6):463. https://doi.org/10.3390/rs8060463

Borgia A (1994) Dynamic basis of volcanic spreading. J Geophys Res 99(B9):17,791-717,804. https://doi.org/10.1029/94JB00578

Borgia A, Delaney PT, Denlinger RP (2000) Spreading volcanoes. Annu Rev Earth Planet Sci 28(1):539–570. https://doi.org/10.1146/annurev.earth.28.1.539

Borselli L, Capra L, Sarocchi D, De la Cruz-Reyna S (2011) Flank collapse scenarios at Volcán de Colima, Mexico: a relative instability analysis. J Volcanol Geotherm Res 208(1–2):51–65. https://doi.org/10.1016/j.jvolgeores.2011.08.004

Boudon G, Komorowski J-C, Villemant B, Semet MP (2008) A new scenario for the last magmatic eruption of La Soufrière of Guadeloupe (Lesser Antilles) in 1530 AD Evidence from stratigraphy radiocarbon dating and magmatic evolution of erupted products. J Volcanol Geotherm Res 178(3):474–490. https://doi.org/10.1016/j.jvolgeores.2008.03.006

Boudon G, Le Friant A, Komorowski J-C, Deplus C, Semet MP (2007) Volcano flank instability in the Lesser Antilles Arc: diversity of scale, processes, and temporal recurrence. J Geophys Res Solid Earth 112(B8). https://doi.org/10.1029/2006JB004674

Brand BD, Bendaña S, Self S, Pollock N (2016) Topographic controls on pyroclastic density current dynamics: insight from 18 May 1980 deposits at Mount St. Helens, Washington (USA). J Volcanol Geotherm Res 321:1–17. https://doi.org/10.1016/j.jvolgeores.2016.04.018

Brantley SR, Waitt RB (1988) Interrelations among pyroclastic surge, pyroclastic flow, and lahars in Smith Creek Valley during first minutes of 18 May 1980 eruption of Mount St Helens, USA. Bull Volcanol 50:304–326. https://doi.org/10.1007/BF01073588

Bravo T (1962) El circo de Las Cañadas y sus dependencias. Bol Real Soc Esp Hist Nat 60:93–108

Brodsky EE, Gordeev E, Kanamori H (2003) Landslide basal friction as measured by seismic waves. Geophys Res Lett 30(24). https://doi.org/10.1029/2003GL018485

Brown SK, Crosweller HS, Sparks RS, Cottrell E, Deligne NI, Guerrero NO, Hobbs L, Kiyosugi K, Loughlin SC, Siebert L, Takarada S (2014) Characterisation of the Quaternary eruption record: analysis of the Large Magnitude Explosive Volcanic Eruptions (LaMEVE) database. J Appl Volcanol 3(1):1–22. https://doi.org/10.1186/2191-5040-3-5

Browning J, Meredith P, Gudmundsson A (2016) Cooling-dominated cracking in thermally stressed volcanic rocks. Geophys Res Lett 43(16):8417–8425. https://doi.org/10.1002/2016GL070532

Bulmer MH, Wilson JB (1999) Comparison of flat-topped stellate seamounts on Earth's seafloor with stellate domes on Venus using side-scan sonar and Magellan synthetic aperture radar. Earth Planet Sci Lett 171(2):277–287. https://doi.org/10.1016/S0012-821X(99)00154-5

Byrne PK, Holohan EP, Kervyn M, van Wyk de Vries B, Troll VR, Murray JB (2013) A sagging-spreading continuum of large volcano structure. Geology 41(3):339–342. https://doi.org/10.1130/G33990.1

Caballero L, Capra L (2011) Textural analysis of particles from El Zaguán debris avalanche deposit, Nevado de Toluca volcano, Mexico: Evidence of flow behavior during emplacement. J Volcanol Geotherm Res 200:75–82. https://doi.org/10.1016/j.jvolgeores.2010.12.003

Camus G, Diament M, Gloaguen M, Provost A, Vincent P (1992) Emplacement of a debris avalanche during the 1883 eruption of Krakatau (Sunda Straits, Indonesia). Geojoumal 28(2):123–128

Capra L, Macías JL (2000) Pleistocene cohesive debris flows at Nevado de Toluca Volcano, central Mexico. J Volcanol Geotherm Res 102(1–2):149–167. https://doi.org/10.1016/S0377-0273(00)00186-4

Capra L, Macías JL (2002) The cohesive Naranjo debris-flow deposit (10 km^3): a dam breakout flow derived from the Pleistocene debris-avalanche deposit of Nevado de Colima Volcano (México). J Volcanol Geotherm Res 117(1–2):213–235. https://doi.org/10.1016/S0377-0273(02)00245-7

Capra L, Macías JL, Scott KM, Abrams M, Garduño-Monroy VH (2002) Debris avalanches and debris flows transformed from collapses in the Trans-Mexican Volcanic Belt, Mexico—behavior, and implications for hazard assessment. J Volcanol Geotherm Res 113:81–110. https://doi.org/10.1016/S0377-0273(01)00252-9

Carey SN, Sigurdsson H (1982) Influence of particle aggregation on deposition of distal tephra from the May 18, 1980, eruption of Mount St. Helens volcano. J Geophys Res 87(B8):7061–7072. https://doi.org/10.1029/JB087iB08p07061

Carracedo JC (1999) Growth, structure, instability and collapse of Canarian volcanoes and comparisons with Hawaiian volcanoes. J Volcanol Geotherm Res 94(1–4):1–19. https://doi.org/10.1016/S0377-0273(99)00095-5

Carrasco-Nuñez G, Vallance JW, Rose WI (1993) A voluminous avalanche-induced lahar from Citlaltepetl volcano, Mexico: implications for hazard assessment. J Volcanol Geotherm Res 59:35–46. https://doi.org/10.1016/0377-0273(93)90076-4

Carrasco-Núñez G, Díaz-Castellón R, Siebert L, Hubbard B, Sheridan MF, Rodríguez SR (2006) Multiple edifice-collapse events in the Eastern Mexican Volcanic Belt: the role of sloping substrate and implications for hazard assessment. J Volcanol Geotherm Res 158(1–2):151–176. https://doi.org/10.1016/j.jvolgeores.2006.04.025

Cashman KV, Thornber CR, Pallister JS (2008) From dome to dust: shallow crystallization and fragmentation of conduit magma during the 2004–2006 dome extrusion of Mount St. Helens, Washington. In: Sherrod DR, Scott WE, Stauffer PH (eds) A volcano rekindled: the renewed eruption of Mount St. Helens, 2004–2006, U S Geol Surv Prof Pap 1750–19:387–413. https://doi.org/10.3133/pp175019

Cashman KV, Hoblitt RP (2004) Magmatic precursors to the 18 May 1980 eruption of Mount St. Helens, USA. Geology 32(2):141–144. https://doi.org/10.1130/G20078.1

Cecchi E, van Wyk de Vries B, Lavest JM (2004) Flank spreading and collapse of weak–cored volcanoes. Bull Volcanol 67:72–91. https://doi.org/10.1007/s00445-004-0369-3

Chadwick WW Jr, De Roy T, Carrasco A (1991) The September 1988 intracaldera avalanche and eruption at Fernandina volcano, Galapagos Islands. Bull Volcanol 53:276–286. https://doi.org/10.1007/BF00414524

Chadwick WW Jr, Dziak RP, Haxel JH, Embley RW, Matsumoto H (2012) Submarine landslide triggered by volcanic eruption recorded by in situ hydrophone. Geology 40(1):51–54. https://doi.org/10.1130/G32495.1

Chadwick WW Jr, Wright IC, Schwarz-Schampera U, Hyvernaud O, Reymond D, de Ronde CEJ (2008) Cyclic eruptions and sector collapses at Monowai submarine volcano, Kermadec arc: 1998–2007. Geochem Geophys Geosyst 9(10). https://doi.org/10.1029/2008GC002113

Chen Y, Remy D, Froger J-L, Peltier A, Villeneuve N, Darrozes J, Perfettini H, Bonvalot S (2017) Long-term ground displacement observations using InSAR and GNSS at Piton de la Fournaise volcano between 2009 and 2014. Remote Sens Environ 194:230–247. https://doi.org/10.1016/j.rse.2017.03.038

Chiba S, Kimura J-I (2001) Geology and growth history of Bandai volcano, Tohoku-Honshu arc, Japan—analysis of volcanic activity by tephrochronology. Jpn Mag Mineral Petrol Sci 30:126–156 (in Jpn with Engl abstr)

Chouet BA (1996) New methods and future trends in seismological volcano monitoring. Monitoring and mitigation of volcano hazards, Springer, Berlin, Heidelberg, 23–97. https://doi.org/10.1007/978-3-642-80087-0_2

Christiansen RL, Peterson DW (1981) Chronology of the 1980 eruptive activity In: Lipman PW, Mullineaux DR (eds) The 1980 eruptions of Mount St. Helens, Washington. U S Geol Surv Prof Pap 1250:17–30

Clarke D, Brenguier F, Froger J-L, Shapiro NM, Peltier A, Staudacher T (2013) Timing of a large volcanic flank movement at Piton de la Fournaise Volcano using noise-based seismic monitoring and ground deformation measurements. Geophys J Int 195(2):1132–1140. https://doi.org/10.1093/gji/ggt276

Clavero JE, Sparks RSJ, Huppert HE, Dade WB (2002) Geological constraints on the emplacement mechanism of the Parinacota debris avalanche, northern Chile. Bull Volcanol 64:40–54. https://doi.org/10.1007/s00445-001-0183-0

Clavero J, Polanco E, Godoy E, Matthews S, Sparks RSJ, van Wyk de Vries B, Pérez de Arce C, Gérman A (2004) Substrata influence in the transport and emplacement mechanism of the Ollagüe debris avalanche (northern Chile). Acta Vulcanol 16(1/2):1–18

Clement BM, Connor CB, Draper G (1993) Paleomagnetic estimate of the emplacement temperature of the long-runout Nevado de Colima volcanic debris avalanche deposit, Mexico. Earth Planet Sci Lett 120:499–510. https://doi.org/10.1016/0012-821X(93)90260-G

Clouard V, Bonneville A (2004) Submarine landslides in French Polynesia. In: Hekinian R, Cheminée JL, Stoffers P (eds) Oceanic hotspots. Springer, Berlin, Heidelberg, 209–238. https://doi.org/10.1007/978-3-642-18782-7_7

Clynne MA, Calvert AT, Wolfe EW, Evarts RC, Fleck RJ, Lanphere MA (2008) The Pleistocene eruptive history of Mount St. Helens, Washington, from 300,000 to 12,800 years before present In Sherrod DR, Scott WE, Stauffer PH (eds) A volcano rekindled: the renewed eruption of Mount St. Helens, 2004–2006. U S Geol Surv Prof Pap 1750:593–627. https://doi.org/10.3133/pp175028

Collard N, Peiffer L, Taran Y (2020) Heat and fluid flow dynamics of a stratovolcano: the Tacaná Volcanic Complex. Mexico-Guatemala. J Volcanol Geotherm Res 400:106916. https://doi.org/10.1016/j.jvolgeores.2020.106916

Coombs ML, White SM, Scholl DW (2007) Massive edifice failure at Aleutian arc volcanoes. Earth Planet Sci Lett 256:403–418. https://doi.org/10.1016/j.epsl.2007.01.030

Cortés A, Macías JL, Capra L, Garduño-Monroy VH (2010) Sector collapse of the SW flank of Volcán de Colima, México—the 3600 yr BP La Lumbre-Los Ganchos debris avalanche and associated debris flows. J Volcanol Geotherm Res 197:52–66. https://doi.org/10.1016/j.jvolgeores.2009.11.013

Cortés A, Komorowski J-C, Macías JL, Capra L, Layer PW (2019) Late Pleistocene-Holocene debris avalanche deposits from Volcán de Colima, México. In: Varley N, Conner CB, Komorowski J-C (eds) Volcán de Colima portrait of a persistently hazardous volcano. Springer, Berlin, 55–79. https://doi.org/10.1007/978-3-642-25911-1_4

Crandell DR (1989) Gigantic debris avalanche of Pleistocene age from ancestral Mount Shasta volcano, California, and debris-avalanche hazard zonation. U S Geol Surv Bull 1861:1–32

Crandell DR, Fahnestock RK (1965) Rockfalls and avalanches from Little Tahoma Peak on Mount Rainier, Washington. U S Geol Surv Bull 1221-A:1–30

Crandell DR, Mullineaux DR, Sigafoos RS, Rubin M (1974) Chaos Crags eruptions and rockfall–avalanches, Lassen Volcanic National Park, California. J Res U S Geol Surv 2(1):49–59

Criswell CW (1987) Chronology and pyroclastic stratigraphy of the May 18, 1980, eruption of Mount St. Helens,. Washington J Geophys Res 92:10237–10266. https://doi.org/10.1029/JB092iB10p10237

Criswell CW (2021) A revised narrative of the May 18, 1980 Plinian eruption of Mount St. Helens: changes in the conduit and magma supply. J Volcanol Geotherm Res 419:107388. https://doi.org/10.1016/j.jvolgeores.2021.107388

Cronin SJ, Ferland MA, Terry JP (2004) Nabukelevu volcano (Mt. Washington), Kadavu–a source of hitherto unknown volcanic hazard in Fiji. J Volcanol Geotherm Res 131:371–396. https://doi.org/10.1016/S0377-0273(03)00414-1

Crosetto M, Monserrat O, Cuevas-González M, Devanthéry N, Crippa B (2016) Persistent scatterer interferometry: a review. ISPRS J Photogramm Remote Sensing 115:78–89. https://doi.org/10.1016/j.isprsjprs.2015.10.011

Crosta GB, Agliardi F (2003) Failure forecast for large rock slides by surface displacement measurements. Can Geotech J 40(1):176–191. https://doi.org/10.1139/t02-085

Cummins J (1981) Chronology of mudflows in the South Fork and North Fork Toutle River following the May 18 eruption. In: Lipman PW, Mullineaux DR (eds) The 1980 eruptions of Mount St. Helens, Washington. U S Geol Surv Prof Pap 1250:479–486

Dai L, Fan X, Jansen JD, Xu Q (2021) Landslides and fluvial response to landsliding induced by the 1933 Diexi earthquake, Minjiang River, eastern Tibetan Plateau. Landslides 18(9):3011–3025. https://doi.org/10.1007/s10346-021-01717-2

Day SJ (1996) Hydrothermal pore fluid pressure and the stability of porous, permeable volcanoes. In: McGuire WJ, Jones AP, Neuberg J (eds) Volcano instability on the Earth and other planets. Geol Soc Lond Spec Publ 110:77–93. https://doi.org/10.1144/GSL.SP.1996.110.01.06

Day SJ (2015) Volcanic tsunamis. In: Sigurdsson H (ed) The encyclopedia of volcanoes, 2nd edn. Academic Press, Amsterdam, 993–1009. https://doi.org/10.1016/B978-0-12-385938-9.00058-4

De Guidi G, Brighenti F, Carnemolla F, Imposa S, Marchese SA, Palano M, Scudero S, Vecchio A (2018) The unstable eastern flank of Mt. Etna volcano (Italy): first results of a GNSS-based network at its southeastern edge. J Volcanol Geotherm Res 357:418–424. https://doi.org/10.1016/j.jvolgeores.2018.04.027

de Silva SL, Davidson JP, Croudace IW, Escobar A (1993) Volcanological and petrological evolution of volcan Tata Sabaya. SW Bolivia J Volcanol Geotherm Res 55(3–4):305–335. https://doi.org/10.1016/0377-0273(93)90043-Q

del Potro R, Hürlimann M (2009) The decrease in the shear strength of volcanic materials with argillic hydrothermal alteration, insights from the summit region of Teide stratovolcano. Tenerife Eng Geol 104(1–2):135–143. https://doi.org/10.1016/j.enggeo.2008.09.005

del Potro R, Hürlimann M, Pinkerton H (2013) Modelling flank instabilities on stratovolcanoes: parameter sensitivity and stability analyses of Teide, Tenerife. J Volcanol Geotherm Res 256:50–60. https://doi.org/10.1016/j.jvolgeores.2013.02.003

Delaney PT (1982) Rapid intrusion of magma into wet rock: groundwater flow due to pore pressure increases. J Geophys Res 87(B9):7739–7756. https://doi.org/10.1029/JB087iB09p07739

Delaney PT, Pollard DD, Ziony JI, McKee EH (1986) Field relations between dikes and joints: emplacement processes and paleostress analysis. J Geophys Res Solid Earth 91(B5):4920–4938. https://doi.org/10.1029/JB091iB05p04920

Delcamp A, van Wyk de Vries B, James MR (2008) The influence of edifice slope and substrata on volcano spreading. J Volcanol Geotherm Res 177(4):925–943. https://doi.org/10.1016/j.jvolgeores.2008.07.014

Delcamp A, Delvaux D, Kwelwa S, Macheyeki A, Kervyn M (2016a) Sector collapse events at volcanoes in the North Tanzanian

divergence zone and their implications for regional tectonics. Bull Geol Soc Am 128:169–186. https://doi.org/10.1130/B31119.1

Delcamp A, Roberti G, van Wyk de Vries B (2016b) Water in volcanoes: evolution, storage and rapid release during landslides. Bull Volcanol 78:87. https://doi.org/10.1007/s00445-016-1082-8

Deligne NI, Coles SG, Sparks RSJ (2010) Recurrence rates of large explosive volcanic eruptions. J Geophys Res Solid Earth 115(B6). https://doi.org/10.1029/2009JB006554

Deplus C, Bonvalot S, Dahrin D, Diament M, Harjono H, Dubois J (1995) Inner structure of the Krakatau volcanic complex (Indonesia) from gravity and bathymetry data. J Volcanol Geotherm Res 64:23–52. https://doi.org/10.1016/0377-0273(94)00038-I

Deplus C, Le Friant A, Boudon G, Komorowski J-C, Villemant B, Harford C, Ségoufin J, Cheminée JL (2001) Submarine evidence for large-scale debris avalanches in the Lesser Antilles Arc. Earth Planet Sci Lett 192:145–157. https://doi.org/10.1016/S0012-821X(01)00444-7

Devoli G, Cepeda J, Kerle N (2009) The 1998 Casita volcano flank failure revisited—new insights into geological setting and failure mechanisms. Eng Geol 105(1–2):65–83. https://doi.org/10.1016/j.enggeo.2008.12.006

Di Traglia F, Intrieri E, Nolesini T, Bardi F, Del Ventisette C, Ferrigno F, Frangioni S, Frodella W, Gigli G, Lotti A, Stefanelli CT, Tanteri L, Leva D, Casagli N (2014a) The ground-based InSAR monitoring system at Stromboli volcano: linking changes in displacement rate and intensity of persistent volcanic activity. Bull Volcanol 76:786. https://doi.org/10.1007/s00445-013-0786-2

Di Traglia F, Nolesini T, Intrieri E, Mugnai F, Leva D, Rosi M, Casagli N (2014b) Review of ten years of volcano deformations recorded by the ground-based InSAR monitoring system at Stromboli volcano: a tool to mitigate volcano flank dynamics and intense volcanic activity. Earth-Sci Rev 139:317–335. https://doi.org/10.1016/j.earscirev.2014.09.011

Di Traglia F, Nolesini T, Ciampalini A, Solari L, Frodella W, Bellotti F, Fumagalli A, De Rosa G, Casagli N (2018) Tracking morphological changes and slope instability using spaceborne and ground-based SAR data. Geomorphology 300:95–112. https://doi.org/10.1016/j.geomorph.2017.10.023

Dick GJ, Eberhardt E, Cabrejo-Liévano AG, Stead D, Rose ND (2015) Development of an early-warning time-of-failure analysis methodology for open-pit mine slopes utilizing ground-based slope stability radar monitoring data. Can Geotech J 54(2):515–529. https://doi.org/10.1139/cgj-2014-0028

Diefenbach AK, Crider JG, Schilling SP, Dzurisin D (2012) Rapid, low-cost photogrammetry to monitor volcanic eruptions: an example from Mount St. Helens, Washington, USA. Bull Volcanol 74:579–587. https://doi.org/10.1007/s00445-011-0548-y

Donnadieu F, Merle O (1998) Experiments on the indentation process during cryptodome intrusions: new insights into Mount St. Helens Deformation. Geology 26(1):79–82. https://doi.org/10.1130/0091-7613(1998)026%3c0079:EOTIPD%3e2.3.CO;2

Donnadieu F, Merle O (2001) Geometrical constraints of the 1980 Mount St. Helens intrusion from analogue models. Geophys Res Lett 28(4):639–642. https://doi.org/10.1029/2000GL011869

Donnadieu F, Merle O, Besson J-C (2001) Volcanic edifice stability during cryptodome intrusion. Bull Volcanol 63:61–72. https://doi.org/10.1007/s004450000122

Druitt TH (1992) Emplacement of the 18 May 1980 lateral blast deposit ENE of Mount St Helens, Washington. Bull Volcanol 54:554–572. https://doi.org/10.1007/BF00569940

Dufresne A, Davies TR (2009) Longitudinal ridges in mass movement deposits. Geomorphology 105:171–181. https://doi.org/10.1016/j.geomorph.2008.09.009

Dufresne A, Geertsema M (2020) Rock slide–debris avalanches: flow transformation and hummock formation, examples from British Columbia. Landslides 17(1):15–32

Dufresne A, Siebert L, Bernard B (2021a) Distribution and geometric parameters of volcanic debris avalanche deposits In: Roverato M, Dufresne A, Procter J (eds) Volcanic debris avalanches. Adv Volcanol 6:75–90. https://doi.org/10.1007/978-3-030-57411-6_4. Springer, Cham

Dufresne A, Zernack A, Bernard K, Thouret JC, Roverato M (2021b) Sedimentology of volcanic debris avalanche deposits. In: Roverato M, Dufresne A, Procter J (eds) Volcanic debris avalanches. Adv Volcanol 6:175–210. https://doi.org/10.1007/978-3-030-57411-6_8. Springer, Cham

Dufresne A, Siebert L, Bernard B, Sparks RSJ, Takarada S, Clavero J, Belousov A, Belousova M (2008) Volcanic debris avalanche deposit database—a progress report. Abstr, IAVCEI general assembly, Reykjavík, Iceland August 17–22, 2008

Dykes AP, Bromhead EN (2018) The Vaiont landslide: re-assessment of the evidence leads to rejection of the consensus. Landslides 15(9):1815–1832. https://doi.org/10.1007/s10346-018-0996-y

Dzurisin D (2003) A comprehensive approach to monitoring volcano deformation as a window on the eruption cycle. Rev Geophys 41(1). https://doi.org/10.1029/2001RG000107

Dzurisin D (2007) Volcano deformation: geodetic monitoring techniques. Springer, Berlin

Ebmeier SK, Biggs J, Mather TA, Amelung F (2013) Applicability of InSAR to tropical volcanoes: insights from Central America. Geol Soc Lond Spec Publ 380(1):15–37. https://doi.org/10.1144/SP380.2

Ebmeier SK, Biggs J, Muller C, Avard G (2014) Thin-skinned mass-wasting responsible for widespread deformation at Arenal volcano. Front Earth Sci 2:35. https://doi.org/10.3389/feart.2014.00035

Ebmeier SK, Andrews BJ, Araya MC, Arnold DWD, Biggs J, Cooper C, Cottrell E, Furtney M, Hickey J, Jay J, Lloyd R, Parker AL, Pritchard ME, Robertson E, Venzke E, Williamson AL (2018) Synthesis of global satellite observations of magmatic and volcanic deformation: implications for volcano monitoring & the lateral extent of magmatic domains. J Appl Volcanol 7(1):1–26. https://doi.org/10.1186/s13617-018-0071-3

Ekström G, Stark CP (2013) Simple scaling of catastrophic landslide dynamics. Science 339(6126):1416–1419. https://doi.org/10.1126/science.1232887

Elsworth D, Voight B (1995) Dike intrusion as a trigger for large earthquakes and the failure of volcano flanks. J Geophys Res, B 100(4):6005–6024. https://doi.org/10.1029/94JB02884

Elsworth D, Voight B (1996) Evaluation of volcano flank instability triggered by dyke intrusion. Geol Soc Lond, Spec Publ 110(1):45–53. https://doi.org/10.1144/GSL.SP.1996.110.01.03

Elsworth D, Voight B (2001) The mechanics of harmonic gas pressurization and failure of lava domes. Geophys J Int 145(1):187–198. https://doi.org/10.1111/j.1365-246X.2001.00370.x

Endo ET, Malone SD, Noson LL, Weaver CS (1981) Locations, magnitudes, and statistics of the March 20–May 18 earthquake sequence. In: Lipman PW, Mullineaux DR (eds) The 1980 eruptions of Mount St. Helens, Washington. U S Geol Surv Prof Pap 1250:93–108

Endo K, Sumida M, Machida M, Furuichi M (1989) The 1984 collapse and debris avalanche deposits of Ontake Volcano, central Japan. In: Latter JH (ed) Volcanic hazards. Springer-Verlag, Berlin, 210–229. https://doi.org/10.1007/978-3-642-73759-6_14

Esposti Ongaro T, Clarke AB, Voight B, Neri A, Widiwijayanti C (2012) Multiphase flow dynamics of pyroclastic density currents during the May 18, 1980 lateral blast of Mount St. Helens. J Geophys Res 117:B06208. https://doi.org/10.1029/2011JB009081

Evans SG, Hungr O, Clague JJ (2001) Dynamics of the 1984 rock avalanche and associated distal debris flow on Mount Cayley, British Columbia, Canada; implications for landslide hazard on dissected volcanoes. Eng Geol 61:29–51. https://doi.org/10.1016/S0013-7952(00)00118-6

Evans SG (2006). Single-event landslides resulting from massive rock slope failure: characterising their frequency and impact on society. In: Evans SG, Mugnozza GS, Strom A, Hermanns RL (eds) Landslides from massive rock slope failure. NATO Science Series 49. Springer, Dordrecht, 53–73. https://doi.org/10.1007/978-1-4020-4037-5_2

Eychenne J, Cashman K, Rust A, Durant A (2015) Impact of the lateral blast on the spatial pattern and grainsize characteristics of the 18 May 1980 Mount St. Helens fallout deposit. J Geophys Res Solid Earth 120:6018–6038. https://doi.org/10.1002/2015JB012116

Fairchild LH (1987) The importance of lahar initiation process. In: Costa JE, Wieczorek GF (eds) Debris flows/avalanches—process, recognition, and mitigation. Geol Soc Am Rev Eng Geol 7:51–61

Farquharson JI, Heap MJ, Baud P (2016) Strain-induced permeability increase in volcanic rock. Geophys Res Lett 43(22):11603–11610. https://doi.org/10.1002/2016GL071540

Farquharson JI, Wild B, Kushnir ARL, Heap MJ, Baud P, Kennedy B (2019) Acid-induced dissolution of andesite: evolution of permeability and strength. J Geophys Res Solid Earth 124(1):257–273. https://doi.org/10.1029/2018JB016130

Favalli M, Karátson D, Mazzarini F, Pareschi MT, Boschi E (2009) Morphometry of scoria cones located on a volcano flank: a case study from Mt. Etna (Italy), based on high-resolution LiDAR data. J Volcanol Geotherm Res 186(3–4):320–330. https://doi.org/10.1016/j.jvolgeores.2009.07.011

Federico A, Popescu M, Elia G, Fidelibus C, Internò G, Murianni A (2012) Prediction of time to slope failure: a general framework. Environ Earth Sci 66(1):245–256. https://doi.org/10.1007/s12665-011-1231-5

Fell R, Glastonbury J, Hunter G (2007) Rapid landslides: the importance of understanding mechanisms and rupture surface mechanics. Quat J Eng Geol Hydrogeol 40:9–27. https://doi.org/10.1144/1470-9236/06-030

Finn CA, Sisson TW, Deszcz-Pan M (2001) Aerogeophysical measurements of collapse-prone hydrothermally altered zones at Mount Rainier volcano. Nature 409:600–603

Finn CA, Deszcz-Pan M, Ball JL, Bloss BJ, Minsley BJ (2018) Three-dimensional geophysical mapping of shallow water saturated altered rocks at Mount Baker, Washington. Implications for slope stability. J Volcanol Geotherm Res 357:261–275. https://doi.org/10.1016/j.jvolgeores.2018.04.013

Finn CA, Deszcz-Pan M, Anderson ED, John DA (2007) Three-dimensional geophysical mapping of rock alteration and water content at Mount Adams, Washington: Implications for lahar hazards. J Geophys Res Solid Earth 112(B10). https://doi.org/10.1029/2006JB004783

Fisher RV (1990) Transport and deposition of a pyroclastic surge across an area of high relief: the 18 May 1980 eruption of Mount St Helens, Washington. Geol Soc Am Bull 102:1038–1054. https://doi.org/10.1130/0016-7606(1990)102%3c1038:TADOAP%3e2.3.CO;2

Fisher RV, Schmincke H-U (1984) Pyroclastic rocks. Springer-Verlag, New York, p 472

Fisher RV, Glicken HX, Hoblitt RP (1987) May 18, 1980, Mount St. Helens deposits in South Coldwater Creek. Washington J Geophys Res 92:10267–10283

Francis PW, Wells GL (1988) Landsat thematic mapper observation of debris avalanche deposits in the Central Andes. Bull Volcanol 50:258–278. https://doi.org/10.1007/BF01047488

Francis PW, Gardeweg M, Ramirez CF, Rother DA (1985) Catastrophic debris avalanche deposit of Socompa volcano, northern Chile. Geology 13:600–603. https://doi.org/10.1130/0091-7613(1985)13%3c600:CDADOS%3e2.0.CO;2

Froger J-L, Famin V, Cayol V, Augier A, Michon L, Lénat J-F (2015) Time-dependent displacements during and after the April 2007 eruption of Piton de la Fournaise, revealed by interferometric data. J Volcanol Geotherm Res 296:55–68. https://doi.org/10.1016/j.jvolgeores.2015.02.014

Frolova JV, Chernov MS, Rychagov SN, Ladygin VM, Sokolov VN, Kuznetsov RA (2021) The influence of hydrothermal argillization on the physical and mechanical properties of tuffaceous rocks: a case study from the Upper Pauzhetsky thermal field. Kamchatka Bull Eng Geol Environ 80(2):1635–1651. https://doi.org/10.1007/s10064-020-02007-2

Frolova J, Ladygin V, Zukhubaya D (2015) Physical and mechanical properties of rocks in the hydrothermal systems of the Kuril-Kamchatka Island Arc. In: Lollino G, Manconi A, Clague J, Shan W, Chiarle M (eds) Engineering geology for society and territory - volume 1. Springer, Cham, 337–340. https://doi.org/10.1007/978-3-319-09300-0_63

Geertsema M, Clague JJ, Schwab JW, Evans SG (2006) An overview of recent large catastrophic landslides in northern British Columbia, Canada. Eng Geol 83(1–3):120–143. https://doi.org/10.1016/j.enggeo.2005.06.028

Germanovich LN, Lowell RP (1995) The mechanism of phreatic eruptions. J Geophys Res Solid Earth 100(B5):8417–8434. https://doi.org/10.1029/94JB03096

Geronimo-Catane (1995) Debris-avalanche occurrence at Philippine volcanoes: an overview. Proceedings workshop on debris avalanche and debris flow of volcanoes, March 7–11, 1995 Tsukuba Japan, Sci Tech Agency Jpn, Nat Inst Earth Sci Disaster Prevention, 59–69

Ghorbani A, Revil A, Coperey A, Ahmed AS, Roque S, Heap MJ, Grandis H, Viveiros F (2018) Complex conductivity of volcanic rocks and the geophysical mapping of alteration in volcanoes. J Volcanol Geotherm Res 357:106–127. https://doi.org/10.1016/j.jvolgeores.2018.04.014

Giampiccolo E, Cocina O, De Gori P, Chiarabba C (2020) Dyke intrusion and stress-induced collapse of volcano flanks: the example of the 2018 event at Mt. Etna (Sicily, Italy). Sci Rep 10(1):1–8. https://doi.org/10.1038/s41598-020-63371-3

Ginibre C, Wörner G (2007) Variable parent magmas and recharge regimes of the Parinacota magma system (N. Chile) revealed by Fe, Mg and Sr zoning in plagioclase. Lithos 98(1–4):118–140. https://doi.org/10.1016/j.lithos.2007.03.004

Glicken H (1986) Rockslide-debris avalanche of May 18, 1980, Mount St. Helens Volcano, Washington. Dissertation, University of California Santa Barbara, California, p 303

Glicken H (1990) The rockslide-debris avalanche of the May 18, 1980, eruption of Mount St. Helens—10th anniversary perspectives. Geosci Can 17:150–153

Glicken H (1991) Sedimentary architecture of large volcanic-debris avalanches. In: Fisher RV, Smith GA (eds) Sedimentation in volcanic settings. SEPM Spec Publ 45:99–106

Glicken H (1996) Rockslide-debris avalanche of May 18, 1980, Mount St. Helens Volcano, Washington. U S Geol Surv Open-file Rep 96–677:1–90 (and 5 plates)

Glicken H, Asmoro P, Lubia H, Frank D, Casadevall TC (1987) The 1772 debris avalanche and eruption at Papandayan volcano, Indonesia, and hazards from future similar events. In: Hawaii symposium on how volcanoes work (abstr) U S Geol Surv Hawaii Volc Observ

Gonzales K, Finizola A, Lénat JF, Macedo O, Ramos D, Thouret JC, Fournier N, Cruz V, Pistre K (2014) Asymmetrical structure, hydrothermal system and edifice stability: the case of Ubinas

volcano, Peru, revealed by geophysical surveys. J Volcanol Geotherm Res 276:132–144. https://doi.org/10.1016/j.jvolgeores.2014.02.020

Gorshkov GS (1959) Gigantic eruption of the volcano Bezymianny. Bull Volcanol 20:77–109. https://doi.org/10.1007/BF02596572

Gorshkov GS, Dubik YM (1970) Gigantic directed blast at Shiveluch volcano (Kamchatka). Bull Volcanol 34:261–288. https://doi.org/10.1007/BF02597790

Griggs RF (1920) The great Mageik landslide. Ohio J Sci 20:325–354

Grosse P, Danišík M, Apaza FD, Guzmán SR, Lahitte P, Quidelleur X, Self S, Siebe C, van Wyk de Vries B, Ureta G, Guillong M, De Rosa R, Le Roux P, Wotzlaw J-F, Bachman O (2022) Holocene collapse of Socompa volcano and pre-and post-collapse growth rates constrained by multi-system geochronology. Bull Volcanol 84(9):1–18. https://doi.org/10.1007/s00445-022-01594-0

Guilbaud MN, Chédeville C, Molina-Guadarrama ÁN, Pineda-Serrano JC, Siebe C (2022) Volcano-sedimentary processes at Las Derrumbadas rhyolitic twin domes, Serdán-Oriental basin, Eastern Trans-Mexican Volcanic Belt. Geol Soc Lond Spec Publ 17:520. https://doi.org/10.1144/SP520-2021-144

Guthrie RH, Friele P, Allstadt K, Roberts N, Evans SG, Delaney KB, Roche D, Clague JJ, Jakob M (2012) The 6 August 2010 Mount Meager rock slide-debris flow, Coast Mountains, British Columbia: characteristics, dynamics, and implications for hazard and risk assessment. Nat Hazard Earth Sys Sci 12(5):1277–1294. https://doi.org/10.5194/nhess-12-1277-2012

Hacker DB, Biek RF, Rowley PD (2014) Catastrophic emplacement of the gigantic Markagunt gravity slide, southwest Utah—implications for hazards associated with sector collapse of volcanic fields. Geology 42(11):943–946. https://doi.org/10.1130/G35896.1

Hadley JB (1978) Madison Canyon Rockslide, Montana, U.S.A. In: Developments in geotechnical engineering 14(A):167–180, Elsevier. https://doi.org/10.1016/B978-0-444-41507-3.50012-X

Hao S, Liu C, Lu C, Elsworth D (2016) A relation to predict the failure of materials and potential application to volcanic eruptions and landslides. Sci Rep 6:27877. https://doi.org/10.1038/srep27877

Hasegawa HS, Kanamori H (1987) Source mechanism of the magnitude 7.2 Grand Banks earthquake of November 1929: double couple or submarine landslide? Bull Seism Soc Am 77(6):1984–2004

Hausback BP (2000) Geologic map of the Sasquatch Steps area, north flank of Mount St. Helens, Washington. U S Geol Surv, Geol Invest Series Map I-2463 scale 1:14,000

Hausback BP, Swanson DA (1990) Record of pre-historic debris avalanches on the north flank of Mount St. Helens. Washington Geosci Can 17:142–145

Heap MJ, Violay MES (2021) The mechanical behaviour and failure modes of volcanic rocks: a review. Bull Volcanol 83(5):1–47. https://doi.org/10.1007/s00445-021-01447-2

Heap MJ, Baud P, Meredith PG, Vinciguerra S, Bell AF, Main IG (2011) Brittle creep in basalt and its application to time-dependent volcano deformation. Earth Planet Sci Lett 307(1–2):71–82. https://doi.org/10.1016/j.epsl.2011.04.035

Heap MJ, Mollo S, Vinciguerra S, Lavallée Y, Hess K-U, Dingwell DB, Baud P, Iezzi G (2013) Thermal weakening of the carbonate basement under Mt. Etna volcano (Italy): implications for volcano instability. J Volcanol Geotherm Res 250:42–60. https://doi.org/10.1016/j.jvolgeores.2012.10.004

Heap MJ, Kennedy BM, Pernin N, Jacquemard L, Baud P, Farquharson JI, Scheu B, Lavallée Y, Gilg HA, Letham-Brake M, Mayer K, Jolly JD, Reuschlé T, Dingwell DB (2015) Mechanical behaviour and failure modes in the Whakaari (White Island volcano) hydrothermal system, New Zealand. J Volcanol Geotherm Res 295:26–42. https://doi.org/10.1016/j.jvolgeores.2015.02.012

Heap MJ, Reuschlé T, Farquharson JI, Baud P (2018) Permeability of volcanic rocks to gas and water. J Volcanol Geotherm Res 354:29–38. https://doi.org/10.1016/j.jvolgeores.2018.02.002

Heap MJ, Troll VR, Kushnir ARL, Gilg HA, Collinson ASD, Deegan FM, Darmawan H, Seraphine N, Neuberg J, Walter TR (2019) Hydrothermal alteration of andesitic lava domes can lead to explosive volcanic behaviour. Nature Commun 10(1):1–10. https://doi.org/10.1038/s41467-019-13102-8

Heap MJ, Gravley DM, Kennedy BM, Gilg HA, Bertolett E, Barker SLL (2020) Quantifying the role of hydrothermal alteration in creating geothermal and epithermal mineral resources: the Ohakuri ignimbrite (Taupō Volcanic Zone, New Zealand). J Volcanol Geotherm Res 390:106703. https://doi.org/10.1016/j.jvolgeores.2019.106703

Heap MJ, Baumann T, Gilg HA, Kolzenburg S, Ryan AG, Villeneuve M, Russell JK, Kennedy LA, Rosas-Carbajal M, Clynne MA (2021a) Hydrothermal alteration can result in pore pressurization and volcano instability. Geology 49(11):1348–1352. https://doi.org/10.1130/G49063.1

Heap MJ, Baumann TS, Rosas-Carbajal M, Komorowski J-C, Gilg HA, Villeneuve M, Moretti R, Baud P, Carbillet L, Harnett C, Reuschlé T (2021b) Alteration-induced volcano instability at La Soufrière de Guadeloupe (Eastern Caribbean). J Geophys Res Solid Earth 126(8):e2021JB022514. https://doi.org/10.1029/2021JB022514

Heap MJ, Wadsworth FB, Heng Z, Xu T, Griffiths L, Velasco AA, Vairé E, Vistour M, Reuschlé T, Troll VR, Deegan FM, Tang C (2021c) The tensile strength of volcanic rocks: experiments and models. J Volcanol Geotherm Res 418:107348. https://doi.org/10.1016/j.jvolgeores.2021.107348

Herrick JA, Siebert L, Rose WI (2013) Large-volume Barriles and Caisán debris avalanche deposits from Volcán Barú, Panama. In: Rose WI, Palma JL, Delgado Granados H, Varley N (eds) Understanding open-vent volcanism and related hazards. Geol Soc Am Spec Pap 498:1–22. https://doi.org/10.1130/2013.2498(09)

Hewitt K (1998) Catastrophic landslides and their effects on the Upper Indus streams, Karakoram Himalaya, northern Pakistan. Geomorphology 26(1–3):47–80. https://doi.org/10.1016/S0169-555X(98)00051-8

Hoblitt RP (2000) Was the 18 May 1980 lateral blast at Mt St Helens the product of two explosions? Phil Trans Roy Soc Lond 358:1639–1661. https://doi.org/10.1098/rsta.2000.0608

Hoblitt RP, Miller CD, Vallance JW (1981) Origin and stratigraphy of the deposit produced by May 18 directed blast. In: Lipman PW, Mullineaux DR (eds) The 1980 eruptions of Mount St. Helens, Washington. U S Geol Surv Prof Pap 1250:401–419

Holcomb RT, Searle RC (1991) Large landslides from oceanic volcanoes. Mar Georesour Geotech 10(1–2):19–32. https://doi.org/10.1080/10641199109379880

Hooper A (2008) A multi-temporal InSAR method incorporating both persistent scatterer and small baseline approaches. Geophys Res Lett 35(16). https://doi.org/10.1029/2008GL034654

Hotta K, Iguchi M, Ohkura T, Yamamoto K (2016) Multiple-pressure-source model for ground inflation during the period of high explosivity at Sakurajima volcano, Japan—combination analysis of continuous GNSS, tilt and strain data. J Volcanol Geotherm Res 310:12–25. https://doi.org/10.1016/j.jvolgeores.2015.11.017

Hotz PE (1977) Geology of Yreka quadrangle, Siskiyou County, California. U S Geol Surv Bull 1436:1–72

Hoyt DV (1978) An explosive volcanic eruption in the Southern Hemisphere in 1928. Nature 275:630–632. https://doi.org/10.1038/275630a0

Hsü KJ (1975) Catastrophic debris streams (Sturzstroms) generated by rockfalls. Geol Soc Am Bull 86:129–140. https://doi.org/10.1130/0016-7606(1975)86%3c129:CDSSGB%3e2.0.CO;2

Huggel C, Caplan-Auerbach J, Waythomas CF, Wessels RL (2007) Monitoring and modeling ice-rock avalanches from ice-capped volcanoes: a case study of frequent large avalanches on Iliamna Volcano, Alaska. J Volcanol Geotherm Res 168(1–4):114–136. https://doi.org/10.1016/j.jvolgeores.2007.08.009

Hughes A, Kendrick JE, Salas G, Wallace PA, Legros F, Di Toro D, Lavallée Y (2020) Shear localisation, strain partitioning and frictional melting in a debris avalanche generated by volcanic flank collapse. J Struct Geol 140:104132. https://doi.org/10.1016/j.jsg.2020.104132

Hunt JE, Talling PJ, Clare MA, Jarvis I, Wynn RB (2014) Long-term (17 Ma) turbidite record of the timing and frequency of large flank collapses of the Canary Islands. Geochem Geophys Geosyst 15:3322–3345. https://doi.org/10.1002/2014GC005232

Hurwitz S, Kipp KL, Ingebritsen SE, Reid ME (2003) Groundwater flow, heat transport, and water table position within volcanic edifices: implications for volcanic processes in the Cascade Range. J Geophys Res 108(B12). https://doi.org/10.1029/2003JB002565

Inokuchi T (1985) The Ontake rockslide and debris avalanche caused by the Naganoken-Seibu earthquake, 1984. In: Proceedings 4th international conference and field workshop on landslides, Tokyo, 329–338

Inokuchi T (1988) Gigantic landslides and debris avalanches on volcanoes in Japan: case studies on Bandai, Chokai, and Iwate Volcanoes. Rep Nat Res Center Disaster Prev 41:163–275 (in Jpn with Engl abstr)

Inokuchi T (2006) Properties of sector-collapse and debris avalanche on quaternary volcanoes in Japan. J Jpn Landslide Soc 42(5):409–420. https://doi.org/10.3313/jls.42.5_409. (in Jpn with Engl abstr)

Inoue K (1999) Shimabara-Shigatusaku earthquake and topographic changes by Shimabara Catastrophe in 1792. J Jpn Soc Erosion Control Eng 54(2):45–54 (in Jpn with Engl Abstr)

Intrieri E, Gigli G (2016) Landslide forecasting and factors influencing predictability. Nat Hazard Earth Syst 16(12):2501–2510. https://doi.org/10.5194/nhess-16-2501-2016

Intrieri E, Di Traglia F, Del Ventisette C, Gigli G, Mugnai F, Luzi G, Casagli N (2013) Flank instability of Stromboli volcano (Aeolian Islands, Southern Italy): integration of GB-InSAR and geomorphological observations. Geomorphology 201:60–69. https://doi.org/10.1016/j.geomorph.2013.06.007

Intrieri E, Carlà T, Gigli G (2019) Forecasting the time of failure of landslides at slope-scale: a literature review. Earth-Sci Rev 193:333–349. https://doi.org/10.1016/j.earscirev.2019.03.019

Iverson RM (1995) Can magma-injection and groundwater forces cause massive landslides on Hawaiian volcanoes? J Volcanol Geotherm Res 66(1–4):295–308. https://doi.org/10.1016/0377-0273(94)00064-N

Iverson RM, Reid ME (1992) Gravity-driven groundwater flow and slope failure potential, 1, elastic effective-stress model. Water Resour Res 28(3):925–938. https://doi.org/10.1029/91WR02694

Janda RJ, Scott KM, Nolan KM, Martinson HA (1981) Lahar movement, effects, and deposits In: Lipman PW, Mullineaux DR (eds) The 1980 eruptions of Mount St. Helens, Washington. U S Geol Surv Prof Pap 1250:461–478

John DA, Sisson TW, Breit GN, Rye RO, Vallance JW (2008) Characteristics, extent and origin of hydrothermal alteration at Mount Rainier Volcano, Cascades Arc, USA: implications for debris-flow hazards and mineral deposits. J Volcanol Geotherm Res 175(3):289–314. https://doi.org/10.1016/j.jvolgeores.2008.04.004

Johnson RW (1987) Large-scale volcanic cone collapse: the 1888 slope failure of Ritter volcano, and other examples from Papua New Guinea. Bull Volcanol 49:669–679. https://doi.org/10.1007/BF01080358

Johnson CG, Kokelaar BP, Iverson RM, Logan M, LaHusen RG, Gray JMNT (2012) Grain-size segregation and levee formation in geophysical mass flows. J Geophys Res-Earth Surf 117:F01032. https://doi.org/10.1029/2011JF002185

Johnson PJ, Valentine GA, Stauffer PH, Lowry CS, Sonder I, Pulgarín BA, Santacoloma CC, Agudelo A (2018) Groundwater drainage from fissures as a source for lahars. Bull Volcanol 80(4):1–13. https://doi.org/10.1007/s00445-018-1214-4

Johnson J, Ramón P, Andrade D, Hall M (2006) Reventador volcano 2002 to present, explosive and effusive activity. In: Fourth conference cities on volcanoes, IAVCEI, Quito-Ecuador, Field Guide, Excursion A 5:1–16

Kanamori H, Given JW (1982) Analysis of long-period seismic waves excited by the May 18, 1980, eruption of Mount St Helens—a terrestrial monopole? J Geophys Res 87:5422–5432. https://doi.org/10.1029/JB087iB07p05422

Kanamori H, Given JW, Lay T (1984) Analysis of seismic body waves excited by the Mount St Helens eruption of May 18, 1980. J Geophys Res 89:1856–1866. https://doi.org/10.1029/JB089iB03p01856

Karakhanian A, Djrbashian R, Trifonov V, Philip H, Arakelian S, Avagian A (2002) Holocene-historical volcanism and active faults as natural risk factors for Armenia and adjacent countries. J Volcanol Geotherm Res 113(1–2):319–344. https://doi.org/10.1016/S0377-0273(01)00264-5

Karstens J, Kelfoun K, Watt SFL, Berndt C (2020) Combining 3D seismics, eyewitness accounts and numerical simulations to reconstruct the 1888 Ritter Island sector collapse and tsunami. Int J Earth Sci 109(8):2659–2677. https://doi.org/10.1007/s00531-020-01854-4

Keefer DK (1984) Landslides caused by earthquakes. Geol Soc Am Bull 95(4):406–421

Keigler R, Thouret J-C, Hodgson KA, Neall VE, Lecointre JA, Procter JN, Cronin SJ (2011) The Whangaehu Formation: Debris-avalanche and lahar deposits from ancestral Ruapehu volcano, New Zealand. Geomorphology 133(1–2):57–79. https://doi.org/10.1016/j.geomorph.2011.06.019

Kendrick JE, Lavallée Y, Ferk A, Perugini D, Leonhardt R, Dingwell DB (2012) Extreme frictional processes in the volcanic conduit of Mount St. Helens (USA) during the 2004–2008 eruption. J Struct Geol 38:61–76. https://doi.org/10.1016/j.jsg.2011.10.003

Kendrick JE, Smith R, Sammonds P, Meredith PG, Dainty M, Pallister JS (2013) The influence of thermal and cyclic stressing on the strength of rocks from Mount St. Helens, Washington. Bull Volcanol 75(7):1–12. https://doi.org/10.1007/s00445-013-0728-z

Kendrick JE, Schaefer LN, Schauroth J, Bell AF, Lamb OD, Lamur A, Miwa T, Coats R, Lavallée Y, Kennedy BM (2021) Physical and mechanical rock properties of a heterogeneous volcano: the case of Mount Unzen. Japan Solid Earth 12(3):633–664. https://doi.org/10.5194/se-12-633-2021

Kereszturi G, Schaefer LN, Miller C, Mead S (2020) Hydrothermal alteration on composite volcanoes: mineralogy, hyperspectral imaging, and aeromagnetic study of Mt Ruapehu, New Zealand. Geochem Geophys Geosyst 21(9):e2020GC009270. https://doi.org/10.1029/2020GC009270

Kereszturi G, Schaefer L, Mead S, Miller C, Procter J, Kennedy B (2021) Synthesis of hydrothermal alteration, rock mechanics and geophysical mapping to constrain failure and debris avalanche hazards at Mt. Ruapehu (New Zealand). New Zeal J Geol Geophys 64(2–3):421–442. https://doi.org/10.1080/00288306.2021.1885048

Kerle N, van Wyk de Vries B, Oppenheimer C (2003) New insight into the factors leading to the 1998 flank collapse and lahar disaster at Casita volcano Nicaragua. Bull Volcanol 65(5):331–345. https://doi.org/10.1007/s00445-002-0263-9

Kern C, Aiuppa A, de Moor JM (2022) A golden era for volcanic gas geochemistry? Bull Volcanol 84:43. https://doi.org/10.1007/s00445-022-01556-6

Kervyn M, van Wyk de Vries B, Walter TR, Njome MS, Suh CE, Ernst GGJ (2014) Directional flank spreading at Mount Cameroon volcano: evidence from analogue modeling. J Geophys Res Solid Earth 119(10):7542–7563. https://doi.org/10.1002/2014JB011330

Kieffer SW (1981a) Blast dynamics at Mount St Helens on 18 May 1980. Nature 291:568–570. https://doi.org/10.1038/291568a0

Kieffer SW (1981b) Fluid dynamics of the May 18 blast at Mount St. Helens. In: Lipman PW, Mullineaux DR (eds) The 1980 eruptions of Mount St. Helens, Washington. U S Geol Surv Prof Pap 1250:379–400

Kieffer SW, Sturtevant B (1988) Erosional furrows formed during the lateral blast at Mount St Helens, May 18, 1980. J Geophys Res 93:14793–14816. https://doi.org/10.1029/JB093iB12p14793

Kilburn CRJ (2003) Multiscale fracturing as a key to forecasting volcanic eruptions. J Volcanol Geotherm Res 125(3–4):271–289. https://doi.org/10.1016/S0377-0273(03)00117-3

Kilburn CRJ (2018) Forecasting volcanic eruptions: beyond the failure forecast method. Front Earth Sci 6:133. https://doi.org/10.3389/feart.2018.00133

Kilburn CRJ, Voight B (1998) Slow rock fracture as eruption precursor at Soufriere Hills volcano, Montserrat. Geophys Res Lett 25(19):3665–3668. https://doi.org/10.1029/98GL01609

Kiyosugi K, Connor C, Sparks RSJ, Crosweller HS, Brown SK, Siebert L, Wang T, Takarada S (2015) How many explosive eruptions are missing from the geologic record? Analysis of the quaternary record of large magnitude explosive eruptions in Japan. J Applied Volcanol 4(1):1–15. https://doi.org/10.1186/s13617-015-0035-9

Koga S (2002) The catastrophe in Shimabara. The 1791–92 eruption of Unzen Fugendake and the sector collapse of Mayu-Yama. Unzen Restoration Office, 21. https://www.qsr.mlit.go.jp/unzen/wlib/pdf/010101b.pdf

Komorowski J-C, Glicken HX, Sheridan MF (1991) Secondary electron imagery of microcracks and hackly fracture surfaces in sand-size clasts from the 1980 Mount St Helens debris-avalanche deposit: implications for particle-particle interactions. Geology 19(3):261–264. https://doi.org/10.1130/0091-7613(1991)019%3c0261:SEIOMA%3e2.3.CO;2

Krastel S, Schmincke H-U, Jacobs CL, Rihm R, Le Bas TP, Alibés B (2001) Submarine landslides around the Canary Islands. J Geophys Res 106(B3):3977–3997. https://doi.org/10.1029/2000JB900413

Krimmel RM, Post A (1981) Oblique aerial photography, March–October 1980. In: Lipman PW, Mullineaux DR (eds) The 1980 eruptions of Mount St. Helens, Washington. U S Geol Surv Prof Pap 1250:31–51

Kuraoka S, Nakashima Y, Doke R, Mannen K (2018) Monitoring ground deformation of eruption center by ground-based interferometric synthetic aperture radar (GB-InSAR): a case study during the 2015 phreatic eruption of Hakone volcano. Earth Planets Space 70(1):1–9. https://doi.org/10.1186/s40623-018-0951-0

Lagmay AMF, Valdivia W (2006) Regional stress influence on the opening direction of crater amphitheaters in Southeast Asian volcanoes. J Volcanol Geotherm Res 158(1–2):139–150. https://doi.org/10.1016/j.jvolgeores.2006.04.020

Lagmay AMF, van Wyk de Vries B, Kerle N, Pyle DM (2000) Volcano instability induced by strike-slip faulting. Bull Volcanol 62(4):331–346. https://doi.org/10.1007/s004450000103

Lambe TW, Whitman RV (1969) Soil mechanics. John Wiley & Sons, New York, p 553

Lamur A, Kendrick JE, Eggertsson GH, Wall RJ, Ashworth JD, Lavallée Y (2017) The permeability of fractured rocks in pressurised volcanic and geothermal systems. Sci Rep 7(1):1–9. https://doi.org/10.1038/s41598-017-05460-4

Lanari R, Lundgren P, Sansosti E (1998) Dynamic deformation of Etna volcano observed by satellite radar interferometry. Geophys Res Lett 25(10):1541–1544. https://doi.org/10.1029/98GL00642

Latter JH (1981) Tsunamis of volcanic origin: summary of causes, with particular reference to Krakatoa, 1883. Bull Volcanol 44(3):467–490. https://doi.org/10.1007/BF02600578

Lavallée Y, Kendrick JE (2021) A review of the physical and mechanical properties of volcanic rocks and magmas in the brittle and ductile regimes. In: Papale P (ed) Forecasting and planning for volcanic hazards, risks, and disasters. Elsevier, Amsterdam, 153–238. https://doi.org/10.1016/B978-0-12-818082-2.00005-6

Lavigne F, Degeai J-P, Komorowski J-C, Guillet S, Robert V, Lahitte P, Oppenheimer C, Stoffel M, Vidal CM, Surono Pratomo I, Wassmer P, Hajdas I, Danang Sri Hadmoko DS, de Belizal E (2013) Source of the great A.D. 1257 mystery eruption unveiled, Samalas volcano, Rinjani Volcanic Complex, Indonesia. Proc Nat Acad Sci 110(42):16742–16747. https://doi.org/10.1073/pnas.1307520110

Legros F (2002) The mobility of long-runout landslides. Eng Geol 63:301–331. https://doi.org/10.1016/S0013-7952(01)00090-4

Legros F, Cantagrel J-M, Devouard B (2000) Pseudotachylyte (frictionite) at the base of the Arequipa volcanic landslide deposit (Peru): implications for emplacement mechanisms. J Geol 108:601–611. https://doi.org/10.1086/314421

Lerner GA, Jenkins SF, Charbonnier SJ, Komorowski J-C, Baxter PJ (2022) The hazards of unconfined pyroclastic density currents: a new synthesis and classification according to their deposits, dynamics, and thermal and impact characteristics. J Volcanol Geotherm Res 421:107429. https://doi.org/10.1016/j.jvolgeores.2021.107429

Lipman PW, Moore JG, Swanson DA (1981) Bulging of the north flank before the May 18 eruption—geodetic data. In: Lipman PW, Mullineaux DR (eds) The 1980 eruptions of Mount St. Helens, Washington. U S Geol Surv Prof Pap 1250:143–155

Lipman PW, Mullineaux DR (eds) (1981) The 1980 eruptions of Mount St. Helens, Washington. U S Geol Surv Prof Pap 1250:1–844. https://doi.org/10.3133/pp1250

Lipovsky PS, Evans SG, Clague JJ, Hopkinson C, Couture R, Bobrowsky P, Ekström G, Demuth MN, Delaney KB, Roberts NJ, Clarke G, Schaeffer A (2008) The July 2007 rock and ice avalanches at Mount Steele, St Elias Mountains, Yukon, Canada. Landslides 5(4):445–455. https://doi.org/10.1007/s10346-008-0133-4

Loew S, Gschwind S, Gischig V, Keller-Signer A, Valenti G (2016) Monitoring and early warning of the 2012 Preonzo catastrophic rockslope failure. Landslides 14(1):141–154. https://doi.org/10.1007/s10346-016-0701-y

López DL, Williams SN (1993) Catastrophic volcanic collapse; relation to hydrothermal processes. Science 260(5115):1794–1796. https://doi.org/10.1126/science.260.5115.1794

Lu Z, Masterlark T, Dzurisin D (2005) Interferometric synthetic aperture radar study of Okmok volcano, Alaska, 1992–2003: magma supply dynamics and postemplacement lava flow deformation. J Geophys Res Solid Earth 110(B2). https://doi.org/10.1029/2004JB003148

Lucas A, Mangeney A, Ampuero JP (2014) Frictional velocity-weakening in landslides on Earth and on other planetary bodies. Nat Commun 5(1):1–9. https://doi.org/10.1038/ncomms4417

Lundgren P, Casu F, Manzo M, Pepe A, Berardino P, Sansosti E, Lanari R (2004) Gravity and magma induced spreading of Mount Etna volcano revealed by satellite radar interferometry. Geophys Res Lett 31:L04602. https://doi.org/10.1029/2003GL018736

Maccaferri F, Richter N, Walter TR (2017) The effect of giant lateral collapses on magma pathways and the location of volcanism. Nature Commun 8:1097. https://doi.org/10.1038/s41467-017-01256-2

Mace CW, Smith L (1987) Effects of frictional heating on the thermal, hydrologic, and mechanical response of a fault. J Geophys Res 92(B7):6249–6272

Macfarlane DG, Wadge G, Robertson DA, James MR, Pinkerton H (2006) Use of a portable topographic mapping millimetre wave radar at an active lava flow. Geophys Res Lett 33:L03301. https://doi.org/10.1029/2005GL025005

Macías JL, Arce JL, García-Palomo A, Mora JC, Layer PW, Espíndola JM (2010) Late-Pleistocene flank collapse triggered by dome growth at Tacaná volcano, México-Guatemala, and its relationship to the regional stress regime. Bull Volcanol 72(1):33–53. https://doi.org/10.1007/s00445-009-0303-9

MacLeod N (1989) Sector-Failure in Indonesian volcanoes. Geol Indon 12(1):563–601

Major JJ, Scott KM (1988) Volcaniclastic sedimentation in the Lewis River valley, Mount St. Helens, Washington—processes, extent, and hazards. U S Geol Surv Bull 1383-D:1–38

Malone SD, Endo ET, Weaver CS, Ramey JW (1981) Seismic monitoring for eruption prediction. In: Lipman PW, Mullineaux DR (eds) The 1980 eruptions of Mount St. Helens, Washington. U S Geol Surv Prof Pap 1250:803–813

Manconi A, Longpré MA, Walter TR, Troll VR, Hansteen TH (2009) The effects of flank collapses on volcano plumbing systems. Geology 37(12):1099–1102. https://doi.org/10.1130/G30104A.1

Mariño J, Samaniego P, Manrique N, Valderrama P, Roche O, van Wyk de Vries B, Guillou H, Zerathe S, Arias C, Liorzou C (2021) The Tutupaca volcanic complex (Southern Peru): eruptive chronology and successive destabilization of a dacitic dome complex. J S Am Earth Sci 109:103227. https://doi.org/10.1016/j.jsames.2021.103227

Martí J (2019) Las Cañadas caldera, Tenerife, Canary Islands: a review, or the end of a long volcanological controversy. Earth-Sci Rev 196:102889. https://doi.org/10.1016/j.earscirev.2019.102889

Masson DG, Watts AB, Gee MJR, Urgeles R, Mitchell NC, Le Bas TP, Canals M (2002) Slope failures on the flanks of the western Canary Islands. Earth Sci-Rev 57(1–2):1–35. https://doi.org/10.1016/S0012-8252(01)00069-1

Masson DG, Le Bas TP, Grevemeyer I, Weinrebe W (2008) Flank collapse and large-scale landsliding in the Cape Verde Islands, off West Africa. Geochem Geophys Geosyst 9(7). https://doi.org/10.1029/2008GC001983

Mastin LG, Carey SN, Van Eaton AR, Eychenne J, Sparks RSJ (2023) Understanding and modeling tephra transport: lessons learned from the 18 May 1980 eruption of Mount St. Helens. Bull Volcanol 85(1):1–21. https://doi.org/10.1007/s00445-022-01613-0

McGovern PJ, Smith JR, Morgan JK, Bulmer MH (2004) Olympus Mons aureole deposits: new evidence for a flank failure origin. J Geophys Res: Planets. 109(E8). https://doi.org/10.1029/2004JE002258

McGuire WJ (1996) Volcano instability: a review of contemporary themes. In: McGuire WJ, Jones AP, Nueberg J (eds) Volcano instability on the Earth and other planets. Geol Soc Lond Spec Publ 110:1–23

McGuire WJ (2006) Lateral collapse and tsunamigenic potential of marine volcanoes. Geol Soc Lond Spec Publ 269(1):121–140. https://doi.org/10.1144/GSL.SP.2006.269.01.08

McGuire WJ, Pullen AD (1989) Location and orientation of eruptive fissures and feederdykes at Mount Etna; influence of gravitational and regional tectonic stress regimes. J Volcanol Geotherm Res 38(3–4):325–344. https://doi.org/10.1016/0377-0273(89)90046-2

McGuire WJ, Pullen AD, Saunders SJ (1990) Recent dyke-induced large-scale block movement at Mount Etna and potential slope failure. Nature 343(6256):357–359. https://doi.org/10.1038/343357a0

McMurtry GM, Watts P, Fryer GJ, Smith JR, Imamura F (2004) Giant landslides, mega-tsunamis, and paleo-sea level in the Hawaiian Islands. Mar Geol 203:219–233. https://doi.org/10.1016/S0025-3227(03)00306-2

McSaveney MJ (1978) Sherman glacier rock avalanche, Alaska, USA. In: Voight B (ed) Natural phenomena. Rockslides and avalanches, vol. 1. Elsevier, New York, 197–258. https://doi.org/10.1016/B978-0-444-41507-3.50014-3

Mehl KW, Schmincke H-U (1999) Structure and emplacement of the Pliocene Roque Nublo debris avalanche deposit, Gran Canaria, Spain. J Volcanol Geotherm Res 94(1–4):105–134. https://doi.org/10.1016/S0377-0273(99)00100-6

Melekestsev IV (2006) Large modern collapses on the active volcanoes of Kamchatka: causes and mechanism of formation. In: Evans, SG, Mugnozza GS, Strom A, Hermanns RL (eds) Landslides from massive rock slope failure. NATO Sci Ser 49:431–444. https://doi.org/10.1007/978-1-4020-4037-5_23. Springer, Dordrecht

Melekestsev IV, Braitseva OA (1988) Giant Collapses on volcanoes. Volcanol Seismol 6:495–508

Merle O, Borgia A (1996) Scaled experiments of volcanic spreading. J Geophys Res Solid Earth 101(B6):13805–13817. https://doi.org/10.1029/95JB03736

Meyer C, Hemley JJ (1997) Wall rock alteration. In: Barnes HL (ed) Geochemistry of hydrothermal ore deposits. John Wiley & Sons, pp 166–235

Miller CA, Schaefer LN, Kereszturi G, Fournier D (2020) Three-dimensional mapping of Mt. Ruapehu volcano, New Zealand, from aeromagnetic data inversion and hyperspectral imaging. J Geophys Res Solid Earth 125(2):e2019JB018247. https://doi.org/10.1029/2019JB018247

Mimura K, Endo H (1997) Repeated collapse and reconstruction of Bandai volcano as revealed in the large outcrop of debris deposits on the Southwest foot. J Volcanol Soc Jpn 42:321–330 (in Jpn with Engl abstr)

Mitchell NC (2003) Susceptibility of mid-ocean ridge volcanic islands and seamounts to large-scale landsliding. J Geophys Res 108(B8):2397. https://doi.org/10.1029/2002JB001997

Mokievsky-Zubok O (1977) Glacier caused slide near Pylon Peak, British Columbia. Can J Earth Sci 14:2657–2662. https://doi.org/10.1139/e77-230

Montanaro C, Beget J (2011) Volcano collapse along the Aleutian Ridge (western Aleutian Arc). Nat Hazards Earth Syst Sci 11(3):715–730. https://doi.org/10.5194/nhess-11-715-2011

Moon V, Bradshaw J, Smith R, de Lange W (2005) Geotechnical characterisation of stratocone crater wall sequences, White Island Volcano, New Zealand. Eng Geol 81:146–178. https://doi.org/10.1016/j.enggeo.2005.07.014

Moore JG (1964) Giant submarine landslides on the Hawaiian Ridge. U S Geol Surv Prof Pap 501-D:95–98

Moore JG, Albee WC (1981) Topographic and structural changes, March–July 1980—photogrammetric data. In: Lipman PW, Mullineaux DR (eds) The 1980 eruptions of Mount St. Helens, Washington. U S Geol Surv Prof Pap 1250:123–134

Moore DP, Mathews WH (1978) The Rubble Creek landslide, southwestern British Columbia. Can J Earth Sci 15(7):1039–1052. https://doi.org/10.1139/e78-112

Moore JG, Rice CJ (1984) Chronology and character of the May 18, 1980, explosive eruptions of Mount St Helens. Explosive volcanism: inception, evolution, and hazards. Nat Acad Press, Washington, DC, pp 133–142

Moore JG, Clague DA, Holcomb RT, Lipman PW, Normark WR, Torresan ME (1989) Prodigious submarine landslides on the Hawaiian Ridge. J Geophys Res 94:17465–17484. https://doi.org/10.1029/JB094iB12p17465

Moore JG, Normark WR, Holcomb RT (1994) Giant Hawaiian landslides. Annu Rev Earth Planet Sci 22:119–144. https://doi.org/10.1146/annurev.ea.22.050194.001003

Moore PL, Iverson NR, Iverson RM (2008) Frictional properties of the Mount St. Helens gouge. In: Sherrod DR, Scott WE, Stauffer PH (eds) A volcano rekindled: the renewed eruption of Mount St. Helens, 2004–2006. U S Geol Surv Prof Pap 1750:415–424. https://doi.org/10.3133/pp175020

Moore JG, Sisson TW (1981) Deposits and effects of the May 18 pyroclastic surge. In: Lipman PW, Mullineaux DR (eds) The 1980 eruptions of Mount St. Helens, Washington. U S Geol Surv Prof Pap 1250:421–438

Mordensky SP, Villeneuve MC, Kennedy BM, Heap MJ, Gravley DM, Farquharson JI, Reuschlé T (2018) Physical and mechanical property relationships of a shallow intrusion and volcanic host rock, Pinnacle Ridge, Mt. Ruapehu, New Zealand. J Volcanol Geotherm Res 359:1–20. https://doi.org/10.1016/j.jvolgeores.2018.05.020

Mordensky SP, Heap MJ, Kennedy BM, Gilg HA, Villeneuve MC, Farquharson JI, Gravley DM (2019) Influence of alteration on the mechanical behaviour and failure mode of andesite: implications for shallow seismicity and volcano monitoring. Bull Volcanol 81:44. https://doi.org/10.1007/s00445-019-1306-9

Muffler LJP, Clynne MA (2015) Geologic field-trip guide to Lassen Volcanic National Park and vicinity, California. US Geol Surv Sci Invest Rep 2015–5067, 67. https://doi.org/10.3133/sir20155067

Mullineaux DR, Crandell DR (1981) The eruptive history of Mount St. Helens. In: Lipman PW, Mullineaux DR (eds) The 1980 eruptions of Mount St. Helens, Washington. U S Geol Surv Prof Pap 1250:3–15

Murray JB, Wooller LK (2002) Persistent summit subsidence at Volcán de Colima, México, 1982–1999: strong evidence against Mogi deflation. J Volcanol Geotherm Res 117(1–2):69–78. https://doi.org/10.1016/S0377-0273(02)00236-6

Murray JB, Voight B, Glot J-P (1994) Slope movment crisis on the east flank of Mt. Etna volcano: models for eruption triggering and forecasting. Eng Geol 38:245–259. https://doi.org/10.1016/0013-7952(94)90041-8

Murray JB, van Wyk de Vries B, Pitty A, Sargent P, Wooller L (2018) Gravitational sliding of the Mt. Etna massif along a sloping basement. Bull Volcanol 80:40. https://doi.org/10.1007/s00445-018-1209-1

Nakamura K (1977) Volcanoes as possible indicators of tectonic stress orientation—principle and proposal. J Volcanol Geotherm Res 2(1):1–16. https://doi.org/10.1016/0377-0273(77)90012-9

Nakamura Y (1978) Geology and petrology of Bandai and Nekoma volcanoes. Tohoku Univ Sci Rep Ser 3(14):67–119

Neall VE (1979) Geological map of New Zealand. 1:50,000 Sheets P19, P20, P21 New Plymouth, Egmont and Manaia, 3 maps and notes. New Zeal Dept Sci Ind Res 36

Neall VE (2002) Review of flank collapses at New Zealand volcanoes. Montagne Pelee 1902–2002 Explosive volcanism in subduction zones, St. Pierre, Martinique, 12–16 May 2002, Abstr p 71

Neri M, Mazzarini F, Tarquini S, Bisson M, Isola I, Behncke B, Pareschi MT (2008) The changing face of Mount Etna's summit area documented with Lidar technology. Geophys Res Lett 35(9). https://doi.org/10.1029/2008GL033740

Newhall CG (1982) A prehistoric debris avalanche from Mount St. Helens (abstr). EOS Trans Am Geophys Union 63:1141

Newhall CG, Self S (1982) The volcanic explosivity index (VEI): an estimate of explosive magnitude for historical volcanism. J Geophys Res 87(C2):1231–1238. https://doi.org/10.1029/JC087iC02p01231

Nishi K, Ono H, Mori H (1999) Global positioning system measurements of ground deformation caused by magma intrusion and lava discharge: the 1990–1995 eruption at Unzendake volcano. Kyushu Japan J Volcanol Geotherm Res 89:23–34. https://doi.org/10.1016/S0377-0273(98)00119-X

Nolesini T, Di Traglia F, Del Ventisette C, Moretti S, Casagli N (2013) Deformations and slope instability on Stromboli volcano: integration of GBInSAR data and analog modeling. Geomorphology 180:242–254. https://doi.org/10.1016/j.geomorph.2012.10.014

Norini G, Lagmay AMF (2005) Deformed symmetrical volcanoes. Geology 33(7):605–608. https://doi.org/10.1130/G21565.1

Norini G, Capra L, Groppelli G, Lagmay AMF (2008) Quaternary sector collapses of Nevado de Toluca volcano (Mexico) governed by regional tectonics and volcanic evolution. Geosphere 4(5):854–871. https://doi.org/10.1130/GES00165.1

Norini G, Bustos E, Arnosio M, Baez W, Zuluaga MC, Roverato M (2020) Unusual volcanic instability and sector collapse configuration at Chimpa volcano, central Andes. J Volcanol Geotherm Res 393:106807. https://doi.org/10.1016/j.jvolgeores.2020.106807

Norini G, Capra L, Groppelli G, Agliardi F, Pola A, Cortes A (2010) Structural architecture of the Colima volcanic complex. J Geophys Res Solid Earth 115(B12). https://doi.org/10.1029/2010JB007649

Normark WR, Moore JG, Torresan ME (1993) Giant volcano-related landslides and the development of the Hawaiian Islands. In: Submarine landslides: selected studies in the US Exclusive Economic Zone. U S Geol Surv Bull 2002:184–196

Nozaki T (2015) Historical and pre-historical gigantic landslides in Tateyama Caldera and their mechanism of occurrence. In: 10th Asian regional conference of international association of engineering geologists, Kyoto University, Japan, 26-29 September 2015

O'Conner JE, Costa JE (2005) The world's largest floods, past and present—their causes and magnitudes. U S Geol Surv Circ 1254:1–13

Oehler J-F, Lénat J-F, Labazuy P (2008) Growth and collapse of the Reunion Island volcanoes. Bull Volcanol 70(6):717–742. https://doi.org/10.1007/s00445-007-0163-0

Okusa S, Anma S, Maikuma H (1987) A gigantic avalanche resulting from the 1984 Naganoken-Seibu earthquake, central Japan. In: Gardiner V (ed) International geomorphology 1986. Proceedings of the first international conference on geomorphology Part I. John Wiley & Sons, Chichester, UK, 406–430

Okyay U, Telling J, Glennie CL, Dietrich WE (2019) Airborne lidar change detection: an overview of Earth sciences applications. Earth-Sci Rev 198:102929. https://doi.org/10.1016/j.earscirev.2019.102929

Olsen S (2016) Eruption: The untold story of Mount St. Helens. WW Norton & Co, New York, p 336

Omira R, Ramalho I, Terrinha P, Baptista MA, Batista L, Zitellini N (2016) Deep-water seamounts, a potential source of tsunami generated by landslides? The Hirondelle Seamount, NE Atlantic. Mar Geol 379:267–280. https://doi.org/10.1016/j.margeo.2016.06.010

Ota K (1969) Study on the collapses in the Mayu-yama—1. On the mechanism of collapse. Rep Shimabara Inst Volcanol Balneol Fac Sci Kyushu Univ 5:6–35

Ota K (1973) A study of hot springs on the Shimabara Peninsula. Sci Rep Shimabara Volc Observ, Fac Sci Kyushu Univ 8:1–33 (in Jpn with Engl abstr)

Paguican EMR, van Wyk de Vries B, Lagmay AMF (2012) Volcanotectonic controls and emplacement kinematics of the Iriga debris avalanches (Philippines). Bull Volcanol 74:2067–2081. https://doi.org/10.1007/s00445-012-0652-7

Paguican EMR, van Wyk de Vries B, Lagmay AMF (2014) Hummocks: how they form and how they evolve in rockslide-debris avalanches. Landslides 11:67–80. https://doi.org/10.1007/s10346-012-0368-y

Paguican EMR, Roverato M, Yoshida H (2021) Volcanic debris avalanche transport and emplacement mechanisms. In: Roverato M, Dufresne A, Procter J (eds) Volcanic debris avalanches. Adv Volcanol 6:143–173. https://doi.org/10.1007/978-3-030-57411-6_7. Springer, Cham

Palano M, Puglisi G, Gresta S (2008) Ground deformation patterns at Mt. Etna from from 1993 to 2000 joint use of InSAR and GPS techniques. J Volcanol Geotherm Res 169(3–4):99–120. https://doi.org/10.1016/j.jvolgeores.2007.08.014

Pallister JS, Cashman KV, Hagstrum JT, Beeler NM, Moran SC, Denlinger RP (2013) Faulting within the Mount St. Helens conduit and implications for volcanic earthquakes. Geol Soc Am Bull 125(3–4):359–376. https://doi.org/10.1130/B30716.1

Pallister JS, Clynne MA, Wright HM, Van Eaton AR, Vallance JW, Sherrod DR, Kokelaar BP (2017) Field-trip guide to Mount St. Helens, Washington—an overview of the eruptive history and petrology, tephra deposits, 1980 pyroclastic density current deposits, and the crater. U S Geol Surv Sci Invest Rep 2017-5022-D:1–6. https://doi.org/10.3133/sir20175022D

Palmer BA, Alloway BV, Neall VE (1991) Volcanic debris-avalanche deposits in New Zealand—lithofacies organization in unconfined, wet-avalanche flows. In: Fisher RV, Smith GA (eds) Sedimentation in volcanic settings. SEPM Spec Publ 45:89–98. https://doi.org/10.2110/pec.91.45.0089

Patanè D, Barberi G, Cocina O, De Gori P, Chiarabba C (2006) Time-resolved seismic tomography detects magma intrusions at Mount Etna. Science 313(5788):821–823. https://doi.org/10.1126/science.1127724

Paul A, Gratier JP, Boudon J (1987) A numerical model for simulating deformation of Mount St. Helens volcano. J Geophys Res 92(B10):10299–10312. https://doi.org/10.1029/JB092iB10p10299

Perinotto H, Schneider J-L, Bachèlery P, Le Bourdonnec F-X, Famin V, Michon L (2015) The extreme mobility of debris avalanches: a new model of transport mechanism. J Geophys Res Solid Earth 120:8110–8119. https://doi.org/10.1002/2015JB011994

Peterson DE, Finn CA, Bedrosian PA (2021) Airborne geophysical imaging of weak zones on Iliamna Volcano, Alaska: implications for slope stability. J Geophys Res Solid Earth 126(3):e2020JB020807. https://doi.org/10.1029/2020JB020807

Petley DN, Bulmer MH, Murphy W (2002) Patterns of movement in rotational and translational landslides. Geology 30(8):719–722. https://doi.org/10.1130/0091-7613(2002)030%3c0719:POMIRA%3e2.0.CO;2

Pierson TC (1985) Initiation and flow behavior of the 1980 Pine Creek and Muddy River lahars, Mount St. Helens, Washington. Geol Soc Am Bull 96:1056–1069. https://doi.org/10.1130/0016-7606(1985)96%3c1056:IAFBOT%3e2.0.CO;2

Pierson TC, Siebert L, Harpel CJ, Scott KM (2018) Geologic field-trip guide of volcaniclastic sediments from snow- and ice-capped volcanoes—Mount St. Helens, Washington, and Mount Hood, Oregon. U S Geol Surv Sci Invest Rep 2017-5022-F:1–97. https://doi.org/10.3133/sir20175022F

Pinel V, Poland MP, Hooper A (2014) Volcanology: lessons learned from synthetic aperture radar imagery. J Volcanol Geotherm Res 289:81–113. https://doi.org/10.1016/j.jvolgeores.2014.10.010

Plafker G, Ericksen GE (1978) Nevados Huascarán avalanches, Peru. In: Voight B (ed) Rockslides and avalanches, 1. Elsevier, Amsterdam, pp 277–314

Pola A, Crosta G, Fusi N, Barberini V, Norini G (2012) Influence of alteration on physical properties of volcanic rocks. Tectonophysics 566:67–86. https://doi.org/10.1016/j.tecto.2012.07.017

Pola A, Crosta GB, Fusi N, Castellanza R (2014) General characterization of the mechanical behaviour of different volcanic rocks with respect to alteration. Eng Geol 169:1–13. https://doi.org/10.1016/j.enggeo.2013.11.011

Polanco E, Naranjo JA (2008) Collapso Holoceno en el Volcán Callaqui (37°55'S), Andes del Sur. Actas del XVII congreso geologico Argentino:1157–1158

Poland M, Hamburger M, Newman A (2006) The changing shapes of active volcanoes: history, evolution, and future challenges for volcano geodesy. J Volcanol Geotherm Res 150(1–3):1–13. https://doi.org/10.1016/j.jvolgeores.2005.11.005

Poland MP, Lisowski M, Dzurisin D, Kramer R, McLay M, Pauk B (2017) Volcano geodesy in the Cascade arc, USA. Bull Volcanol 79:59. https://doi.org/10.1007/s00445-017-1140-x

Ponomareva VV, Melekestsev IV, Dirksen OV (2006) Sector collapses and large landslides on Late Pleistocene-Holocene volcanoes in Kamchatka. Russia J Volcanol Geotherm Res 158(1–2):117–138. https://doi.org/10.1016/j.jvolgeores.2006.04.016

Pouliquen O, Delour J, Savage SB (1997) Fingering in granular flows. Nature 386:816–817. https://doi.org/10.1038/386816a0

Prager C, Zangerl C, Nagler T (2009) Geological controls on slope deformations in the Köfels rockslide area (Tyrol, Austria). Austrian J Earth Sci 102(2):4–19

Primulyana S, Bani P, Harris A (2017) The effusive-explosive transitions at Rokatenda 2012–2013: unloading by extrusion of degassed magma with lateral gas flow. Bull Volcanol 79:22. https://doi.org/10.1007/s00445-017-1104-1

Priyanto WS, Hunt JE, Hanif M, Tappin DR, Permana H, Susilohadi Cassidy M, Yulianto E (2021) Bathymetry and shallow seismic imaging of the 2018 flank collapse of Anak Krakatau. Front Earth Sci 8:577448. https://doi.org/10.3389/feart.2020.577448

Procter JN, Cronin SJ, Zernack AV, Lube G, Stewart RB, Nemeth K, Keys H (2014) Debris flow evolution and the activation of an explosive hydrothermal system; Te Maari, Tongariro, New Zealand. J Volcanol Geotherm Res 286:303–316. https://doi.org/10.1016/j.jvolgeores.2014.07.006

Procter JN, Zernack AV, Cronin SJ (2021) Computer simulation of a volcanic debris avalanche from Mt. Taranaki, New Zealand. In: Roverato M, Dufresne A, Procter J (eds). Adv Volcanol 6:281–310. https://doi.org/10.1007/978-3-030-57411-6_11

Pulgarín B, Capra L, Cepeda H, Macías JL (2004) Late Pleistocene deposits associated with a southern flank collapse of the Nevado del Huila volcanic complex (Colombia). Acta Vulcanol 16(1–2):37–58

Qi S, Xu Q, Zhang B, Zhou Y, Lan H, Li L (2011) Source characteristics of long runout rock avalanches triggered by the 2008 Wenchuan earthquake, China. J Asian Earth Sci 40(4):896–906. https://doi.org/10.1016/j.jseaes.2010.05.010

Quartau R, Ramalho RS, Madeira J, Santos R, Rodrigues A, Roque C, Carrara G, Brum da Silveira A (2018) Gravitational, erosional and depositional processes on volcanic ocean islands: insights from the submarine morphology of Madeira Archipelago. Earth Planet Sci Lett 82:288–299. https://doi.org/10.1016/j.epsl.2017.11.003

Reiche P (1937) The toreva-block—a distinctive landslide type. J Geol 45:538–548

Reid ME (2004) Massive collapse of volcano edifices triggered by hydrothermal pressurization. Geology 32(5):373–376. https://doi.org/10.1130/G20300.1

Reid ME, Brien DL (2006) Assessing massive flank collapse at stratovolcanoes using 3-D slope stability analysis. In: Evans SG, Mugnozza GS, Strom A, Hermanns RL (eds) Landslides from massive rock slope failure. NATO Sci Ser 49:445–458. https://doi.org/10.1007/978-1-4020-4037-5_24

Reid ME, Iverson RM (1992) Gravity-driven groundwater flow and slope failure potential: 2. Effects of slope morphology, material properties, and hydraulic heterogeneity. Water Resour Res 28(3):939–950. https://doi.org/10.1029/91WR02695

Reid ME, Christian SB, Brien DL (2000) Gravitational stability of three-dimensional stratovolcano edifices. J Geophys Res 105(B3):6043–6056. https://doi.org/10.1029/1999JB900310

Reid ME, Sisson TW, Brien DL (2001) Volcano collapse promoted by hydrothermal alteration and edifice shape, Mount Rainier. Wash Geol 29(9):779–782. https://doi.org/10.1130/0091-7613(2001)029%3c0779:VCPBHA%3e2.0.CO;2

Reid ME, Brien DL, Waythomas CF (2010a) Preliminary slope-stability analysis of Augustine Volcano. In: Power JA, Coombs ML, Freymueller JT (eds) The 2006 eruption of Augustine Volcano, Alaska. U S Geol Surv Prof Pap 1769:321–332

Reid ME, Keith TEC, Kayen RE, Iverson NR, Iverson RM, Brien DL (2010b) Volcano collapse promoted by progressive strength reduction: new data from Mount St. Helens. Bull Volcanol 72:761–766. https://doi.org/10.1007/s00445-010-0377-4

Revil A, Finizola A, Sortino F, Ripepe M (2004) Geophysical investigations at Stromboli volcano, Italy: implications for ground water flow and paroxysmal activity. Geophys J Int 157(1):426–440. https://doi.org/10.1111/j.1365-246X.2004.02181.x

Revil A, Coperey A, Heap MJ, Carbillet L (2020) A geophysical index to map alteration, permeability, and mechanical properties within volcanoes. Application to the soft volcanic rocks from Whakaari/White Island (New Zealand). J Volcanol Geotherm Res 401:106945. https://doi.org/10.1016/j.jvolgeores.2020.106945

Richards JP, Villeneuve M (2001) The Llullaillaco volcano, northwest Argentina: construction by Pleistocene volcanism and destruction by sector collapse. J Volcanol Geotherm Res 105:77–105. https://doi.org/10.1016/S0377-0273(00)00245-6

Roberti G, Friele P, van Wyk de Vries B, Ward B, Clague JJ, Perotti L, Giardino M (2017) Rheological evolution of the Mount Meager 2010 debris avalanche, southwestern British Columbia. Geosphere 13(2):369–90. https://doi.org/10.1130/GES01389.1

Rodríguez C, Bommer JJ, Chandler RJ (1999) Earthquake-induced landslides: 1980–1997. Soil Dyn Earthq Eng 18(5):325–346. https://doi.org/10.1016/S0267-7261(99)00012-3

Romero C, Galindo I, Sánchez N, Martín-González E, Vegas J (2020) Syn-eruptive lateral collapse of monogenetic volcanoes: the case of Mazo Volcano from the Timanfaya Eruption (Lanzarote, Canary Islands). Németh K (ed) Updates in volcanology — Transdisciplinary nature of volcano science, IntechOpen. https://doi.org/10.5772/intechopen.93882

Rosas-Carbajal M, Komorowski J-C, Nicollin F, Gibert D (2016) Volcano electrical tomography unveils edifice collapse hazard linked to hydrothermal system structure and dynamics. Sci Rep 6(1):1–11. https://doi.org/10.1038/srep29899

Rose ND, Hungr O (2007) Forecasting potential rock slope failure in open pit mines using the inverse-velocity method. Int J Rock Mech Mining Sci 44(2):308–320. https://doi.org/10.1016/j.ijrmms.2006.07.014

Rosenbaum JG, Waitt RB (1981) Summary of eyewitness accounts of the May 18 eruption. In: Lipman PW, Mullineaux DR (eds) The 1980 eruptions of Mount St. Helens, Washington. U S Geol Surv Prof Pap 1250:53–67

Rouwet D, Sandri L, Marzocchi W, Gottsmann J, Selva J, Tonini R, Papale P (2014) Recognizing and tracking volcanic hazards related to non-magmatic unrest: a review. J Appl Volcanol 3:17. https://doi.org/10.1186/s13617-014-0017-3

Roverarto M, Cronin S, Procter J, Capra L (2015) Textural features as indicators of debris avalanche transport and emplacement, Taranaki volcano. Geol Soc Am Bull 127:3–18. https://doi.org/10.1130/B30946.1

Roverato M (2016) The Montesbelos mass-flow (southern Amazonian craton, Brazil): a Paleoproterozoic volcanic debris avalanche deposit? Bull Volcanol 78:49. https://doi.org/10.1007/s00445-016-1043-2

Roverato M, Capra L (2013) Características microtexturales como indicadores del transporte y emplazamiento de dos depósitos de avalancha de escombros del volcán de Colima. Rev Mex Cien Geol 30:512–525

Roverato M, Di Traglia F, Procter J, Paguican E, Dufresne A (2021a) Factors contributing to volcano lateral collapse. In: Roverato M, Dufresne A, Procter J (eds) Volcanic debris avalanches: from collapse to hazard. Adv Volcanol 6:91–119. https://doi.org/10.1007/978-3-030-57411-6_5. Springer, Cham

Roverato M, Dufresne A, Procter J (eds) (2021b) Volcanic debris avalanches: from collapse to hazard. Advances in Volcanology. Springer, Cham, 358. https://doi.org/10.1007/978-3-030-57411-6

Rowberry M, Klimeš J, Blahůt J, Balek J, Kusák M (2023) A global database of giant landslides on volcanic islands. In: Sassa K, Konagai K, Tiwari B, Arbanas Ž, Sassa S (eds) Progress in landslide research and technology. Springer, Cham 1(1):295–304. https://doi.org/10.1007/978-3-031-16898-7_22

Rowley PD, Kuntz MA, Macleod NS (1981) Pyroclastic-flow deposits. In: Lipman PW, Mullineaux DR (eds) The 1980 eruptions of Mount St. Helens, Washington. U S Geol Surv Prof Pap 1250:489–512

Rulon JJ, Freeze RA (1985) Multiple seepage faces on layered slopes and their implications for slope-stability analysis. Can Geotech J 22(3):347–356. https://doi.org/10.1139/t85-047

Runqiu H (2009) Some catastrophic landslides since the twentieth century in the southwest of China. Landslides 6(1):69–81. https://doi.org/10.1007/s10346-009-0142-y

Saito M (1965) Forecasting the time of occurrence of slope failure. Proceedings 6th international conference soil mechancis and foundation engineering. Montreal 2:537–541

Salt G (1988) Landslide mobility and remedial measures. In: Bonnard C (ed) Landslides: Glissements de terrain. Proceedings of the fifth international symposium on landslides. A.A. Balkema, Rotterdam 757–762

Samaniego P, Valderrama P, Mariño J, van Wyk de Vries B, Roche O, Manrique N, Chédeville C, Liorzou C, Fidel L, Malnati J (2015) The historical (218 ± 14 a BP) explosive eruption of Tutupaca volcano (Southern Peru). Bull Volcanol 77:51. https://doi.org/10.1007/s00445-015-0937-8

Sanford WE, Knoikow LF, Rowe GL Jr, Brantley SL (1995) Groundwater transport of crater-lake brine at Poás Volcano. Costa Rica J Volcanol Geotherm Res 64(3–4):269–293. https://doi.org/10.1016/0377-0273(94)00080-Z

Sarna-Wojcicki AM, Shipley S, Waitt RB, Dzurisin D, Wood SH (1981) Areal distribution, thickness, mass, volume, and grain size of air-fall ash from the six major eruptions of 1980. In: Lipman PW, Mullineaux DR (eds) The 1980 eruptions of Mount St. Helens, Washington. U S Geol Surv Prof Pap 1250:577–60

Sassa K, Dang K, Yanagisawa H, He B (2016) A new landslide-induced tsunami simulation model and its application to the 1792 Unzen-Mayuyama landslide-and-tsunami disaster. Landslides 13(6):1405–1419. https://doi.org/10.1007/s10346-016-0691-9

Satake K, Kato Y (2001) The 1741 Oshima-Oshima eruption: extent and volume of submarine debris avalanche. Geophys Res Lett 28(3):427–430. https://doi.org/10.1029/2000GL012175

Scarpa R, Tilling RI (eds) (2012) Monitoring and mitigation of volcano hazards. Springer Verlag, Berlin, p 841

Schaefer LN, Oommen T, Corazzato C, Tibaldi A, Escobar-Wolf R, Rose WI (2013) An integrated field-numerical approach to assess slope stability hazards at volcanoes: the example of Pacaya. Guatemala Bull Volcanol 75:720. https://doi.org/10.1007/s00445-013-0720-7

Schaefer LN, Kendrick JE, Oommen T, Lavallée Y, Chigna G (2015a) Geomechanical rock properties of a basaltic volcano. Front Earth Sci 3:29. https://doi.org/10.3389/feart.2015.00029

Schaefer LN, Lu Z, Oommen T (2015b) Dramatic volcanic instability revealed by InSAR. Geology 43(8):743–746. https://doi.org/10.1130/G36678.1

Schaefer LN, Wang T, Escobar-Wolf R, Oommen T, Lu Z, Kim J, Lundgren P, Waite G (2017) Three-dimensional displacements of a large volcano flank movement during the May 2010 eruptions at Pacaya Volcano, Guatemala. Geophys Res Lett 44(1):135–142. https://doi.org/10.1002/2016GL071402

Schaefer LN, Di Traglia F, Chaussard E, Lu Z, Nolesini T, Casagli N (2019) Monitoring volcano slope instability with synthetic aperture radar: a review and new data from Pacaya (Guatemala) and Stromboli (Italy) volcanoes. Earth-Sci Rev 192:236–257. https://doi.org/10.1016/j.earscirev.2019.03.009

Schmidt R, Schmincke H-U (2002) From seamount to oceanic island, Porto Santo, central East-Atlantic. Int J Earth Sci 91(4):594–614. https://doi.org/10.1007/s00531-001-0243-x

Schneider JL, Fisher RV (1998) Transport and emplacement mechanisms of large volcanic debris avalanches: evidence from the northwest sector of Cantal Volcano (France). J Volcanol Geotherm Res 83:141–165. https://doi.org/10.1016/S0377-0273(98)00016-X

Schuster R (1996) The 25 most catastrophic landslides of the 20th century. In: Landslides, Proceedings 8th international conference and field workshop, Granada, Spain 27–28 September 1996

Schuster RL, Alford D (2004) Usoi landslide dam and Lake Sarez, Pamir mountains, Tajikistan. Environ Eng Geosci 10(2):151–168. https://doi.org/10.2113/10.2.151

Schuster RL, Salcedo DA, Valenzuela L (2002) Overview of catastrophic landslides of South America in the twentieth century. Rev Eng Geol 15:1–34

Scott KM (1988a) Origins, behavior, and sedimentology of lahars and lahar-runout flows in the Toutle-Cowlitz River system, Mount St. Helens Washington. U S Geol Surv Prof Pap 1447-A:1–74

Scott KM (1988b) Origins, behavior, and sedimentology of prehistoric catastrophic lahars at Mount St. Helens, Washington. Geol Soc Am Spec Pap 229:23–36. https://doi.org/10.1130/SPE229-p23

Scott KM (1989) Magnitude and frequency of lahars in the Toutle-Cowlitz River system, Mount St. Helens, Washington. U S Geol Surv Prof Pap 1447-B:1–33

Scott KM, Vallance JW, Pringle PT (1995) Sedimentology, behavior, and hazards of debris flows at Mount Rainier, Washington. U S Geol Surv Prof Pap 1547:1–56

Scott KM, Macías JL, Naranjo JA, Rodríguez S, McGeehin JP (2001) Catastrophic debris flows transformed from landslides in volcanic terrains: mobility, hazard assessment, and mitigation strategies. U S Geol Surv Prof Pap 1630:1–59

Scott KM, Vallance JW, Kerle N, Macías JL, Strauch W, Devoli G (2005) Catastrophic precipitation-triggered lahar at Casita volcano, Nicaragua: occurrence, bulking and transformation. Earth Surf Proc Land 30:59–79. https://doi.org/10.1002/esp.1127

Scutter CR, Cas RAF, Moore CL, De Rita D (1998) Facies architecture and origin of a submarine rhyolitic lava flow-dome complex, Ponza, Italy. J Geophys Res: Solid Earth 10.103(B11):27551–66. https://doi.org/10.1029/98JB01121

Segalini A, Valletta A, Carri A (2018) Landslide time-of-failure forecast and alert threshold assessment: a generalized criterion. Eng Geol 245:72–80. https://doi.org/10.1016/j.enggeo.2018.08.003

Segall P (2013) Volcano deformation and eruption forecasting. Geol Soc Lond Spec Publ 380(1):85–106. https://doi.org/10.1144/SP380.4

Segall P, Cervelli P, Owen S, Lisowski M, Miklius A (2001) Constraints on dike propagation from continuous GPS measurements. J Geophys Res Solid Earth 106(B9):19301–19317. https://doi.org/10.1029/2001JB000229

Sekiya S, Kikuchi Y (1889) The eruption of Bandai-san. Tokyo Imp Univ Coll Sci J 3(2):91–172

Shea T, van Wyk de Vries B (2008) Structural analysis and analogue modeling of the kinematics and dynamics of rockslide avalanches. Geosphere 4(4):657–686. https://doi.org/10.1130/GES00131.1

Shea T, van Wyk de Vries B, Pilato M (2008) Emplacement mechanisms of contrasting debris avalanches at Volcán Mombacho (Nicaragua), provided by structural and facies analysis. Bull Volcanol 70(8):899–921. https://doi.org/10.1007/s00445-007-0177-7

Sherrod DR, Vallance JW, Tapia Espinosa A, McGeehin JP (2007) Volcán Barú—eruptive history and volcano-hazards assessment. US Geol Surv Open-File Report 2007–1401, 33 pp, 1 plate, scale 1:100,000.

Shimano T, Geshi N, Kobayashi T (2013) Geological map of Suwanosejima volcano. Geol Surv Jpn, 1:20,000 scale map and explanatory text (in Jpn)

Shreve RL (1968) The Blackhawk landslide. Geol Soc Am Spec Pap 108:1–47

Siebe C, Komorowski J-C, Sheridan MF (1992) Morphology and emplacement of an unusual debris-avalanche deposit at Jocotitlán volcano, central Mexico. Bull Volcanol 54:573–589. https://doi.org/10.1007/BF00569941

Siebe C, Salinas S, Arana-Salinas L, Macías JL, Gardner J, Bonasia R (2017) The ~ 23,500 y ^{14}C BP White Pumice Plinian eruption and associated debris avalanche and Tochimilco lava flow of Popocatépetl volcano, México. J Volcanol Geotherm Res 15(333):66–95. https://doi.org/10.1016/j.jvolgeores.2017.01.011

Siebert L (1984) Large volcanic debris avalanches: characteristics of source areas, deposits, and associated eruptions. J Volcanol Geotherm Res 22:163–197. https://doi.org/10.1016/0377-0273(84)90002-7

Siebert L (2002) Landslides resulting from structural failure of volcanoes. In: Evans SG, DeGraff JV (eds) Catastrophic landslides: effects, occurrence, and mechanisms. Geol Soc Am Rev Eng Geol 15:209–235. https://doi.org/10.1130/REG15-p209

Siebert L, Glicken H, Ui T (1987) Volcanic hazards from Bezymianny- and Bandai-type eruptions. Bull Volcanol 49:435–459. https://doi.org/10.1007/BF01046635

Siebert L, Glicken H, Kienle J (1989) Debris avalanches and lateral blasts at Mount St. Augustine volcano, Alaska. Nat Geog Res 5(2):232–249

Siebert L, Begét JE, Glicken H (1995) The 1883 and late-prehistoric eruptions of Augustine volcano, Alaska. J Volcanol Geotherm Res 66:367–395. https://doi.org/10.1016/0377-0273(94)00069-S

Siebert L, Kimberly P, Pullinger CR (2004) The voluminous Acajutla debris avalanche from Santa Ana volcano, western El Salvador, and comparison with other Central American edifice-failure events. In: Rose WI, Bommer JJ, López DL, Carr MJ, Major JJ (eds) Natural hazards in El Salvador. Geol Soc Am Spec Pap 375:5–23. https://doi.org/10.1130/0-8137-2375-2.5

Siebert L, Alvarado GE, Vallance JW, van Wyk de Vries B (2006) Large-volume volcanic edifice failures in Central America and associated hazards. In: Rose WI, Bluth GJS, Carr MJ, Ewert

JW, Patino LC, Vallance JW (eds) Volcanic hazards in Central America. Geol Soc Am Spec Pap 412:1–26. https://doi.org/10.1130/2006.2412(01)

Siebert L, Simkin T, Kimberly P (2011) Volcanoes of the world, 3rd edn. University of California Press, Berkeley

Siebert L, Roverato M (2021) A historical perspective on lateral collapse and debris avalanches. In: Roverato M, Dufresne A, Procter J (eds) Volcanic debris avalanches: from collapse to hazard. Advances in Volcanology. Springer, Cham 6:11–50. https://doi.org/10.1007/978-3-030-57411-6_2

Siebert L, Vallance JW (2017) Large volume edifice failures in the Cascade Range of southern British Columbia to northern California. IAVCEI 2017 scientific assembly, Portland Oregon, August 14–18, 2017, abstr VH23A-181

Siebert L, Reid ME, Vallance JW, Pierson TC (2019) When volcanoes fall down—catastrophic collapse and debris avalanches (ver 1.2, August 2019). U S Geol Surv Fact Sheet 2019–3023, 6 https://doi.org/10.3133/fs20193023

Silver E, Day S, Ward S, Hoffman G, Llanes P, Driscoll N, Appelgate B, Saunders S (2009) Volcano collapse and tsunami generation in the Bismarck volcanic arc, Papua New Guinea. J Volcanol Geotherm Res 186:210–222. https://doi.org/10.1016/j.jvolgeores.2009.06.013

Simmons J, Elsworth D, Voight B (2005) Classification and idealized limit-equilibrium analyses of dome collapses at Soufrière Hills volcano, Montserrat, during growth of the first lava dome: November 1995–March 1998. J Volcanol Geotherm Res 139(3–4):241–258. https://doi.org/10.1016/j.jvolgeores.2004.08.009

Skilling IP, White JDL, McPhie J (2002) Peperite: a review of magma–sediment mingling. J Volcanol Geotherm Res 114(1–2):1–17. https://doi.org/10.1016/S0377-0273(01)00278-5

Smoot NC, King RE (1993) Three-dimensional secondary surface geomorphology of submarine landslides on northwest Pacific plate guyots. Geomorphology 6(2):151–173. https://doi.org/10.1016/0169-555X(93)90044-3

Solaro G, Acocella V, Pepe S, Ruch J, Neri M, Sansosti E (2010) Anatomy of an unstable volcano from InSAR: multiple processes affecting flank instability at Mt. Etna, 1994–2008. J Geophys Res Solid Earth 115(B10). https://doi.org/10.1029/2009JB000820

Sousa J, Voight B (1995) Multiple-pulsed debris avalanche emplacement at Mount St Helens in 1980. Evidence from numerical continuum flow simulations. J Volc Geotherm Res 66:227–250. https://doi.org/10.1016/0377-0273(94)00067-Q

Sparks RSJ, Moore JG, Rice CJ (1986) The initial giant umbrella cloud of the May 18th, 1980, explosive eruption of Mount St. Helens J Volc Geotherm Res 28:257–274. https://doi.org/10.1016/0377-0273(86)90026-0

Sparks RSJ, Barclay J, Calder ES, Herd RA, Komorowski J-C, Luckett R, Norton GE, Ritchie LJ, Voight B, Woods AW (2002) Generation of a debris avalanche and violent pyroclastic density current on 26 December (Boxing Day) 1997 at Soufriere Hills Volcano, Montserrat. Geol Soc Lond Mem 21(1):409–434. https://doi.org/10.1144/GSL.MEM.2002.021.01.18

Sruoga P, Rubinstein N, Hinterwimmer G (2004) Porosity and permeability in volcanic rocks: a case study on the Serie Tobífera, South Patagonia, Argentina. J Volcanol Geotherm Res 132(1):31–43. https://doi.org/10.1016/S0377-0273(03)00419-0

Staudigel H, Clague DA (2010) The geological history of deep-sea volcanoes: biosphere, hydrosphere, and lithosphere interactions. Oceanography 23(1):58–71

Stevens NF, Wadge G, Williams CA (2001) Post-emplacement lava subsidence and the accuracy of ERS InSAR digital elevation models of volcanoes. Int J Remote Sens 22(5):819–828. https://doi.org/10.1080/01431160051060246

Stix J, de Moor JM (2018) Understanding and forecasting phreatic eruptions driven by magmatic degassing. Earth Planets Space 70(1):1–19. https://doi.org/10.1186/s40623-018-0855-z

Stoffel KL (1980) The May 18, 1980 eruption of Mount St. Helens, a view from the top. Wash State Dept Nat Resour Inf Circ 71:9–11

Strom A, Li L, Lan H (2019) Rock avalanche mobility: optimal characterization and the effects of confinement. Landslides 16:1437–1452. https://doi.org/10.1007/s10346-019-01181-z

Sturkell E, Einarsson P, Sigmundsson F, Geirsson H, Olafsson H, Pedersen R, de Zeeuw-van DE, Linde AT, Sacks SI, Stefánsson R (2006) Volcano geodesy and magma dynamics in Iceland. J Volcanol Geotherm Res 150(1–3):14–34. https://doi.org/10.1016/j.jvolgeores.2005.07.010

Takahashi R, Yahata M (2018) Effects of subvolcanic hydrothermal systems on edifice collapses and phreatic eruptions at Tokachidake volcano, Japan. J Volcanol Geotherm Res 352:117–129. https://doi.org/10.1016/j.jvolgeores.2018.01.014

Takarada S, Ui T, Yamamoto Y (1999) Depositional features and transportation mechanism of valley-filling Iwasegawa and Kaida debris avalanches, Japan. Bull Volcanol 60:508–522. https://doi.org/10.1007/s004450050248

Tamura C, Hayakawa Y (1995) Reconstruction of the sequence of the 1783 Asama Eruption from the ancient literature. J Geog 104(6):843–864 (in Jpn with Engl abstr)

Terzaghi K (1950) Mechanisms of landslides. In: Paige S (ed) Application of geology to engineering practice; Berkey volume. Geol Soc Am, New York, 83–123. https://doi.org/10.1130/Berkey.1950.83

Thomas ME, Petford N, Bromhead EN (2004) Volcanic rock-mass properties from Snowdonia and Tenerife: implications for volcano edifice strength. J Geol Soc Lond 161(6):939–946. https://doi.org/10.1144/0016-764903-166

Tibaldi A (2003) Influence of volcanic cone morphology on dikes, Stromboli, Italy. J Volcanol Geotherm Res 126:79–95. https://doi.org/10.1016/S0377-0273(03)00118-5

Tibaldi A (2015) Structure of volcano plumbing systems: a review of multi-parametric effects. J Volcanol Geotherm Res 298:85–135. https://doi.org/10.1016/j.jvolgeores.2015.03.023

Tibaldi A, Lagmay AMF, Ponomareva VV (2005) Effects of basement structural and stratigraphic heritages on volcano behaviour and implications for human activities (the UNESCO/IUGS/IGCP project 455). Episodes 28(3):158–170. https://doi.org/10.18814/epiiugs/2005/v28i3/002

Tinti S, Pagnoni G, Zaniboni F (2006) The landslides and tsunamis of the 30th of December 2002 in Stromboli analysed through numerical simulations. Bull Volcanol 68:462–479. https://doi.org/10.1007/s00445-005-0022-9

Tost M, Cronin SJ, Procter JN (2014) Transport and emplacement mechanisms of channelised long-runout debris avalanches, Ruapehu volcano, New Zealand. Bull Volcanol 76:881. https://doi.org/10.1007/s00445-014-0881-z

Trofimovs J, Cas RAF, Davis BK (2004) An archean submarine volcanic debris avalanche deposit, Yilgarn Craton, western Australia, with komatiite, basalt and dacite megablocks: the product of dome collapse. J Volcanol Geotherm Res 138:111–126. https://doi.org/10.1016/j.jvolgeores.2004.06.008

Tsuchiya S, Sasahara K, Shuin S, Ozono S (2009) The large-scale landslide on the flank of caldera in South Sulawesi, Indonesia. Landslides 6(1):83–88. https://doi.org/10.1007/s10346-009-0143-x

Tucholke BE (1992) Massive submarine rockslide in the rift-valley wall of the Mid-Atlantic Ridge. Geology 20(2):129–132. https://doi.org/10.1130/0091-7613(1992)020%3c0129:MSRITR%3e2.3.CO;2

Ui T (1983) Volcanic dry avalanche deposits-identification and comparison with nonvolcanic debris streams deposits. J Volcanol

Geotherm Res 18:135–150. https://doi.org/10.1016/0377-0273(83)90006-9
Ui T, Aramaki S (1983) Volcanic dry avalanche deposit in 1980 eruption of Mt. St. Helens, USA. Bull Volcanol Soc Jpn 28:289–300 (in Jpn with Engl abstr)
Ui T, Glicken H (1986) Internal structural variations in a debris-avalanche deposit from ancestral Mount Shasta, California, USA. Bull Volcanol 48:189–194. https://doi.org/10.1007/BF01087673
Ui T, Yamamoto H, Suzuki-Kamata K (1986) Characterization of debris avalanche deposits in Japan. In: Kushiro I (ed) M Sakuyama and H Fukuyama memorial volume. J Volcanol Geotherm Res 29:231–243. https://doi.org/10.1016/0377-0273(86)90046-6
Ui T, Takarada S, Yoshimoto M (2000) Debris avalanches. In: Sigurdsson H, Houghton B, McNutt SR, Rymer H, Stix J (eds) The encyclopedia of volcanoes. Academic Press, Amsterdam, pp 617–626
Usui Y, Ogawa Y, Aizawa K, Kanda W, Hashimoto T, Koyama T, Yamaya Y, Kagiyama T (2017) Three-dimensional resistivity structure of Asama Volcano revealed by data-space magnetotelluric inversion using unstructured tetrahedral elements. Geophys J Int 208(3):1359–1372. https://doi.org/10.1093/gji/ggw459
Valderrama P, Roche O, Samaniego P, van Wyk de Vries B, Bernard K, Mariño J (2016) Dynamic implications of ridges on a debris avalanche deposit at Tutupaca volcano (Southern Peru). Bull Volcanol 78:14. https://doi.org/10.1007/s00445-016-1011-x
Valderrama P, Roche O, Samaniego P, van Wyk de Vries B, Araujo G (2018) Granular fingering as a mechanism for ridge formation in debris avalanche deposits: laboratory experiments and implications for Tutupaca volcano, Peru. J Volcanol Geotherm Res 349:409–418. https://doi.org/10.1016/j.jvolgeores.2017.12.004
Vallance JW, Scott KM (1997) The Osceola Mudflow from Mount Rainier: sedimentology and hazard implications of a huge clay-rich debris flow. Geol Soc Am Bull 109:143–163. https://doi.org/10.1130/0016-7606(1997)109%3C0143:TOMFMR%3E2.3.CO;2
Vallance JW, Siebert L, Rose WI Jr, Girón JR, Banks NG (1995) Edifice collapse and related hazards in Guatemala. J Volcanol Geotherm Res 66(1–4):337–355. https://doi.org/10.1016/0377-0273(94)00076-S
Vallance JW, Iverson RM (2015) Lahars and their deposits. In: Sigurdsson H, Houghton B, McNutt SR, Rymer H, Stix J (eds) The encyclopedia of volcanoes, 2nd edn. Academic Press, Amsterdam, 649–664. https://doi.org/10.1016/B978-0-12-385938-9.00037-7
van Wyk de Vries B, Borgia A (1996) The role of basement in volcano deformation. Geol Soc London, Spec Publ 110(1):95–110. https://doi.org/10.1144/GSL.SP.1996.110.01.07
van Wyk de Vries B, Francis PW (1997) Catastrophic collapse at stratovolcanoes induced by gradual volcano spreading. Nature 387(6631):387–390. https://doi.org/10.1038/387387a0
van Wyk de Vries B, Matela R (1998) Styles of volcano-induced deformation: numerical models of substratum flexure, spreading and extrusion. J Volcanol Geotherm Res 81(1–2):1–18. https://doi.org/10.1016/S0377-0273(97)00076-0
van Wyk de Vries B, Merle O (1996) The effect of volcanic constructs on rift fault patterns. Geology 24(7):643–646. https://doi.org/10.1130/0091-7613(1996)024%3c0643:TEOVCO%3e2.3.CO;2
van Wyk de Vries B, Self S, Francis PW, Keszthelyi L (2001) A gravitational spreading origin for the Socompa debris avalanche. J Volcanol Geotherm Res 105:225–247. https://doi.org/10.1016/S0377-0273(00)00252-3
van Wyk de Vries B, Davies TR (2015) Landslides, debris avalanches, and volcanic gravitational deformation. In: Sigurdsson H (ed) The encyclopedia of volcanoes, 2nd edn. Academic Press, Amsterdam, 665–685. https://doi.org/10.1016/B978-0-12-385938-9.00038-9
van Wyk de Vries B, Delcamp A (2015) Volcanic debris avalanches. In: Shroder JF, Davies T (eds) Landslide hazards, risks and disasters. Academic Press, San Diego 131–157. https://doi.org/10.1016/B978-0-12-396452-6.00005-7
Vidal N, Merle O (2000) Reactivation of basement faults beneath volcanoes: a new model of flank collapse. J Volcanol Geotherm Res 99(1–4):9–26. https://doi.org/10.1016/S0377-0273(99)00194-8
Voight B (1978) Lower Gros Ventre slide, Wyoming, USA. In: Developments in geotechnical engineering 14(A):113–162, Elsevier. https://doi.org/10.1016/B978-0-444-41507-3.50011-8
Voight B (1981) Time scale for the first moments of the May 18 eruption. In: Lipman PW, Mullineaux DR (eds) The 1980 eruptions of Mount St. Helens, Washington. U S Geol Surv Prof Pap 1250:69–86
Voight B (1989) A relation to describe rate-dependent material failure. Science 243:200–203. https://doi.org/10.1126/science.243.4888.200
Voight B (2000) Structural stability of andesitic volcanoes and lava domes. Phil Trans Roy Soc Lond A 358:1663–1703. https://doi.org/10.1098/rsta.2000.0609
Voight B, Elsworth D (1997) Failure of volcano slopes. Geotechnique 47(1):1–31. https://doi.org/10.1680/geot.1997.47.1.1
Voight B, Elsworth D (2000) Instability and collapse of hazardous gas-pressurized lava domes. Geophys Res Lett 27(1):1–4. https://doi.org/10.1029/1999GL008389
Voight B, Sousa J (1994) Lessons from Ontake-san: a comparative analysis of debris avalanche dynamics. Eng Geol 38:261–297. https://doi.org/10.1016/0013-7952(94)90042-6
Voight B, Glicken H, Janda RJ, Douglass PM (1981) Catastrophic rockslide avalanche of May 18. In: Lipman PW, Mullineaux DR (eds) The 1980 eruptions of Mount St. Helens, Washington. U S Geol Surv Prof Pap 1250:347–377
Voight B, Janda RJ, Glicken H, Douglass PM (1983) Nature and mechanics of the Mount St. Helens rockslide-avalanche of 18 May 1980. Geotechnique 33:243–273. https://doi.org/10.1680/geot.1983.33.3.243
Voight B, Komorowski J-C, Norton GE, Belousov AB, Belousova M, Boudon G, Francis PW, Franz W, Heinrich P, Sparks RSJ, Young SR (2002) The 26 December (Boxing Day) 1997 sector collapse and debris avalanche at Soufriere Hills volcano, Montserrat. Geol Soc Lond Mem 21(1):363–407. https://doi.org/10.1144/GSL.MEM.2002.021.01.17
Wadge G, Francis PW, Ramirez CF (1995) The Socompa collapse and avalanche event. J Volcanol Geotherm Res 66:309–336. https://doi.org/10.1016/0377-0273(94)00083-S
Wadge G, Macfarlane DG, Robertson DA, Hale AJ, Pinkerton H, Burrell RV, Norton GE, James MR (2005) AVTIS: a novel millimetre-wave ground based instrument for volcano remote sensing. J Volcanol Geotherm Res 146(4):307–318. https://doi.org/10.1016/j.jvolgeores.2005.03.003
Wadge G, Macfarlane DG, Odbert HM, James MR, Hole JK, Ryan G, Bass V, De Angelis S, Pinkerton H, Robertson DA, Loughlin SC (2008) Lava dome growth and mass wasting measured by a time series of ground-based radar and seismicity observations. J Geophys Res 113:B08210. https://doi.org/10.1029/2007JB005466
Waitt RB (1981) Devastating pyroclastic density flow and attendant air fall of May 18—stratigraphy and sedimentology of deposits. In: Lipman PW, Mullineaux DR (eds) The 1980 eruptions of Mount St. Helens, Washington. U S Geol Surv Prof Pap 1250:439–458
Waitt RB (1989) Swift snowmelt and floods (lahars) caused by great pyroclastic surge at Mount St. Helens volcano, Washington, 18 May 1980. Bull Volcanol 52:138–157. https://doi.org/10.1007/BF00301553
Waitt RB (2015) In the path of destruction: eyewitness chronicles of Mount St. Wash State Univ Press, Helens, p 413

Waitt RB, Begét, JE (2009) Volcanic processes and geology of Augustine Volcano, Alaska: U S Geol Surv Prof Pap 1762:1–78, 2 plates, scale 1:25,000

Waitt RB, Major JJ, Hoblitt RP, Van Eaton AR, Clynne MA (2019) Field trip guide to Mount St. Helens, Washington—recent and ancient volcaniclastic processes and deposits. U S Geol Surv Sci Invest Rep 2017–5022–E, 68. https://doi.org/10.3133/sir20175022E

Walker GPL (1971) Grain-size characteristics of pyroclastic deposits. J Geol 79:696–714

Wang X, Aoki Y, Chen J (2019) Surface deformation of Asama volcano, Japan, detected by time series InSAR combining persistent and distributed scatterers, 2014–2018. Earth Planets Space 71(1):121. https://doi.org/10.1186/s40623-019-1104-9

Ward SN, Day S (2006) Particulate kinematic simulations of debris avalanches: interpretation of deposits and landslide seismic signals of Mount Saint Helens, 1980 May 18. Geophys J Int 167(2):991–1004. https://doi.org/10.1111/j.1365-246X.2006.03118.x

Watters RJ, Zimbelman DR, Bowman SD, Crowley JK (2000) Rock mass strength assessment and significance to edifice stability, Mount Rainier and Mount Hood, Cascade Range volcanoes. Pure Appl Geophys 157:957–976. https://doi.org/10.1007/s000240050012

Watters RJ, Delahaut WD (1995) Effect of argillic alteration on rock mass stability. In: Haneburg WC, Anderson SA (eds) Clay and shale slope instability. Geol Soc Am Rev Eng Geol, 139–150

Waythomas CF (2012) Landslides at stratovolcanoes initated by volcanic unrest. In: Clague JJ, Stead D (eds) Landslides: types, mechanisms and modeling. Cambridge Univ Press, 37–49

Weidinger JT, Korup O, Munack H, Altenberger U, Dunning SA, Tippelt G, Lottermoser W (2014) Giant rockslides from the inside. Earth Planet Sci Lett 389:62–73. https://doi.org/10.1016/j.epsl.2013.12.017

Wicks CW Jr, Dzurisin D, Ingebritsen S, Thatcher W, Lu Z, Iverson J (2002) Magmatic activity beneath the quiescent Three Sisters volcanic center, central Oregon Cascade Range, USA. Geophys Res Lett 29(7):26-1–26-4. https://doi.org/10.1029/2001GL014205

Wooller L, van Wyk de Vries B, Murray JB, Rymer H, Meyer S (2004) Volcano spreading controlled by dipping substrata. Geology 32(7):573–576. https://doi.org/10.1130/G20472.1

Wooller L, van Wyk de Vries B, Cecchi E, Rymer H (2009) Analogue models of the effect of long-term basement fault movement on volcanic edifices. Bull Volcanol 71(10):1111–1131. https://doi.org/10.1007/s00445-009-0289-3

Worni R, Huggel C, Stoffel M, Pulgarín B (2012) Challenges of modeling current very large lahars at Nevado del Huila Volcano, Colombia. Bull Volcanol 74(2):309–324. https://doi.org/10.1007/s00445-011-0522-8

Wright IC, Worthington TJ, Gamble JA (2006) New multibeam mapping and geochemistry of the 30°–35° S sector, and overview, of southern Kermadec arc volcanism. J Volcanol Geotherm Res 149(3–4):263–296. https://doi.org/10.1016/j.jvolgeores.2005.03.021

Wright HM, Cashman KV, Gottesfeld EH, Roberts JJ (2009) Pore structure of volcanic clasts: measurements of permeability and electrical conductivity. Earth Planet Sci Lett 280(1–4):93–104. https://doi.org/10.1016/j.epsl.2009.01.023

Wyering LD, Villeneuve MC, Wallis IC, Siratovich PA, Kennedy BM, Gravley DM, Cant JL (2014) Mechanical and physical properties of hydrothermally altered rocks, Taupo Volcanic Zone, New Zealand. J Volcanol Geotherm Res 288:76–93. https://doi.org/10.1016/j.jvolgeores.2014.10.008

Yamagishi H (1996) Destructive mass movements associated with quaternary volcanoes in Hokkaido, Japan. Geol Soc Lond Spec Publ 110:267–279. https://doi.org/10.1144/GSL.SP.1996.110.01.21

Yoshida H (2013) Decrease of size of hummocks with downstream distance in the rockslide-debris avalanche deposit at Iriga volcano, Philippines: similarities with Japanese avalanches. Landslides 10:665–672. https://doi.org/10.1007/s10346-013-0414-4

Yoshida H (2014) Hummock alignment in Japanese volcanic debris avalanches controlled by pre-avalanche slope of depositional area. Geomorphology 223:67–80. https://doi.org/10.1016/j.geomorph.2014.06.024

Yoshida H, Sugai T (2010) Grain size distribution of the sediments from the 24 ka sector collapse of Asama volcano, Japan. Trans Jpn Geomorph Union 31(2):193–201

Yoshida H, Sugai T, Ohmori H (2012) Size-distance relationships for hummocks on volcanic rockslide-debris avalanche deposits in Japan. Geomorphology 136:76–87. https://doi.org/10.1016/j.geomorph.2011.04.044

Yoshida H (2016) Magnitude-frequency distribution of slope failures in Japan: statistical approach to a true perspective on volcanic mega-collapses. In: Nemeth K (ed) Updates in volcanology—from volcano modelling to volcano geology. InTech, Croatia, 191–219. https://doi.org/10.3390/geosciences6010005

Yoshimoto M, Ui T (1998) The 1640 sector collapse of Hokkaido Komagatake volcano, northern Japan. Bull Volcanol Soc Jpn 43:137–148 (in Jpn with Engl abstr)

Young SR, Voight B, Barclay J, Herd RA, Komorowski J-C, Miller AD, Sparks RS, Stewart RC (2002) Hazard implications of small-scale edifice instability and sector collapse: a case history from Soufrière Hills Volcano, Montserrat. Geol Soc Lond Mem 21(1):349–362. https://doi.org/10.1144/GSL.MEM.2002.021.01.16

Yudhicara Y, Bani P, Darmawan A (2015) Geothermal system as the cause of the 1979 landslide tsunami in Lembata Island, Indonesia. Indon J Geosci 2(2):91–99

Zernack AV (2021) Volcanic debris-avalanche deposits in the context of volcaniclastic ring plain successions—a case study from Mt. Taranaki. In: Roverato M, Dufresne A, Procter J (eds) Volcanic debris avalanches. Adv Volcanol 6:211–254. https://doi.org/10.1007/978-3-030-57411-6_9. Springer, Cham

Zernack AV, Procter JN, Cronin SJ (2009) Sedimentary signatures of cyclic growth and destruction of stratovolcanoes: a case study from Mt. Taranaki, New Zealand. Sed Geol 220(3–4):288–305. https://doi.org/10.1016/j.sedgeo.2009.04.024

Zernack AV, Cronin SJ, Neall VE, Procter JN (2011) A medial to distal volcaniclastic record of an andesite stratovolcano: detailed stratigraphy of the ring-plain succession of south-west Taranaki, New Zealand. Int J Earth Sci (geol Rundsch) 100:1937–1966. https://doi.org/10.1007/s00531-010-0610-6

Zimbelman DR, Watters RJ, Firth IR, Breit GN, Carrasco-Núñez G (2004) Stratovolcano stability assessment methods and results from Citlaltépetl. Mexico Bull Volcanol 66(1):66–79. https://doi.org/10.1007/s00445-003-0296-8

Zimbelman DR, Rye RO, Breit GN (2005) Origin of secondary sulfate minerals on active andesitic stratovolcanoes. Chem Geol 215(1–4):37–60. https://doi.org/10.1016/j.chemgeo.2004.06.056